DISSERTATION

Next Generation Mesenchymal Stromal Cells for Regenerative Purposes - Manipulation of the Cellular Phenotype Using Biomaterials and Non-viral Gene Transfer

Mesenchymale Stromazellen der nächsten Generation für regenerative Zwecke - Manipulation des Zellphänotyps durch Biomaterialien und nichtviralen Gentransfer

zur Erlangung des akademischen Grades
Medical Doctor - Doctor of Philosophy (MD/PhD)

vorgelegt der Medizinischen Fakultät

Charité – Universitätsmedizin Berlin

von

Norman M. Drzeniek

Erstbetreuer*in: Prof. Dr. med. Hans-Dieter Volk

Datum der Promotion: 23. März 2024

Table of Contents

List of Tables

List of Figures

List of Abbreviations

4E-BP1	eukaryotic translation initiation factor 4E-binding protein 1
5mC	5-methyl-cytidine
5moU	5-methoxy-uridine
ANGPT1	angiopoietin 1
ANOVA	analysis of variance
C	cytidine
CD	cluster of differentiation
Col-HA	type-I collagen and hyaluronic acid hydrogel
CXCL1	chemokine (C-X-C motif) ligand 1
DAPI	4′,6-diamidino-2-phenylindole
DMEM	Dulbecco's modified eagle medium
DNA	desoxyribonucleic acid
ECM	extracellular matrix
ELISA	enzyme-linked immunosorbent assay
EtOH	ethanol
FCS	fetal calf (or bovine) serum
FCS	forward scatter
Gel-HA	Gelatin-HA hydrogel
GFP	(enhanced) green fluorescent protein
GTP	guanosine-5'-triphosphate
HA	hyaluoronic acid
HGF	hepatocyte growth factor
IE-mRNA	immuno-engineered mRNA
IL-8	interleukin 8

IL-10	interleukin 10
INF-β	interferon beta
IVT	in vitro transcription
LF	lipofectamine MessengerMax
LOD	limit of detection
m1ψ	n1-methyl-pseudouridine
mRNA	messenger ribonucleic acid
MSC	mesenchymal stem/ stromal cell
NPX	normalized protein expression
ORF	open reading frame
PBS	phosphate buffered saline
PEG	polyethylene glycol
PEGDA	polyethylene glycol diacrylate
RT	room temperature
RT-PCR	reverse transcription polymerase chain reaction
SARS-CoV2	severe acute respiratory syndrome coronavirus 2
SD	standard deviation
SEM	standard error of the mean
SSC	side scatter
TCP	tissue culture plastic
U	uridine
U-mRNA	unmodified / uridine-containing mRNA
UV-A	long-wave ultraviolet light
VEGF	vascular endothelial growth factor
ψ	pseudouridine

Zusammenfassung

Die Summe verschiedener Reize aus dem Mikromilieu reguliert den Phänotyp und das Verhalten von Zellen. Synergistische Strategien, welche diese Multimodalität berücksichtigen, könnten genutzt werden, um die Funktion therapeutischer Zellen präzise zu kontrollieren. In dieser Arbeit habe ich eine Kombination aus Biomaterialeinbettung und mRNA Transfektion etabliert, um das parakrine Profil Mesenchymaler Stromazellen (MSCs) zu formen. MSCs sind ein sekretorisch aktiver Zelltyp, welcher sich in klinischen Studien als sicher, aber nicht immer wirkungsvoll erwiesen hat.

Um Wachstumsfaktorsekretion mittels Zell-Material-Interaktionen zu stimulieren, wurden MSCs in Kollagen-HA (Col-HA) Hydrogel eingebettet. Als Kontrolle dienten HA-, PEG- und Gelatinegele. MSCs in Col-HA wiesen stärkere Elongation und ein expandiertes Sekretionsprofil mit unterschiedlichen Kinetiken für HGF und VEGF auf.

MSCs wurden mittels Lipofektamin mit in vitro transkribierter mRNA transfiziert, welche GFP bzw. VEGF kodiert. Uridin wurde durch Varianten wie 5-Methoxy-Uridin (5moU) ersetzt. Unmodifizierte mRNA löste eine Typ-I Interferonantwort aus, erhöhte die Ausschüttung proinflammatorischer Zytokine und senkte proangiogene Faktoren. 5moU-mRNA löste keine detektierbare Interferonantwort aus und erlaubte eine verlängerte Genexpression, ohne Beeinträchtigung des natürlichen Sekretionsprofils.

Zuletzt wurde die mRNA Transfektion sequentiell mit der Hydrogeleinbettung kombiniert. Nur 5moU-mRNA, nicht jedoch unmodifizierte mRNA erlaubte die sequentielle Kombination beider Methoden bei hoher Zellviabilität und erhaltenen Hydrogeleffekten auf die Faktorfreisetzung. Umgekehrt wurde auch der Einfluss der Matrixadhäsion auf die mRNA Transfektion untersucht. GFP Expression und VEGF Sekretion wurden in Col-HA versus PEG-HA, welches keine Integrinliganden enthält, verglichen. In Col-HA sezernierten die MSCs mehr mRNA-kodiertes VEGF als in PEG-HA. Das GFP Signal war vergleichbar, was nahelegt, dass nicht die Translation, sondern die Sekretion adhäsionssensitiv ist.

Die Ergebnisse zeigen, dass die breite Sekretomstimulation durch Zell-Material-Interaktionen orthogonal mit mRNA Überexpression eines ausgewählten Schlüsselmediators kombiniert werden kann, um das MSC Sekretom auf meheren Ebenen zu formen. 5moU-

mRNA kann zur Expression eines gewünschten Gens verwendet werden, ohne den übrigen Zellphänotyp zu beeinträchtigen. Zudem konnten wir einen Synergismus zwischen Zelladhäsion und der Freisetzung mRNA-kodierter Faktoren identifizieren.

Offen bleibt die Frage nach den genauen Mechanismen, durch welche die Zell-Material-Interaktionen zu zeitlichen Veränderungen im Sekretionsprofil führen. Außerdem muss der therapeutische Nutzen eines solchen multimodalen Systems gezeigt werden. Das hier vorgeschlagene Konzept könnte zu allgemeineren Stimulom-Modellen synergistischer bzw. antagonistischer Reizinteraktionen erweitert werden.

Abstract

The sum of different microenvironment stimuli precisely regulates cell phenotype and behavior. Synergistic strategies, which make use of this multimodality could be harnessed to precisely control functions of therapeutic cells. In this thesis I have established and applied a combination of biomaterial encapsulation and mRNA transfection to shape the paracrine profile of mesenchymal stromal cells (MSCs), a secretory active cell type shown to be safe but not always efficacious in clinical trials.

To stimulate growth factor secretion through cell-material interactions, MSCs were encapsulated in collagen and HA (Col-HA) hydrogel, or control hydrogels made from HA, PEG, and gelatin. MSC showed stronger elongation and an expanded growth factor profile in Col-HA with distinct upregulation kinetics for HGF versus VEGF.

MSCs were transfected with in vitro transcribed mRNA coding for GFP and VEGF using lipofectamine. Uridine was substituted by different chemically modified derivates, including 5-methoxy-uridine (5moU). Unmodified mRNA triggered a type-I interferon response in MSCs and upregulated pro-inflammatory cytokine secretion, while downregulating pro-angiogenic growth factors. 5moU-mRNA did not trigger a detectable type-I interferon response and allowed for prolonged gene overexpression without disturbing the MSC's natural secretome.

Finally, a protocol for sequential mRNA transfection and hydrogel encapsulation was developed. The effects of mRNA transfection on cell-material interactions were evaluated. Only 5moU-mRNA, but not unmodified mRNA, allowed for sequential transfection and encapsulation with high cell viability and preserved hydrogel-dependent effects on growth

factor secretion. Conversely, the effect of cell-matrix adhesion on mRNA transfection was investigated by comparing GFP expression and VEGF secretion in Col-HA, which contains integrin ligand motifs, versus a PEG-HA control gel, which does not. In Col-HA, MSCs secreted higher levels of mRNA-encoded VEGF than in PEG-HA, but no difference in GFP fluorescence was observed, suggesting that secretion, but not translation of mRNA-encoded protein is adhesion-sensitive.

The results show that broad secretome stimulation by cell-material interactions can be orthogonally combined with high mRNA overexpression of a selected key factor, to shape the MSC secretome on multiple levels. Additionally, we identified a synergy between secretion of targeted mRNA-encoded factors and cell adhesion. Importantly, 5moU-mRNA can be used to express a gene of interest while leaving the remaining cellular phenotype largely unaffected.

Open questions include elucidating mechanistic connections between cell-material interactions and the temporal changes in secretion profile, as well as showing a therapeutic utility of such a multimodal system. The concept proposed here could be expanded into generalized stimulome models of synergies and antagonisms between different cell-instructive stimuli.

1 Introduction

1.1 Mesenchymal Stromal/Stem Cells (MSCs) and their therapeutic potential

Mesenchymal stromal cells or mesenchymal stem cells (MSCs) are fibroblast-shaped adherent cells that can be isolated from a variety of tissues such as bone marrow, adipose tissue or perinatal tissues. These cells are characterized by their osteogenic, chondrogenic and adipogenic differentiation potential and a characteristic surface marker profile. The originally proposed paradigm that they promote tissue regeneration directly by differentiation and cell replacement has shifted toward a paracrine mode of action promoting endogenous regeneration [1]. MSCs secrete a broad cocktail of angiogenic, immunomodulatory and pro-regenerative growth factors and cytokines, known as the MSC secretome [2]. MSCs have shown promise for a variety of regenerative indications, including musculoskeletal, neurological, ischemic and immune disorders in preclinical models and more than 1000 clinical trials are registered for MSC-related products. However, while safety of MSC transplantation has been demonstrated, the therapeutic efficacy in clinical trials is limited [3-5]. Therefore, there is a need for bioengineering strategies that improve MSCs' therapeutic potential, specifically the qualitative and quantitative composition of their growth factor secretome.

1.2 Cells as processors of different stimulus modalities

To improve therapeutic functionality of MSCs, a broad variety of approaches have been proposed, ranging from cytokine conditioning during culture or encapsulating the cells in a biomaterial to direct genetic modification.

In coordinated biological processes such as tissue development and repair, cells receive different types of stimuli, including contact-dependent signaling through cell-matrix or cell-cell contacts (which can also transmit mechanical forces), gradients of paracrine factors such as growth factors, morphogens or cytokines, and -for some cell types even electrical signals. I propose to summarize all biological, chemical and physical stimuli a cell receives under the term "stimulome" in analogy to the "secretome" or "interactome". Although the effects of a single stimulus might be broad and lack selectivity, cells act as information processors which summate all synergistic and antagonistic stimuli within their stimulome and respond with highly specific phenotype and function (Fig. 1a). In addition, direct programming of cell identity and function can be achieved through introduction of

nucleic acid like DNA or mRNA into the cell. In contrast to the unselective stimulation by external cues, gene transfer allows for overexpression of precisely defined key factors, which can drive a biological process. While the high specificity is an important advantage, narrow modification of only one or few genes might not be as effective in driving complex biological processes without supporting synergistic cues.

Combining overexpression of a selected key factor in MSCs with the broad stimulatory effects of contact-dependent stimuli or cell-material interaction, could result in a multifactorial, yet targeted paracrine response (Fig 1b). Furthermore, the two modalities could possibly interact with each other through convergent intracellular processing, resulting in emergent effects, which favor a multimodal strategy over the different individual approaches of MSC engineering.

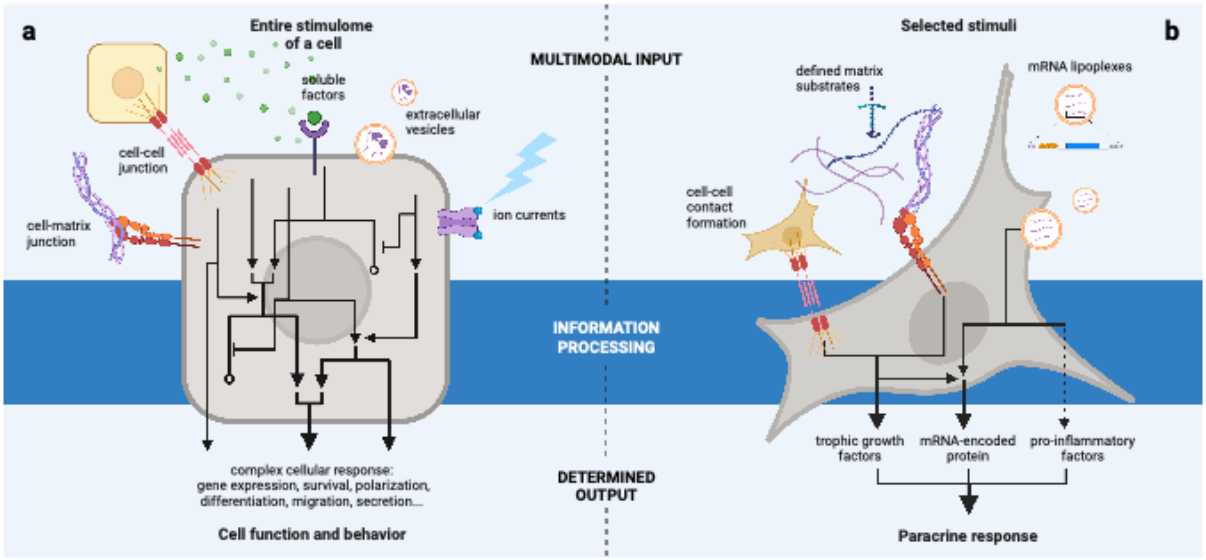

Figure 1: Model of cells as information processing units, own representation.

(a) Generalized model of the stimulome and its cellular processing: A cell is exposed to a complex microenvironment of multimodal stimuli, i.e. its stimulome (top panel). This multimodal input is summated by the cell through a myriad of synergistic and antagonistic pathways (middle) and results in a complex but determined cellular response toward the cell's stimulome (bottom). (b) In this work, a simplified model is investigated experimentally, where MSCs are subjected to different biopolymer substrates and allowed to elongate and form cell-cell contacts. IVT-mRNA coding for a selected protein is introduced by lipofection (top). Possible synergies between matrix-related effects and mRNA expression are investigated (middle). The paracrine response (secretome) serves as the main readout (bottom).

1.3 Biomaterial-based manipulation of the MSC secretome

While injecting or implanting the cells in a pre-designed biomaterial microenvironment is an emerging strategy to protect the cells from the in vivo microenvironment, retain their localization and extend their persistence, biomaterials can also be used to modulate the MSC phenotype by providing biologically relevant cues [2].

The MSC phenotype is regulated by interactions between receptors on the cell surface, such as integrins, and adhesion ligands present on extracellular matrix (ECM) components or on other cells. Integrins are a family of heterodimeric receptors consisting of an α and β subunit, have different ligand specificity and can be targeted for modulation of cell adhesion, migration, differentiation, and paracrine signaling. Integrin receptor subunits expressed by MSCs include α1, α3, α5, αV, β1 and β3 and according to some sources α2, α5, α6, α7, α10, αIIb, β4 and β5 [6-8]. Bioinert biomaterials, such as polyethylene glycol or alginate do not possess ligands for adhesion receptors, such as integrins, and are not enzymatically degradable. Biopolymers are often naturally present within the extracellular matrix, are enzymatically degradable and can be divided into those which provide cell adhesion sites, such as collagen, gelatin or laminin or those that do not, such as hyaluronic acid (HA) [9].

Type-I collagen in its native form contains the triple-helical motif GxOGER, which binds to β1-containing integrins such as α1β1, α2β1 and α10β [10, 11]. Integrin signaling in type-1-collagen has been shown to enhance the pro-angiogenic effects of MSCs [12].

The denatured and less organized form of collagen, gelatin, interacts primarily with α5β1 and αvβ3 through the tripeptide sequence RGD [10, 11]. Therefore, despite sharing the same amino acid (aa) sequence, cells interact differently with collagen vs gelatin environments [11, 13]. RGD is also present on vitronectin, fibronectin and other ECM components [14]. Laminin, whose microanatomical localization is the basal lamina, has its own specific receptors including α3β1, α6β1 and α7β1 [15]. MSCs grown on laminin showed an αvβ3-dependent increased secretion of pro-angiogenic factors HGF, IL-8 and CXCL1 [16].

Not only the biochemical composition, but also physical cues such as porosity, topography and mechanical parameters, contribute to the interface between materials and tissues. Especially porous scaffolds have been shown to promote cell-matrix and cell-cell interactions and a stromal, elongated morphology of MSCs which correlate with increased growth factor secretion and pro-regenerative capacity [17]. However, scaffolds need to

be prefabricated and then seeded with cells, a process which may be difficult to execute reliably in a clinical environment. Also, not all scaffolds are injectable, restricting their use to applications, where scaffolds can be implanted. Hydrogels, polymer networks which swell in aqueous environments, allow for rapid and homogenous cell encapsulation by simple mixing. They can be injected in a soluble phase and crosslinked through temperature-, pH- or light-dependent mechanisms, making them attractive carriers for cell delivery [9, 18]. However, a study which compared MSC encapsulation in an RGD-functionalized alginate hydrogel versus microporous scaffold found that the alginate hydrogel impaired the MSC paracrine activity, while the porous hydrogel augmented it [17]. This suggests that hydrogels are a valuable tool for MSC delivery only if they provide a sufficient density of biologically relevant cues and allow for cell elongation and cell-cell contact formation. The combination of injectability, easy handling and favorable interactions with cells is a challenge in the engineering of biomaterials for cell delivery.

1.4 Direct cell manipulation using IVT-mRNA technology

Beside indirect stimulation of MSCs through cues from the microenvironment, direct genetic modification of MSCs has been suggested to selectively overexpress target genes coding for secreted factors, transcription factors or homing receptors [19]. Viral gene transfer methods, such as lentiviral or adeno-associated virus or non-viral integrating methods, such as transposon are efficient in vivo gene delivery vectors but come with several limitations such as cytotoxicity, immunogenicity, and potential disruption of tumor suppressor genes by uncontrolled chromosomal integration of transfected DNA fragments [20, 21].The recent success of messenger RNA (mRNA) vaccines against SARS-CoV2 has showcased in vitro transcribed (IVT)-mRNA as a safe and effective technology to express a gene of interest [22]. Using IVT-mRNA for cell manipulation comes with important advantages compared to DNA-based methods [23]: Instead of integrating into the cell’s genome, mRNA is translated to protein and degraded after a limited amount of time. This eliminates any risk for genomic integration and putative genotoxicity. Because the nucleus does not need to be reached for translation, the expression is fast, efficient and independent of cell cycle. Currently IVT-mRNA has two major limitations: In most cases, expression last only hours to a few days, with a distinct peak around 24 h post-transfection [23]. Prolonging or even tailoring IVT-mRNA expression kinetics to the desired application would make it an even more versatile tool for a variety of indications.

The other limitation of IVT-mRNA is its strong immunogenicity, which is related to recognition of exogenous IVT-mRNA by pattern recognition receptors, such as toll like receptors 7 and 8 [24]. The recognition triggers an anti-viral type-I interferon-mediated immune response, which has been shown to accelerate mRNA degradation and arrest protein translation [25, 26]. While some immune stimulation may be favorable as a vaccine adjuvant, its consequences on the function of therapeutic cell products, such as MSCs are not understood. Use of chemically modified nucleotides, especially uridine derivates, during IVT has been shown to modulate the immune response toward mRNA [26-28]. However, over the years several uridine modifications have been proposed based on experiments with cell lines, which have rarely been compared with each other [27-29]. As such, the effects and functional consequences of mRNA nucleotide-modification on the phenotype of transfected primary cells, and MSCs in particular, remain poorly understood.

1.5 Aims of this work

The aim of this work was to establish two different approaches of cell manipulation and explore synergies between them. In this work, the cell manipulation was carried out on MSCs as a model cell type to augment their paracrine activity, which is considered their therapeutically relevant mode of action. Important criteria for selection of the manipulation strategies were (I) potential translatability into a clinically applicable protocol and (II) controlled / minimized side effects on cell fitness and characteristics. For the gene transfer strategy this excluded the use of viral or integrating approaches.
Key research questions within this project included:

a) designing an injectable hydrogel for favorable stimulation of the MSC secretome
b) uncoupling the IVT-mRNA immunogenicity from its protein-expressing functionality in MSCs through substitution of uridine with different derivates, thereby minimizing side effects of mRNA-triggered innate immune response
c) combining the mRNA transfection and biomaterial encapsulation into a protocol which minimizes cell stress and is applicable in a clinical setting
d) investigating synergies between mRNA transfection and biomaterial stimulation as a multimodal strategy to orchestrate the MSC secretome (Fig 1b)

2 Materials & Methods

2.1 Mesenchymal stromal cells

Primary mesenchymal stromal/stem cells (MSCs) from human bone marrow were kindly provided by the core facility "Cell and Tissue Harvesting" at the BIH Center for Regenerative Therapies (BCRT). MSCs had been isolated from bone marrow biopsies of patients undergoing hip replacement at Charité—Universitätsmedizin Berlin, as previously stated [16]. Written informed consent was given, and ethics approval was obtained from the local ethics committee/ institutional review board of the Charité— Universitätsmedizin Berlin (number of approval: EA2/089/20). MSCs obtained from the core facility were seeded in tissue culture flasks at a density of at least $1.7x10^3$ cells/cm^2 culture surface and expanded in low glucose DMEM supplemented with 10% v/v fetal calf serum (FCS), 1% v/v penicillin/streptomycin (both Biochrom AG), and 1% v/v Glutamax (Thermo Fisher Scientific Inc., Waltham, MA) at 37 °C in a humidified 5% CO2 atmosphere. Culture medium was changed at least every 2 - 3 days. Cells were passaged around 80% confluence and not used for experiments beyond passage 6. Cells were detached from culture plastic using trypsin-EDTA (0.04%, 0.03%) or TrypLE select (Thermo Fisher) and either passaged for further expansion or experiments or aliquoted in cryo medium (either Cryo SFM from Promocell, Heidelberg, Germany or culture medium with 10% DMSO) for storage. After thawing, cells were allowed to adhere for at least 24 h prior before being used for experiments. All experiments were performed using primary cells from at least two different donors, to monitor for biological variability between donors.

2.2 Biomaterials and 3D cell culture

2.2.1 Formulation of Col-HA

The hydrogels used in this study are all photo-crosslinkable formulations, in which thioethers are formed from thiol- or alkene-functionalized biopolymers through a free-radical addition (Fig 2a). This reaction was catalyzed by the radical donator 2-hydroxy-4'-(2-hydroxyethoxy)-2-methylpropiophenone (Irgacure 2959; Sigma Aldrich, St. Louis, MO) upon UVA irradiation (1 J/cm^2). The collagen-HA hydrogel (Col-HA) was prepared from methacrylated type 1 collagen (Advanced Biomatrix, Carlsbad, CA) and hyaluronic acid functionalized with sulfhydryl groups (HyStem; Advanced Biomatrix or Sigma Aldrich, St.

Louis, MO). Lyophilized collagen was dissolved in 20 mM acetic acid to a concentration of 8 mg/ml. Thiolated HA was dissolved in PBS containing 0.1% (w/v) of Irgacure 2959 to a concentration of 10 mg/ml. Collagen was mixed with HA and DMEM or PBS at a ratio of 3 : 1 : 2 parts, resulting in final concentrations of 4mg/ml collagen, 1.67mg/ml HA and ~0.17 mg/ml Irgacure 2959. This hydrogel was based on the collagen-HA bioink first introduced by Mazzocchi et al [30] with identical components formulated at different proportions. Reformulating the hydrogel mix to include a volume of DMEM or PBS allowed to incorporate further components within or instead of this volume. Mouse laminin (Thermo Fisher) or human plasma fibronectin (Sigma) were functionalized with sulfhydryl groups using a protein thiolation kit (Expedeon, Over Cambridgeshire, UK) and included in this PBS volume for a final concentration of 0.33 mg/ml.

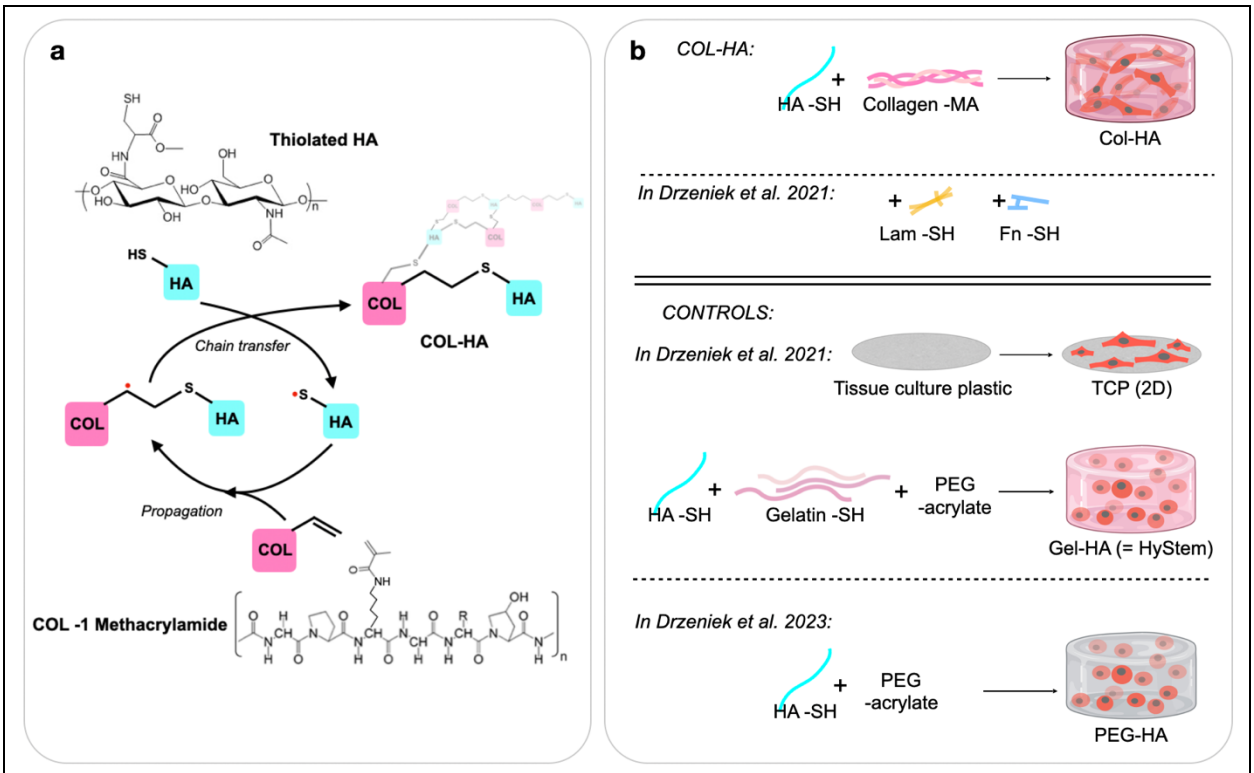

Figure 2: Col-HA hydrogel and control hydrogels, from *Drzeniek et al. 2021 [13]* and own representation.

(a) Schematic: thiol-ene reaction between methacrylated type-I collagen and thiolated hyaluronic acid crosslinks the collagen-HA hydrogel (Col-HA) without the need for any additional crosslinkers. (b) Overview of comparisons made between Col-HA and controls. *Item a from Drzeniek et al. 2021 [13], b own representation.*

2.2.2 Control hydrogels

The control hydrogel Gel-HA soft, which corresponds to the commonly used HyStem-C kit (Sigma Aldrich, St. Louis, MO), was prepared according to the manufacturer's manual. Briefly, thiolated porcine type A gelatin (Gelin-S) and the same HA component as for Col-HA were dissolved with PBS. Irgacure 2959 was included in the HA aliquot, as described above. Since both the gelatin and the HA were functionalized with thiol groups, polyethylene glycol (PEG) functionalized with acrylate groups had to be used as a crosslinker. For the standard HyStem formulation, the linear PEG diacrylate provided with the kit was used, resulting in a very soft gel. To match the higher stiffness of Col-HA, 4-arm PEG acrylate linkers (2 kDa, 10 kDa, 20 kDa MW; Creative PEGWorks, Durham, NC) at 0.5 mM (1 mM; 5 mM; 10 mM) concentrations were tested (Tab 1). Elastic modulus of the crosslinked hydrogels was assessed through a uniaxial compression test using a Discovery HR-2 (TA Instruments, New Castle, DE). The 20 kDa linker at a concentration of 5 mM was used to formulate the Gel-HA stiff control gel. To generate a control hydrogel which provided a 3D environment but no integrin-mediated adhesion, the methacrylated collagen was replaced by PEG diacrylate (PEGDA) solution and mixed with thiolated HA solution at a 1 : 4 ratio.

Table 1: Relationship between PEG crosslinker type and concentration and resulting bulk hydrogel stiffness in gelatin-HA control gels, adapted from *Drzeniek et al. 2021 [13]*

Linker type	Linear PEGDA *	4 arm-PEG	4 arm-PEG	4 arm-PEG	4 arm-PEG	4 arm-PEG	4 arm-PEG *	8 arm-PEG
Linker size (MW in kDa)	3.5	2	10	10	10	20	20	20
Linker arm length (kDa/n arms)	1.75	1	2.5	2.5	2.5	5	5	2.5
Molar concentration (μmol ml^{-1})	2.86	5	1	5	10	0.5	5	0.5
Mass concentration (% w/v)	1	1	1	5	10	1	10	1
Hydrogel stiffness (Pa); SD	6069; 691	6180; 788	6845; 1723	14048; 1491	22760; 429	8680; 2766	28744; 4724	6822; 388

The two conditions highlighted with an asterisk (*) were used as control hydrogels in this study. SD = standard deviation.

2.2.3 Cell encapsulation and 3D culture

MSCs were detached from culture plastic and centrifuged into a pellet at 250-270 x g for 5-7min. The pellet was resuspended in the respective hydrogel formulation to a cell concentration of ~3.5- 5x 10^6/ ml.10 µl droplets were pipetted and UV-crosslinked into microspheres at a dose of ~1J/ cm^2 using a UV-A spot lamp (Dymax, Torrington, CT). The microspheres were cultured in 48 well plates (1 microsphere per well) and media were changed at least every other day. To determine cell viability, microspheres were stained with calcein AM (green; 1:2000) and ethidium homodimer-1 (red; 1:1000) (Thermo Fisher) in culture medium at 37 °C for 1-2 h before imaging on a Leica TCS LSI macro-confocal microscope (Leica, Wetzlar Germany). Cells were manually counted in Image J to determine live/dead ratio. Elongation was also quantified from images using the “analyze particles” function in Image J and expressed as the reciprocal of the circularity value. As a complementary method to assess cell viability, activity of caspases 3 and 7 was measured using the Caspase-Glo 3/7 3D kit, as described below for conventional 2D culture.

2.3 mRNA

2.3.1 mRNA synthesis

For GFP-mRNA synthesis the plasmid vector pRNA2-(A)128 (gift from Stephen Ikeda; Addgene plasmid # 174006; RRID:Addgene_174006; http://n2t.net/addgene:174006) was used as a template [31]. It consists of a T7 promoter, followed by a short 5′-UTR including a multiple cloning site, a Kozak sequence and start codon for translation initiation, an enhanced green fluorescent protein (GFP) coding sequence, a head-to-tail duplicated β-globin 3'-UTR sequence and a 128 bp poly(A) tail sequence. A DNA plasmid template for human vascular endothelial growth factor A isoform 165 (VEGF-165) mRNA synthesis (Fig 3) was designed in silico using SnapGene (GSL Biotech LLC, Boston, MA). The fragment containing the VEGF coding sequence (Tab 2) was ordered from Integrated DNA Technologies (Coralville, IA) and cloned into the pRNA2-(A)128 vector using restriction endonucleases HindIII and NotI (New England Biolabs, Ipswich, MA) to replace the GFP coding sequence. The resulting plasmid and the original plasmid were linearized using BaeI and BspMI (NEB) and the resulting overhangs of the BaeI digestion were blunted (Quick Blunting kit; NEB). The fragments of the restriction products were separated by non-denaturing agarose gel electrophoresis and the gel fragment containing the correct DNA template band was cut out with a scalpel for both constructs respectively.

The DNA from this fragment was extracted, purified (Gel Clean-up kit; Macherey-Nagel, Düren, Germany) and used as a template for in vitro transcription. Synthetic mRNA for EGFP and VEGF-165 was transcribed from the purified DNA template using the TranscriptAid T7 High Yield Transcription Kit (Thermo Fisher). The DNA template was mixed with ribonucleotides at a concentration of 5 mM and an anti-reverse cap analog and mRNA was transcribed by a T7 polymerase within 2-3h at 37°C. GTP was used at a concentration of 1.5 mM to increase capping efficiency. To avoid excessive recognition of the mRNA by pattern recognition receptors, for some of the mRNA conditions pyrimidines in the IVT reaction were completely substituted. Uridine was substituted either by pseudouridine (ψ), n1-methyl-pseudouridine (m1ψ) or 5-methoxy-uridine (5moU). For some VEGF-mRNA conditions cytidine was replaced by 5-methyl cytidine (5mC; all from Jena Bioscience, Jena, Germany). No post-transcriptional polyadenylation was necessary because the sequence for 128(A) was included in the DNA template. DNA was removed by DNaseI treatment for 20 min and all transcripts were precipitated with lithium chloride overnight at −20°C (Thermo Fisher). Upon centrifugation at 18,000 × g at 4°C for 30 min, IVT products were washed with 70% EtOH, and the air-dried pellets were then resuspended in sterile nuclease-free water. mRNA concentration was adjusted to 1 mg/ml using UV/Vis-spectroscopy (NanoDrop 1000; Peqlab, Erlangen, Germany).

Table 2: Coding sequences for enhanced GFP and VEGF, own representation

Name	Coding sequence	Source
enhanced GFP	ATGGTGAGCAAGGGCGAGGAGCTGTTCACCGGGGTGGTGCCCATCCTGGTCGAGC TGGACGGCGACGTAAACGGCCACAAGTTCAGCGTGTCCGGCGAGGGCGAGGGCG ATGCCACCTACGGCAAGCTGACCCTGAAGTTCATCTGCACCACCGGCAAGCTGCCC GTGCCCTGGCCCACCCTCGTGACCACCCTGACCTACGGCGTGCAGTGCTTCAGCC GCTACCCCGACCACATGAAGCAGCACGACTTCTTCAAGTCCGCCATGCCCGAAGG CTACGTCCAGGAGCGCACCATCTTCTTCAAGGACGACGGCAACTACAAGACCCGC GCCGAGGTGAAGTTCGAGGGCGACACCCTGGTGAACCGCATCGAGCTGAAGGGCA TCGACTTCAAGGAGGACGGCAACATCCTGGGGCACAAGCTGGAGTACAACTACAAC AGCCACAACGTCTATATCATGGCCGACAAGCAGAAGAACGGCATCAAGGTGAACTT CAAGATCCGCCACAACATCGAGGACGGCAGCGTGCAGCTCGCCGACCACTACCAG CAGAACACCCCCATCGGCGACGGCCCCGTGCTGCTGCCCGACAACCACTACCTGA GCACCCAGTCCGCCCTGAGCAAAGACCCCAACGAGAAGCGCGATCACATGGTCCT GCTGGAGTTCGTGACCGCCGCCGGGATCACTCTCGGCATGGACGAGCTGTACAAG TAA	GenBank: MN989412.1 (https://www.ncbi.nlm.nih.gov/nuccore/MN989412); [31]
human VEGF-A isoform 165	ATGAACTTTCTGCTGTCTTGGGTGCATTGGAGCCTTGCCTTGCTGCTCTACCTCCAC CATGCCAAGTGGTCCCAGGCTGCACCCATGGCAGAAGGAGGAGGGCAGAATCATC ACGAAGTGGTGAAGTTCATGGATGTCTATCAGCGCAGCTACTGCCATCCAATCGAG ACCCTGGTGGACATCTTCCAGGAGTACCCTGATGAGATCGAGTACATCTTCAAGCC ATCCTGTGTGCCCCTGATGCGATGCGGGGGCTGCTGCAATGACGAGGGCCTGGAG TGTGTGCCCACTGAGGAGTCCAACATCACCATGCAGATTATGCGGATCAAACCTCA CCAAGGCCAGCACATAGGAGAGATGAGCTTCCTACAGCACAACAAATGTGAATGCA GACCAAAGAAAGATAGAGCAAGACAAGAAAATCCCTGTGGGCCTTGCTCAGAGCGG AGAAAGCATTTGTTTGTACAAGATCCGCAGACGTGTAAATGTTCCTGCAAAAACACA GACTCGCGTTGCAAGGCGAGGCAGCTTGAGTTAAACGAACGTACTTGCAGATGTGA CAAGCCGAGGCGGTGA	GenBank: AB021221.1 (https://www.ncbi.nlm.nih.gov/nuccore/4996350); [32] ; [33]

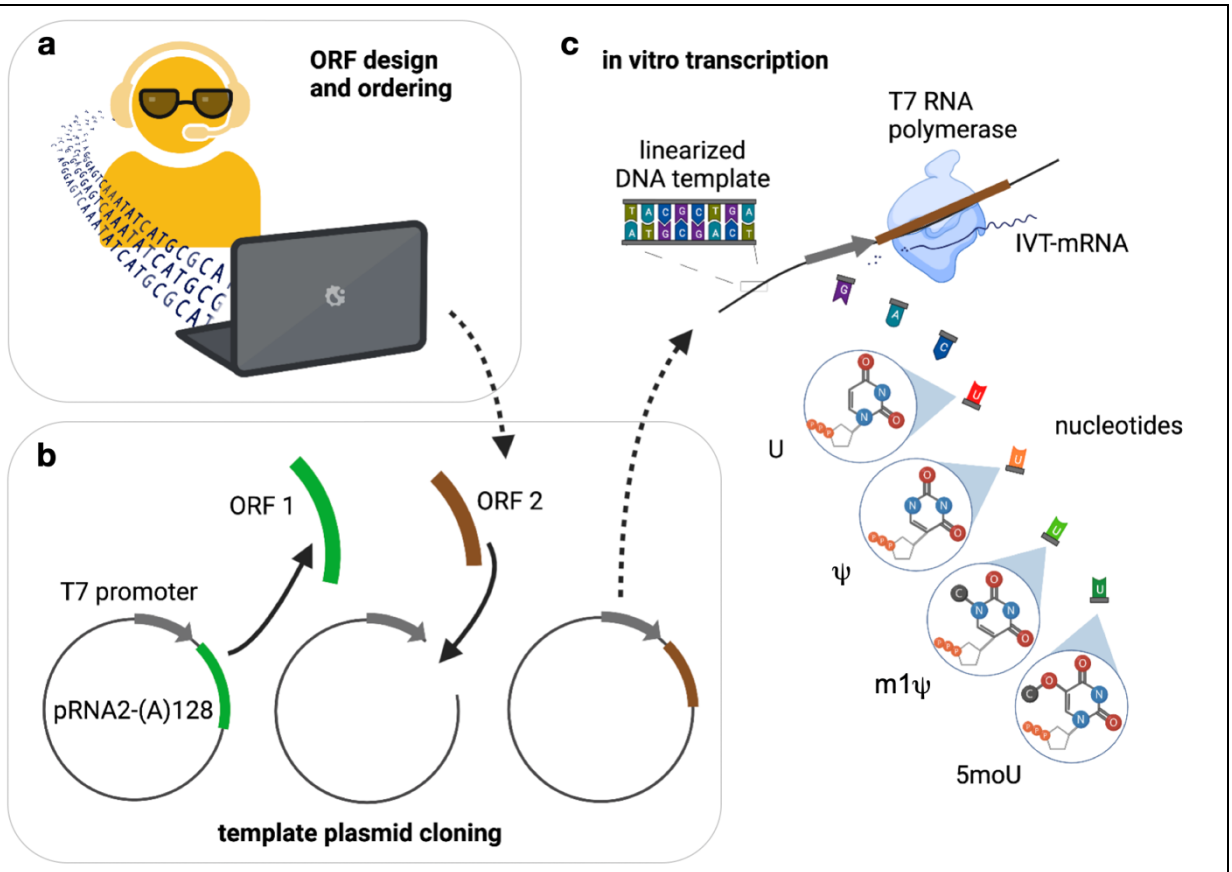

Figure 3: mRNA synthesis process, own representation

(a) First, the coding sequence or open reading frame (ORF) is designed in silico and the DNA sequence, flanked by restriction sites, is ordered. (b) The new ORF is cloned into the template vector containing a T7 promoter. (c) The DNA template is then linearized and used for in vitro transcription: A T7 polymerase transcribes the IVT-mRNA from the template sequence, incorporating the provided nucleotides and a 5' cap (not shown). Nucleotides can be chemically modified derivates of uridine, such as pseudouridine (ψ), n1-methyl-pseudouridine (m1ψ) or 5-methoxy-uridine (5moU), or the cytidine derivate 5-methyl cytidine (not shown).

2.3.2 mRNA transfection

For mRNA transfection, MSCs were cultured until ~80-95% confluence and at least for 24h before adding mRNA. mRNA was complexed with Lipofectamine MessengerMAX (LF; Thermo Fischer) at a ratio of 0.5mg mRNA/ ml LF. First, LF was diluted in OptiMEM (Thermo Fischer) according to manufacturer's instructions, vortexed and incubated at RT for 10min. Then, mRNA diluted in the same volume of OptiMEM was added gently and incubated at RT for another 5-10min. The mRNA-lipoplex solution was added dropwise to culture wells. Untransfected cells or cells to which only OptiMEM and LF was added

were included as control groups. A series of mRNA concentrations was tested for expression and cell toxicity and a concentration of 125ng mRNA/ cm^2 was selected for experiments, unless indicated otherwise (Fig 4).

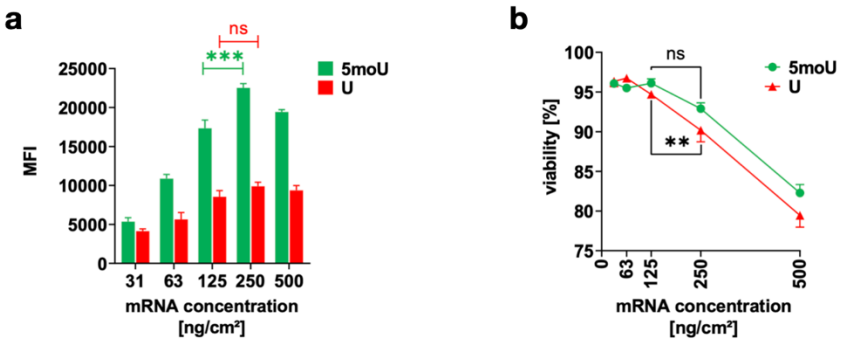

Figure 4: mRNA dose response, from *Drzeniek et al. 2023 [34]*

(a) Mean fluorescence intensity of MSCs transfected with different doses of GFP-mRNA per culture area. (b) Viability of MSCs transfected with different doses of GFP-mRNA per culture area, as measured by DAPI staining and flow cytometry. Both n = 4, two-way ANOVA. **p < 0.01; ***p < 0.001; ns = not significant. Error bars: SEM.

2.3.3 Evaluation of transfection efficiency, GFP expression and cell viability

GFP transfected cells were observed using a Nikon Eclipse Ti fluorescence microscope (Nikon Instruments Inc., Tokyo, Japan) at different time points post-transfection. To quantify fluorescence and cell viability, cells were detached, resuspended in PBS, stained with DAPI (1:1000) and analyzed using flow cytometry (MACSQuant VYB; Miltenyi Biotec, Bergisch Gladbach, Germany). Flow cytometry data was analyzed with FlowJo V10 using the gating strategy depicted in Fig 5. First, forward scatter (FSC) was plotted against side scatter (SSC), then doublets were excluded by plotting FSC-area against FSC-height (FSC-A, FSC-H). Dead cells were identified using a $DAPI^+$ negative control and within the live population, GFP^+ cells quantified in relation to untransfected cells.

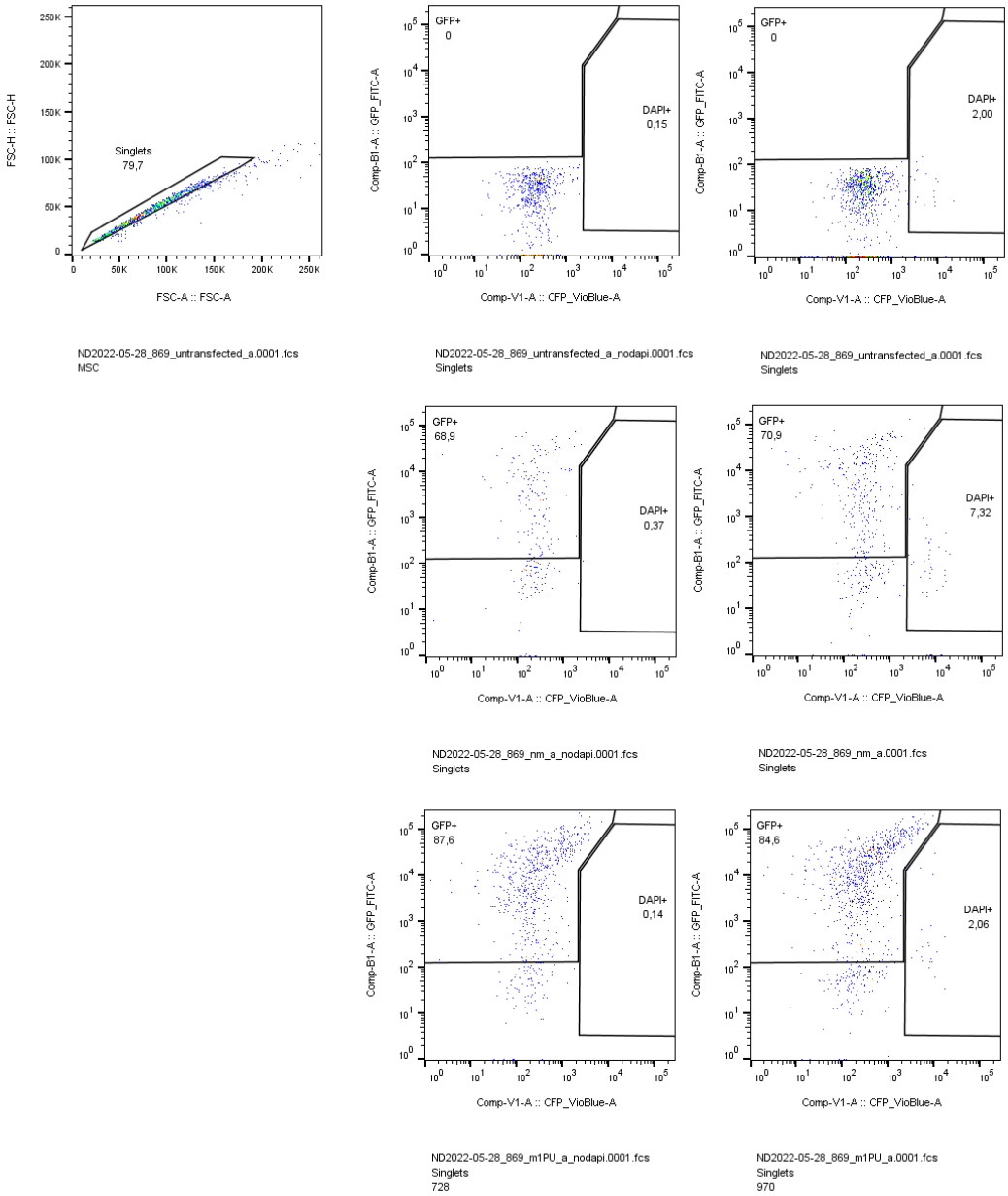

Figure 5: Exemplary flow cytometry gating strategy, from *Drzeniek et al. 2023 [34] supplementary data*

MSCs were stained with DAPI (1:1000) prior to measurement. Cells were gated for single cells, then for $DAPI^+$ (V1-A channel) and for GFP^+ (B1-A) channel. Gates for GFP^+ and $DAPI^+$ populations were placed based on negative controls: untransfected cells and unstained ("nodapi") cells respectively. Differences in GFP expression intensity can be observed between the three exemplary conditions: untransfected MSCs; "nm" = transfected with unmodified mRNA; "m1PU" = transfected with n1-methyl-pseudouridine mRNA.

VEGF expression was quantified by measuring cell-secreted VEGF in culture supernatants, as described below. To assess how mRNA-lipoplex incubation time reduced transfection efficacy of exposed cells, the mRNA-lipoplexes were removed at the indicated timepoints with two additional washing steps using warm medium, ensuring complete removal of the mRNA. GFP expression was quantified 24 h after the lipoplexes were added.

2.3.4 Metabolic activity and caspase activity of transfected cells

Metabolic activity of MSCs was quantified using the resazurin-based PrestoBlue cell viability kit (Thermo Fisher) on days 0, 1 and 5 post mRNA-transfection. Cells were incubated in a 1:10 ratio of reagent : culture medium at 37 °C. After 1h fluorescence was measured using a fluorescent plate reader (Tecan, Männedorf, Switzerland).
Activity of caspases 3 and 7 was measured using the Caspase-Glo 3/7 kit for 2D culture (Promega, Madison, WI). Cells were incubated in a 1:2 mix of reagent and culture medium for 1 h at room temperature (RT). The reagent mix was transferred to an appropriate imaging plate and luminescence was measured with a GloMax luminometer (Promega). Because this method is also affected by absolute cell count / well which could vary slightly between experiments, activity was expressed relative to the value obtained for the untreated control group.

2.4 Protein detection

2.4.1 ELISA

Cell culture supernatants were collected from MSC culture at different timepoints post-transfection and MSC-conditioned media were stored at −80 °C until analysis. Unconditioned but fully supplemented culture media samples from the same respective experiments were also stored and used as a blank or negative control. Hepatocyte growth factor (HGF), vascular endothelial growth factor (VEGF) and interferon-β (IFN-β) secreted by MSCs were quantified using enzyme-linked immunosorbent assays (ELISA; all R&D Systems, Minneapolis, MN) according to the manufacturer's instructions.

2.4.2 Secretome profiling

To understand changes in the paracrine activity of MSCs in response to different hydrogels or to different mRNA chemistry, concentrations of 266 proteins in the MSC culture supernatant were measured using an Olink Target 96 proximity extension assay (Olink

Bioscience, Uppsala, Sweden). Cell culture supernatants were shipped on dry ice to Uppsala and measurements were carried out by the company. Details on this technology, including detection limits, validation data and reproducibility can be found on the company's website (www.olink.com/downloads). Briefly, samples are mixed with a proprietary mix of cytokine-specific antibodies barcoded with DNA oligonucleotides. When two distinct specific antibody probes bind an analyte, the DNA barcodes anneal via complementary sequences. This forms the basis for an amplicon which is then quantified by RT-PCR. Measurement results were received as relative concentration values, expressed in normalized protein expression (NPX) units. An analyte was considered detected if more than three samples in any group had NPX values exceeding its limit of detection (LOD). The latter was defined as the larger of either the LOD defined by the manufacturer or the LOD estimated from our own negative controls (blank medium measurements) plus three standard deviations. Analyses were performed using R version 4.0.2 or 4.1.1. Heatmaps were generated with the ComplexHeatmap package. The assay was carried out in quadruplicates for Fig 7 and in triplicates for Fig 8. Two replicates were culture supernatants from the same cell donor and the third (and fourth) replicate was derived from cells of a different donor.

2.5 Statistical analysis and data visualization

Levels of statistical significance were set at $*p < 0.05$, $**p < 0.01$, $***p < 0.001$. Statistical analysis was carried out in GraphPad Prism 9.0 (GraphPad Software Inc., USA) and R version 4.0.2 or 4.1.1. One or two-way ANOVA with an appropriate post-hoc test or a mixed-effects analysis (if values were missing) was used to test for significant differences between groups (details in figure legends). Values are depicted as mean ± standard deviation (SD) or standard error of the mean (SEM), as indicated in figure legends. Schematics were created using Biorender.com.

3. Main results

I am showing data from two publications (Drzeniek et al. 2021 [13]) and Drzeniek et al. 2023 [34]) side by side. Taken out of context the figure items may differ slightly in their visual style and sometimes in the controls or comparisons used in the two respective studies. In some cases, I have changed the visualization of the data to better fit the overarching narrative of this dissertation and address research questions, which overarch both publications.

3.1 Photo-crosslinkable collagen-HA hydrogel supports viability and elongation of MSCs

A photo-crosslinkable hydrogel consisting of methacrylated type-I collagen and thiolated hyaluronic acid (Col-HA) was compared against a softer and a stiffness-matched variant of an industry standard gelatin-HA-PEG (Gel-HA soft and stiff) hydrogel kit [13] or against a hydrogel, where the thiolated HA was crosslinked by PEG-acrylate instead of methacrylated collagen [34] (Fig 2b; details in section 2 Materials & Methods). All hydrogels could be photo-crosslinked using UVA light and transitioned from an aqueous phase, in which cells could be resuspended and injected through a syringe, to a gel phase in which the hydrogel disk could be held with forceps (Fig 6a). Upon encapsulation and 3D culture, MSCs showed excellent viability in Col-HA for 10 days and slightly lower viability in all tested control hydrogels (Fig 6b). Only in Col-HA did the MSCs assume a stromal morphology and potentially establish cell-cell contacts. Elongation was usually observable from day 4 post-encapsulation, with variations between cell donors. In contrast, in the control hydrogels, the cells remained round and isolated (Fig 6c).

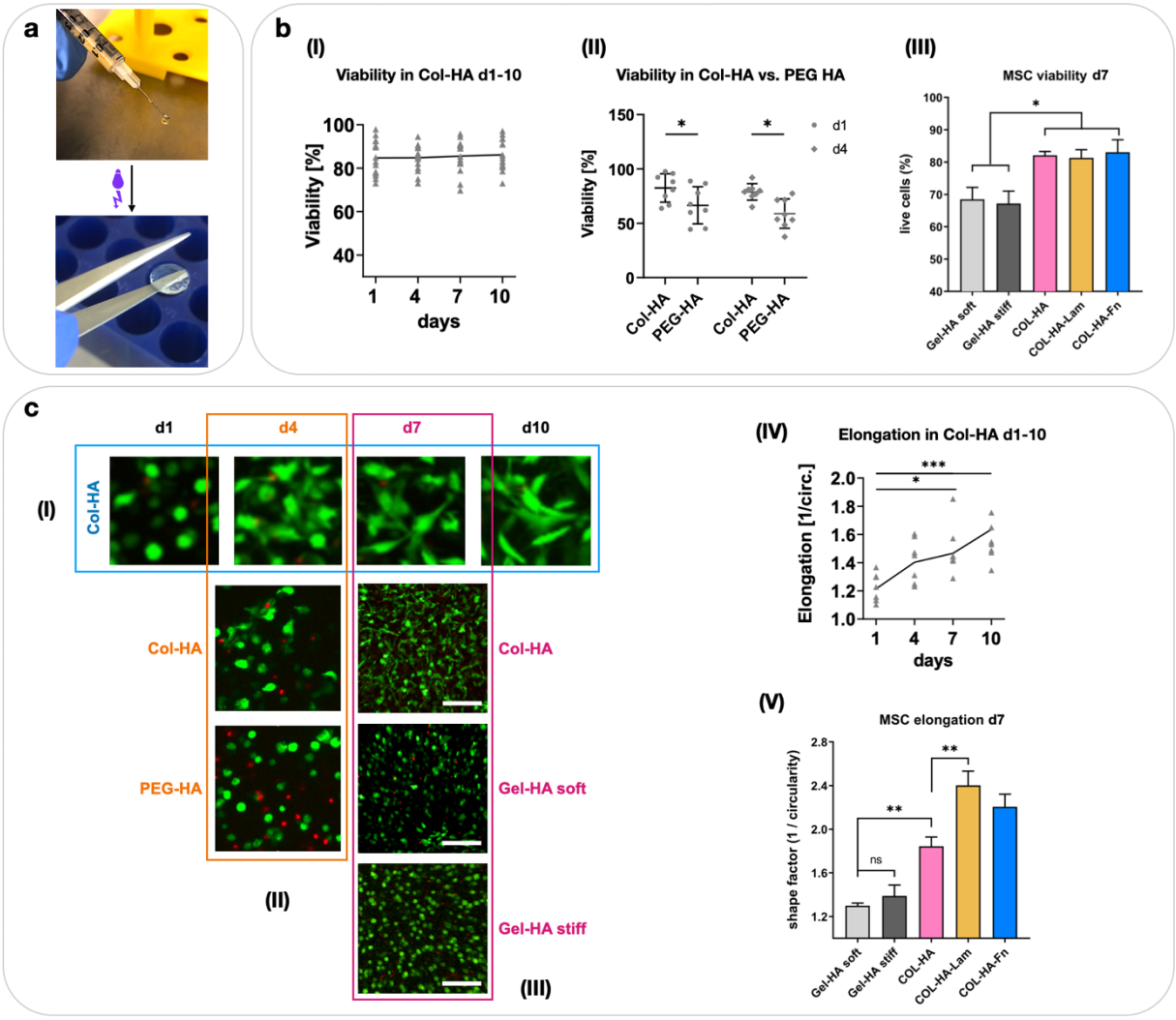

Figure 6: The Col-HA hydrogel promotes viability and stromal morphology of MSCs, adapted from *Drzeniek et al. 2021 [13]* and *Drzeniek et al. 2023 [34]*

(a) Pictures of Col-HA before and after crosslinking. (b) MSC viability in Col-HA: (I) viability over 10 days post-encapsulation. n = 16. (II) viability in Col-HA vs. PEG-HA on days 1 and 4. n=8, two-way ANOVA. (III) viability in different hydrogel conditions on day 7. n ≥ 3, one-way ANOVA. (c) MSC morphology in hydrogels across different projects: longitudinal observation of MSC morphology in Col-HA (I, blue frame). MSC morphology on day 4 in Col-HA vs. PEG-HA (II, orange frame). Morphology on day 7 in Col-HA vs. Gel-HA soft (= conventional HyStem protocol) and Gel-HA stiff (= stiffness matches Col-HA; III, magenta frame). Green = calcein AM in (I, III) or GFP in (II), red = ethidium homodimer. Scale bar = 250 µm, picture fragments = 200 µm. (IV) quantified elongation of MSCs over 10 days. n = 8, two-way ANOVA. (V) quantified elongation in different hydrogels. n ≥ 3, one-way ANOVA. *p < 0.05; **p < 0.01; ***p < 0.001; ns = not significant. Error bars: SEM. *Items b (I), (II), c (II), (IV) data from Drzeniek et al. 2023*

[34]. Items a, b (III), c (III), (V) from Drzeniek et al. 2021 [13]; c (I) modified from Drzeniek et al. 2023 [34].

3.2 Encapsulation in Col-HA hydrogel expands the MSC secretome in an adhesion-sensitive manner

Seven days after encapsulation and 3D culture, MSCs in the Col-HA hydrogels secreted increased levels of several proteins compared to MSCs cultured on tissue culture plastic (TCP) or in Gel-HA with lower (soft) or matched (stiff) bulk stiffness (Fig 7a). These proteins included angiogenic, neuro-regenerative and immune modulatory mediators. The secretome of MSCs in Gel-HA soft showed more similarity with the Col-HA group than with the 2D TCP group. Functionalization of the collagen-HA gel with a small amount of thiolated laminin or fibronectin did not result in any qualitative changes in the secretome pattern of encapsulated MSCs.

To elucidate the temporal aspect of the observed effects, MSCs were cultured in Col-HA for 10 days and the secretion of two surrogate markers, HGF and VEGF, was measured on days 1, 4, 7 and 10 (Fig 7b). HGF secretion increased within the first 4 days and remained above initial levels for the remaining days. Interestingly, VEGF levels did not significantly change throughout the observation period.

To investigate whether the effects of collagen-HA were dependent on the presence of integrin motifs for cell adhesion, PEG-HA was used as a control hydrogel which provides a 3D culture environment but no integrin ligands, instead of the gelatin-containing Gel-HA. MSCs were cultured in both hydrogels side by side and the levels of VEGF and HGF were measured on 4 consecutive days (Fig 7c). Again, VEGF levels remained constant but were higher in the collagen-HA group. HGF levels in the collagen-HA group showed a steady increase over 4 days as observed before. In the PEG-HA group, an increase in HGF secretion was also present, albeit much lower than for Col-HA.

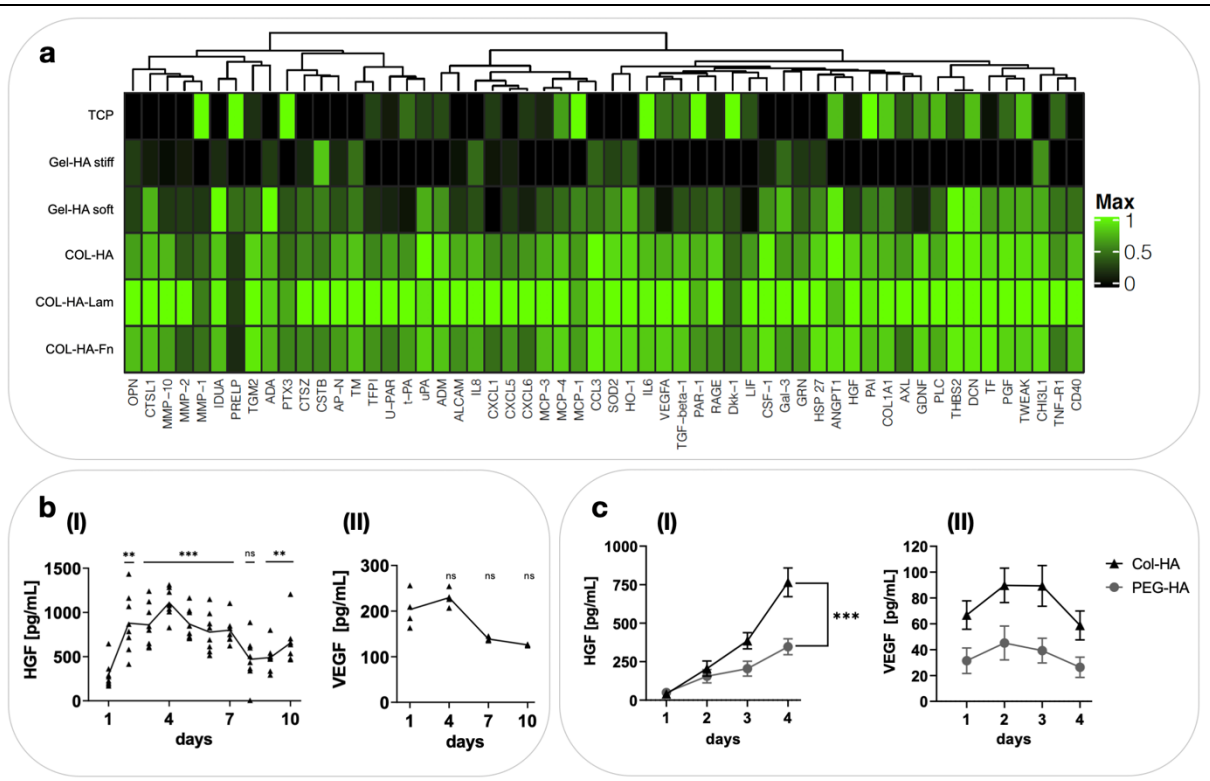

Figure 7: The Col-HA hydrogel promotes growth factor secretion from MSCs, adapted from *Drzeniek et al. 2021 [13]* and *Drzeniek et al. 2023 [34]*

(a) Secretome profiles of MSCs cultured in Col-HA versus other conditions. Analysis includes proteins related to angiogenesis, neuroprotection/regeneration, immune response, homeostasis and ECM remodeling. The color brightness indicates the relative concentration of an analyte in an experimental group, compared to the mean value for this analyte across all groups. n=4. (b) Longitudinal measurement of HGF (I) and VEGF (II) secretion from MSCs cultured in Col-HA. n = 8 and 4 respectively, repeated measures one-way ANOVA. Significance shown in relation to d1. (c) Secretion of HGF (I) and VEGF (II) in Col-HA (black triangles; cell adhesion) versus PEG-HA (grey circles; no cell adhesion) at early timepoints post-encapsulation. n = 12 and 11 respectively, two-way ANOVA. **p < 0.01; ***p < 0.001; ns = not significant. Error bars: SEM. *Item a from Drzeniek et al. 2021 [13]. Items b and c altered representation based on data from Drzeniek et al. 2023 [34].*

3.3 Chemical nucleotide modification in IVT-mRNA affects expression kinetics and cell viability

IVT-mRNA coding for GFP was transcribed in vitro using uridine (U) or substituting it with pseudouridine (ψ), n1-methyl-pseudouridine (m1ψ) or 5-methoxy-uridine (5moU). Transfection of MSCs resulted in high transfection efficacy for all mRNAs. However, cell fluorescence intensity (MFI) and kinetics thereof were different between mRNA groups (Fig 8a). ψ-mRNA was not significantly different from U and both groups showed a rapid decline in GFP signal after peak fluorescence at day 1. m1ψ-MRNA yielded the highest peak fluorescence, which also declined rapidly. 5moU-mRNA yielded slightly lower initial fluorescence than m1ψ but maintained the highest GFP signal at days 4 and 7 post-transfection, resulting in a different expression kinetic than all other groups.
IVT-mRNA did not affect cell viability, except U-mRNA. This was also reflected in caspase activity, which was only elevated in U-mRNA-transfected MSCs but became elevated also for ψ-mRNA at a 4-fold higher mRNA dose (Fig 8b). Proliferation was impaired in U- and ψ-mRNA groups but not in m1ψ- and 5moU, as quantified by change in mitochondrial metabolic activity (Fig 8c).

3.4 Replacement of uridine with 5moU reduces the immune response triggered by IVT-mRNA and its side effects on MSC paracrine activity

The anti-viral mediator interferon-β (IFN-β) was secreted in high amounts by U-mRNA transfected MSCs and was detectable in all other mRNA groups except for 5moU-mRNA (Fig 8d), implicating an innate immune response against those IVT-mRNAs. To understand the consequences of this immune response on therapeutically relevant functions of MSCs, changes in the paracrine response in cells transfected with U-mRNA versus 5moU-mRNA were investigated (Fig 8e). U-mRNA transfected cells secreted higher levels of pro-inflammatory cytokines and eukaryotic translation initiation factor 4E-binding protein 1 (4E-BP1) compared to untreated cells. Pro-angiogenic growth factors like VEGF, HGF or angiopoietin 1 (ANGPT1) were secreted less from U-mRNA transfected MSCs. 5moU-mRNA transfected cells clustered with untreated cells and did not show any discernible secretome pattern shifts.

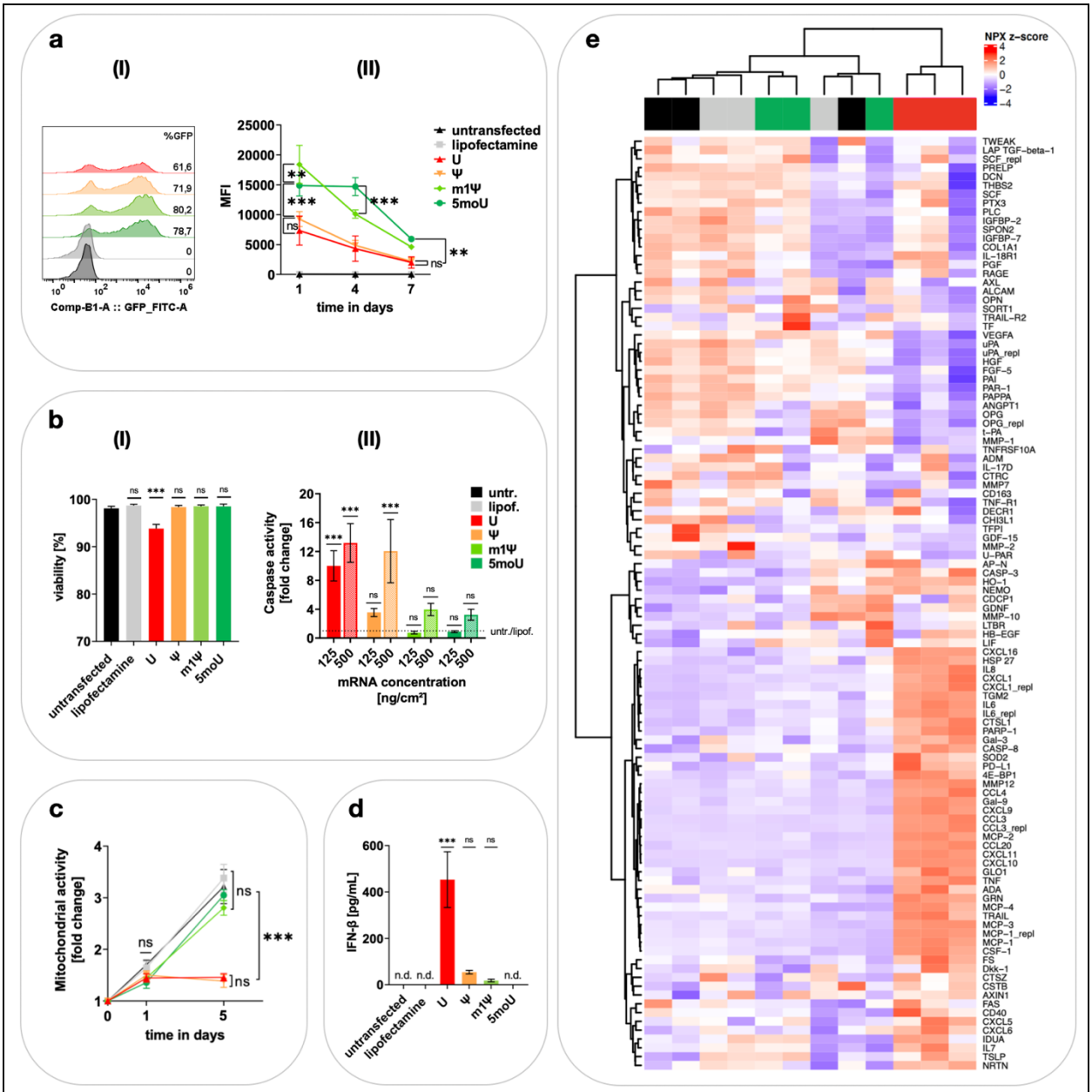

Figure 8: Nucleotide-modification of mRNA prolongs expression and minimizes cellular immune response, from *Drzeniek et al. 2023 [34]*

(a) Transfection efficacy (I) and fluorescence intensity (II) after transfection of MSCs with differently nucleotide-modified GFP mRNA. n = 4, two-way ANOVA. (b) Cell viability measured by DAPI staining and flow cytometry (I) and caspase activity (II) after transfection of MSCs with differently uridine-modified mRNA. n = 4 and 6 respectively, one-way ANOVA. Significance shown in relation to untransfected. (c) Changes in metabolic activity of MSCs. n = 4, two-way ANOVA. Significance shown in relation to day 0, unless indicated otherwise. (d) Interferon-β secretion 24h post-transfection. n=4, one-way ANOVA. (e) Semiquantitative array of MSC-secreted factors at 24h. The color red (=high) or blue (=low) indicates the relative concentration of an analyte in a sample, compared to the mean value for this analyte across all samples. n=3

per group. Symbols and color code in (a II) relate to all items in this figure. **p < 0.01; ***p < 0.001; ns = not significant, n.d. = not detected. Error bars: SEM.

3.5 Cell-material interactions are not affected by transfection with modified IVT-mRNA

To investigate whether the material-mediated effects on MSCs (3.1., 3.2.) are affected by mRNA-transfection, the phenotype of transfected and untransfected cells encapsulated in Col-HA was compared. VEGF-mRNA modified with 5moU and 5mC nucleotides was used as an "immuno-engineered" mRNA (IE-mRNA), while U and C containing mRNA (U-mRNA) was included as a control.

MSCs could be detached and encapsulated as early as 1h post-transfection. This short incubation with mRNA was sufficient to preserve an acceptable transfection efficacy of > 33% (Fig 9a). Cell viability in Col-HA was not affected by transfection with IE-mRNA, although caspase activity was slightly higher compared to untransfected cells. U-mRNA transfected cells did not tolerate encapsulation, as viability was < 50% and caspase activity was increased > 10-fold (Fig 9b). Morphology and elongation of live cells was not affected by any mRNA (Fig 9c). U-mRNA treated cells secreted barely detectable levels of HGF. Adhesion-sensitive increase in HGF secretion was comparable between IE-mRNA transfected cells and untreated cells. Both groups responded very similarly to culture in Col-HA versus PEG-HA (Fig 9d).

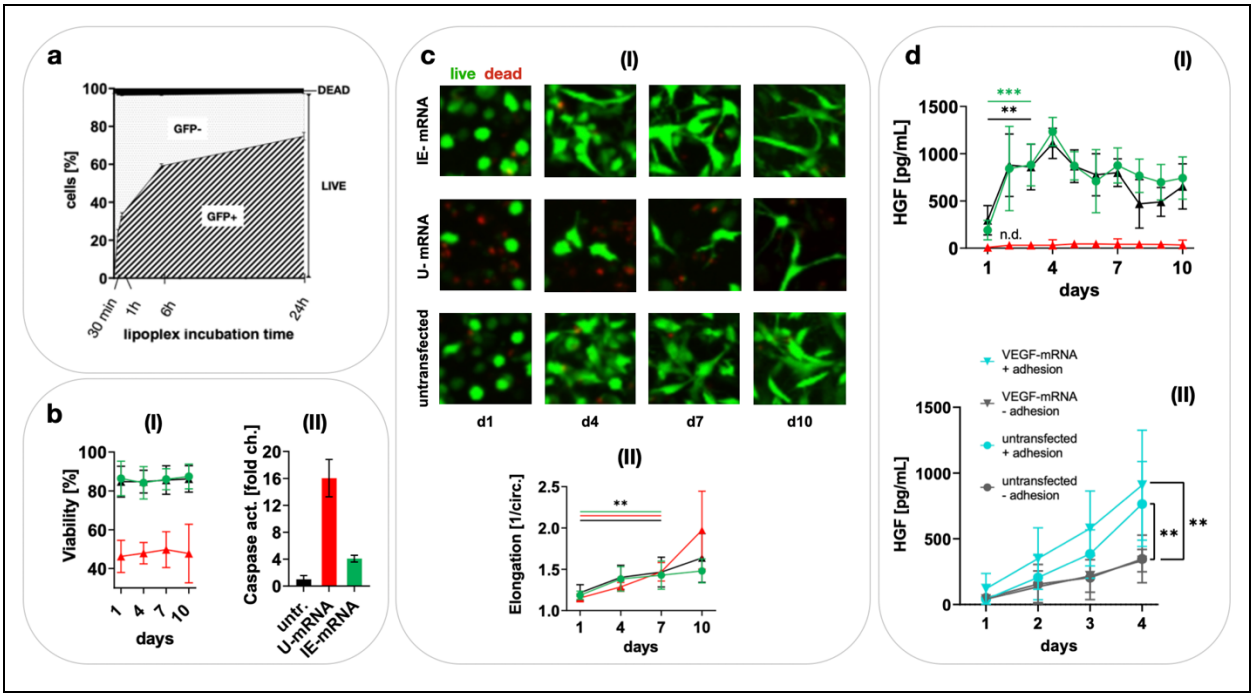

Figure 9: mRNA transfection can be combined with hydrogel encapsulation without disturbing cell-material interactions, from *Drzeniek et al. 2023 [34]*

(a) Relationship between transfection efficacy and incubation time of mRNA lipoplexes on MSC layer. n = 4. (b) Cell viability (I) and caspase Morphology (I) and quantified elongation (II) of mRNA-transfected and untransfected MSCs in Col-HA. n = 4, mixed effect analysis. Significance shown in relation to day 1. n = 8. (d) HGF activity (II) of mRNA-transfected and untransfected MSCs in Col-HA. n = 16 and 10 respectively. (c) secretion in Col-HA (I) or Col-HA versus PEG-HA (II) from untransfected versus mRNA-transfected cells. Teal and grey colors represent Col-HA and PEG-HA respectively. n = 8 and 12 respectively, two-way ANOVA. Color code in (b II) relates to all items in this figure, if applicable: untransfected = black triangles, U-mRNA = red triangles, IE-mRNA = green circles. **p < 0.01; ***p < 0.001. n.d. not detected. Error bars: SD. *Item a published as supplementary material to Drzeniek et al. 2023 [34].*

3.6 Secretion of IVT-mRNA encoded protein is modulated by cell-material interactions

Next, it was investigated whether the expression or secretion of IVT-mRNA-encoded protein is affected by different biomaterial microenvironments. MSCs transfected with GFP-mRNA and cultured in Col-HA versus PEG-HA did not show any observable difference in fluorescence intensity, implicating that protein expression per se was not sensitive to cell adhesion (Fig 10a).

To evaluate the influence of cell adhesion on protein secretion, MSCs were transfected with the unmodified or immuno-engineered VEGF-mRNA, encapsulated in Col-HA after 1h and cultured for 10 days. Increased levels of VEGF were secreted from IE-mRNA transfected cells for 8 days, but secretion kinetics were not qualitatively different from MSCs in TCP culture (Fig 10b). However, in direct comparison with the PEG-HA control hydrogel which lacks integrin adhesion motifs, VEGF secretion from VEGF-transfected cells was 4-fold higher in Col-HA (Fig 10c).

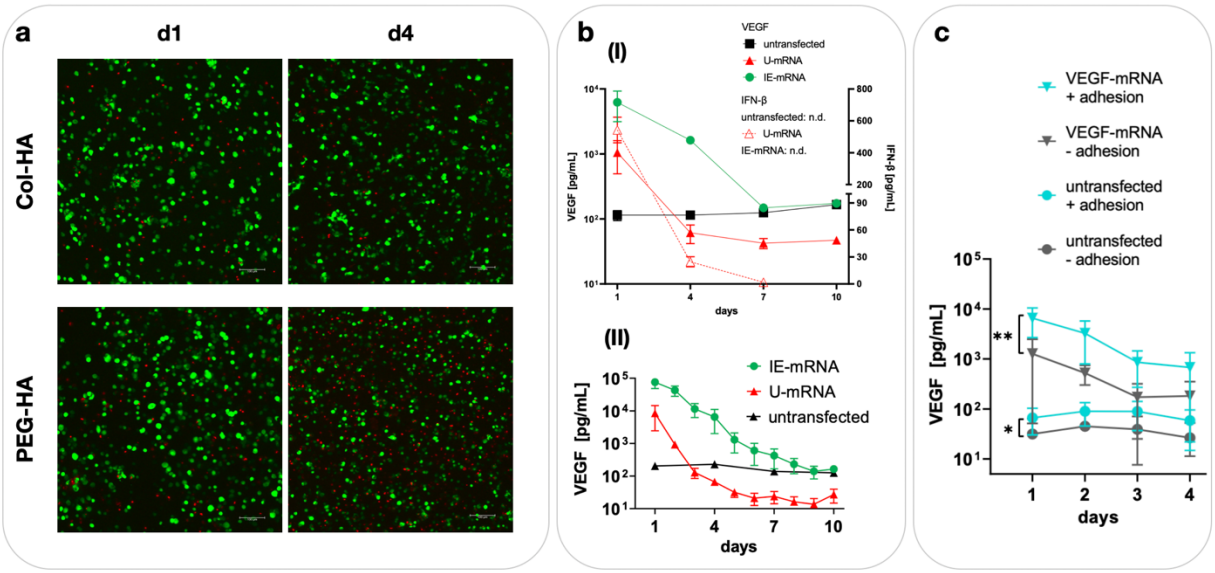

Figure 10: Cell-material interactions increase the secretion of mRNA-encoded growth factor, from *Drzeniek et al. 2023 [34]*

(a) GFP fluorescence of mRNA-transfected cells in Col-HA vs PEG-HA. (b) Comparison of VEGF secretion kinetics from VEGF-mRNA transfected MSCs cultured on TCP (I) versus in Col-HA (II). n = 4. (c). Secretion of naturally transcribed (circles) and IVT-mRNA-encoded (triangles) VEGF in Col-HA (teal) versus PEG-HA (grey). n = 11, two-way ANOVA. *p<0.05; **p < 0.01, n.d. not detected. Error bars: SD. *Item a only published as supplementary material to Drzeniek et al. 2023 [34].*

4. Discussion and conclusion

To discuss the results presented within my thesis and the two publications it is based upon, I chose the plural form i.e., "our results" or "we measured" in recognition of the team effort behind each project. My contributions to the publications are specified below and in the publications themselves.

4.1 Interpretation

In this thesis I have investigated two methods of cell engineering: cell-material-interactions and transient gene expression in MSCs as a model system for multimodal control of cellular phenotype.

MSCs were cultured in different biopolymer hydrogels to investigate whether the Col-HA hydrogel would induce a different cellular phenotype compared to a commercially available standard 3D culture hydrogel composed of gelatin, HA and PEG (Gel-HA soft). Initially, we observed that MSCs in the Col-HA hydrogel had slightly higher viability and elongated faster and stronger than in Gel-HA (Fig 6). Based on my colleagues' previous work [17], I hypothesized that stronger elongation in Col-HA would correlate with stronger growth factor secretion. This was was confirmed (Fig 7a), although the differences between MSCs in hydrogels versus on tissue culture plastic were more pronounced than differences between Col-HA and Gel-HA soft. Surprisingly, the stiffness-matched control Gel-HA stiff resulted in the lowest growth factor secretion among all groups (Fig 7a), which suggests that the effects of Col-HA compared to Gel-HA soft did not stem primarily from a difference in bulk modulus. It could also mean that the higher proportion of bioinert PEG component in Gel-HA stiff impaired cell-material interactions. Here we saw an advantageous feature of Col-HA, which consists of functionalized collagen and HA and does not require any additional components for photo-crosslinking.

To follow up on the relationship between cell morphology and secretome, in our second study (Drzeniek et al. 2023 [34]), we measured HGF and VEGF as surrogate markers for the proangiogenic secretome over the course of 10 days and compared with the cell elongation which occurred over time in Col-HA. While HGF secretion increased within the first 4 days post-encapsulation as cells elongated, to our surprise VEGF did not show any increase over time (Fig 7b) but was higher in Col-HA than in PEG-HA already on d1 (Fig

7c). This suggests that while HGF secretion seems to be indeed dependent on cell elongation or on cell-cell contacts forming as a consequence of this elongation, VEGF secretion is rather sensitive to cell-matrix adhesion, which occurs within the first 24h.

The material-mediated secretome shifts we observed were of a rather broad nature and we were interested in overexpressing a selected key factor using mRNA to shape the MSC secretome in a more defined direction, such as VEGF for angiogenesis. Transfection of MSCs using mRNA complexed with Lipofectamine yielded >60% transfected cells and a cell viability >90% (Fig 8a, b) 24h post-transfection. Because the short expression window of unmodified IVT-mRNA and the cellular immune response it triggers upon recognition pose critical limitations to its application, we used three different uridine derivates to fully replace uridine in the IVT process and observed an increased or prolonged GFP expression and reduced anti-viral interferon response for m1ψ and 5moU compared to U-containing mRNA (Fig 8a, d). We were interested in how this would be reflected in the MSC paracrine profile. Secretome measurement and our subsequent analysis revealed that U-mRNA stimulated the secretion of pro-inflammatory mediators and reduced the secretion of pro-angiogenic growth factors. 5moU-mRNA transfected MSCs clustered with untransfected controls, showing a minimal footprint of the IVT-mRNA on cellular function and phenotype (Fig 8e). The fact that the translation repressor 4E-BP1 was upregulated in U-mRNA transfected cells could represent a mechanistic link between the anti-viral response and the reduced production of growth factors and of mRNA-encoded protein. The results obtained with GFP-mRNA were confirmed using VEGF-encoding mRNA (in Drzeniek et al. 2023 [34], not shown here) and demonstrate that the cellular responses triggered by IVT-mRNA with different nucleotide chemistries are comparable between different sequences and represent an additional level of cell modulation, which can be uncoupled from the mRNA's protein coding function.

Having identified 5moU-mRNA as a low-footprint tool for gene overexpression, we sought to combine the selective overexpression of VEGF with the material-mediated pro-angiogenic secretome stimulation of Col-HA. We observed a moderate increase in caspase activity but no reduction of live:dead cell ratio or of elongation in encapsulated 5moU-mRNA transfected cells (Fig 9b,c). Natural HGF secretion was also comparable to and followed a similar kinetic as for untransfected cells (Fig 9d). In contrast, U-mRNA transfected cells showed poor viability <50% and minimal HGF secretion after encapsulation, implicating that U-mRNA reduced the cells' resilience and ability to adapt to a new microenvironment. However, viable cells in the U-mRNA group elongated strongly (Fig. 9c).

Given the low transfection rate of <40% after 1h of mRNA exposure (Fig 9a) and the barely detectable HGF secretion it is probable that those cells within the U-mRNA treated samples which elongated were not transfected, while most of the cells which were really transfected died. Together these results indicate that only minimally immunogenic mRNA can be used as a building block in tissue engineering, as it does not negatively impact cell viability and cell-material interactions.

Conversely, we were curious if the cell-material-interactions would impact the mRNA expression of VEGF. In Col-HA, VEGF secretion from 5moU-mRNA transfected MSCs remained above baseline levels for 8 days, displaying a very similar kinetic to transfected MSCs on culture plastic (Fig 10b), which means that the Col-HA gel did not qualitatively change the expression kinetics. However, a quantitative increase in VEGF-secretion was revealed when Gel-HA was compared against the PEG-HA control. This shows that the presence of integrin adhesion motifs increases the secretion of VEGF, regardless of whether it is naturally expressed or overexpressed at the mRNA level. Because fluorescence levels of GFP transfected MSCs in both hydrogels were comparable (Fig 10a), we conclude that secretion, but not translation of mRNA-encoded protein is affected by the substrate.

The combination of biomaterial encapsulation and mRNA transfection is synergistic, insofar as the mRNA sequence determines precisely which protein is to be overexpressed, while the material composition determines how much of that protein is secreted and what other proteins are also secreted by the cells, thereby possible resulting in additional synergisms on a bioactivity level. This finding also has implications for locally administered mRNA drugs in general, the effect of which would be modulated by the microenvironment of the transfected cells.

4.2 Comparison to other studies

Many published studies investigate secretome engineering of MSCs using biomaterials, as reviewed by Wechsler et al [2]. Previous work in this direction conducted by colleagues at our institute revealed that an important advantage of a lyophilized, RGD-functionalized alginate scaffold, compared to a hydrogel of the same biochemical composition, was the stronger facilitation of MSC elongation and cell-cell contact formation in the scaffold. This resulted in stronger paracrine activity compared to the alginate hydrogel, in which the MSCs remained round and isolated [17], which is consistent with the key result of this

thesis, that in Col-HA, which promoted their elongation, MSCs secreted an expanded growth factor profile. In contrast to my colleagues' previous work, who had to implant their scaffold surgically, all hydrogels used in my thesis projects are injectable and easy to mix homogenously with MSCs by pipetting, while still providing an environment which promotes MSC adhesion, elongation, and augmented growth factor secretion.

The favorable effect of type-I collagen on MSC growth factor secretion has also been recently demonstrated by Thomas et al [12]. They also showed that this effect was mediated by integrin receptors, which were upregulated on MSCs during culture in collagen. While we did not explicitly investigate the integrin-specificity behind our cell-material interactions, this mechanism would explain the differences in secretome pattern between hydrogels with versus without collagen. In contrast to Thomas et al. our collagen formulation is photo-crosslinkable and we compared it with other biopolymer hydrogels, such as gelatin-based and HA-based hydrogels to show that not any gel, but especially the collagen-I containing one, promotes strong secretion of regenerative growth factors.

A comparison between gelatin and collagen as culture substrates has also been carried out by Davidenko et al [11]. The authors proposed that although collagen and gelatin share the same amino acid sequence, their different tertiary structure results in different availability of RGD (on gelatin) versus GxOGER (on collagen) motifs, which engage different integrins respectively. Our comparison of collagen and gelatin-based hydrogels fits well with this model, although the mechanistic link between differences in secretome and differences in substrate integrin specificity alone was not entirely clarified in our study, as discussed below in the limitations section.

IVT-mRNA has been previously used in several other studies to overexpress selected genes in MSCs. Among those studies, the first and most influential one was published in 2013 by Levy and colleagues [29]. Here, IL-10 and a homing receptor were encoded as IVT-mRNA and introduced into MSCs. Although this study showed important proof of concept, it was conducted using early-stage mRNA technology and remained without follow up for many years. For instance, Levy et al. used ψ-modified mRNA, which performed only slightly better than unmodified mRNA in our experiments. In contrast, our study included the more recently proposed uridine derivates m1ψ [27] and 5moU [28], the former of which was used in Moderna's and BioNTech's SARS-CoV2 vaccines [35]. Importantly and in contrast to Levy et al., our study focused not only on demonstrating successful expression, but rather on characterizing the side effects that mRNA with different synthetic nucleotide chemistries can cause in transfected cells. As mRNA technology has

recently evolved into a new mature drug class with a variety of potential applications, such a focus on characterization and safety seemed of great translational importance to us.
Recently, there seems to be a growing appreciation for the concept that phenotypic plasticity of cell therapeutics and tissue engineered products can be harnessed most effectively by simultaneously controlling multiple levels of the complex information that a cell receives. The concept of multiplexing cell instructive cues for tighter control of cell function has been very recently suggested for cell therapies in a review article by Lim [36] and demonstrated also recently for tissue engineering by Kit-Anan et al., who have multiplexed topography or shape and mechanical cues to control the phenotype of cardiomyocytes, following a rational very similar to ours [37]. Multimodal cell-instructive strategies have also been extensively studied in a slightly different context for nerve guidance channel implants, where combinations of optimized adhesion molecules, channel microstructure, trophic and chemotactic molecules, as well as electrical stimulation or substrate conductivity are often required to effectively promote regeneration of axons in transected peripheral nerves [38]. Finally, the relationship between genetic engineering and cell culture substrate / microenvironment has been investigated in the past for DNA transfection [39, 40], but to the best of our knowledge we first explored it for state-of-the-art IVT mRNA transfection.

4.3 Strengths and limitations

A strength of this work is that the two publications build well upon one another and lead to many new questions, which would be exciting to address. The results from Drzeniek et al. 2023 [34] addressed questions posed by the initial comparison between Col-HA and the industry standard control gel in Drzeniek et al. 2021 [13], such as the temporal dynamics of growth factor upregulation or comparison with a gel completely devoid of integrin adhesion ligands, as stated above in section 4.1. However, the results obtained thus far, do not allow to pinpoint which specific (integrin) receptor mediates the effects observed for Col-HA, Gel-HA and PEG-HA. Nor can we say with certainty to which extent the differences observed between Col-HA and Gel-HA can be attributed to the different integrin specificity of type I collagen versus gelatin, as opposed to other possible variables such as PEG content, crosslinking mechanism or internal structure (cf 4.2).
Addressing these two questions would require for instance presenting recombinant integrin ligands, such as the RGD or GxOGER motifs in an otherwise neutral, bioinert and

consistent environment. The difficulty here is always to create biomaterial controls which are different in only one variable but truly identical in all other aspects such as biochemical composition, crosslinking mechanism, modulus, internal structure etc.

It should be noted that although PEG-HA hydrogel was used as a negative control for cell adhesion, some cell types, especially immune cells, can bind to HA through CD44 [41, 42]. However, HA is not an integrin ligand, and we did not observe any elongation of MSCs in PEG-HA, which is why we chose it as a negative control condition to study the relationship between elongation and growth factor secretion. The interaction through CD44 is especially important for immune cells and although a role for CD44 in MSC biology has been proposed in specific scenarios, such as engineered CD44 with altered ligand specificity or for CD44-expressing MSC cell lines [43-45], there is no strong consensus on the expression and the role of CD44 in primary human MSCs.

The concept of understanding and using the multiplicity of cell-instructive cues is quite general, but in this dissertation only one cell type was used to multiplex material effects with transfection. Further investigations with more cell types and better-defined receptor ligands would be necessary to build a systematic understanding of the cellular stimulome.

It should be noted that the concept proposed here is reductionist in nature and to what extent it can be used to understand emergent cellular behavior is debatable, although this critique could in principle be extended to most if not all mechanistic investigations in cell biology.

Finally, although this work was driven also by translational aims, we have not yet studied the therapeutic use of the proposed system. Col-HA has been developed here as a potential delivery vehicle for MSCs, yet its injectability has only been shown by passing it through a syringe and its in vivo performance has not been characterized to date. These steps, although very important, lie outside the scope of my dissertation.

4.4 Outlook

In the early days of regenerative medicine, a lot of hope was placed in simple, monofactorial approaches, such as the systemic administration of a single key growth factor. With a growing understanding of cellular self-organization, however, these approaches were updated with the notion that regenerative processes are orchestrated by spatiotemporal cascades of stimuli. Cell therapies play a central role in this concept as they are able to both dynamically adapt to their spatiotemporally specific microenvironment and

respond in a complex, multifactorial manner. It is this capability to integrate and sum different modalities of external stimuli and the hypothesized synergisms between said stimuli, which lie at the conceptual center of this work. Although a strongly simplified model was used here, the growing understanding of how cell biology can be controlled effectively through complementary techniques could lead to new categories of multifactorial therapies.

The mechanistic link between observed cell-material interactions and changes in cell phenotype could be further elucidated for example using chemically defined hydrogels with recombinant receptor ligands. Chemically defined hydrogels offer two advantages compared to the naturally derived hydrogel substrates used here: first, characterization and batch-to-batch consistency are far easier to control in chemically defined and recombinant components, which could be an advantage in clinical translation. Second, a reductionist investigation of selected, isolated cues can be implemented in a more controlled environment, as also discussed in 4.3.

An interesting follow-up would also be to investigate the suspected dependency of VEGF and HGF secretion on cell-matrix contact versus cell-cell contact respectively. We are currently investigating this by reducing the cell density in hydrogels and using anti-N-cadherin antibody to prevent cell-cell contact formation in Col-HA.

More classes of stimuli, such as topographical cues or electrical stimulation and additional readouts such as migration studies, transcriptomics and other omics could be investigated to form a generalized understanding of how the stimulome is processed by cells.

More classes of stimuli, such as topographical cues or electrical stimulation and additional readouts such as migration studies, transcriptomics and other omics could be investigated to form a generalized understanding of how the stimulome is processed by cells.

While this work has addressed some current limitations of mRNA drugs, important further development could include controlled-release strategies for mRNA transfection complexes to control their pharmacokinetics, in situ transfection with controlled biodistribution rather the in vitro transfection shown here, and in an even bigger picture the stability, storage, scalability and affordability of mRNA drugs.

Importantly, the therapeutic use of the proposed mRNA transfection and material encapsulation should be investigated in an appropriate disease model, such as revascularization of ischemic tissue or orchestration of regenerative cascades, which could benefit from a complex input rather than a traditional mono-therapeutic approach.

References

1. Caplan, A.I. and D. Correa, *The MSC: an injury drugstore.* Cell Stem Cell, 2011. **9**(1): p. 11-5.
2. Wechsler, M.E., V.V. Rao, A.N. Borelli, and K.S. Anseth, *Engineering the MSC Secretome: A Hydrogel Focused Approach.* Adv Healthc Mater, 2021. **10**(7): p. e2001948.
3. Doorn, J., G. Moll, K. Le Blanc, C. van Blitterswijk, and J. de Boer, *Therapeutic applications of mesenchymal stromal cells: paracrine effects and potential improvements.* Tissue Eng Part B Rev, 2012. **18**(2): p. 101-15.
4. Caplan, H., S.D. Olson, A. Kumar, M. George, K.S. Prabhakara, P. Wenzel, S. Bedi, N.E. Toledano-Furman, F. Triolo, J. Kamhieh-Milz, G. Moll, and C.S. Cox, Jr., *Mesenchymal Stromal Cell Therapeutic Delivery: Translational Challenges to Clinical Application.* Front Immunol, 2019. **10**: p. 1645.
5. Rodriguez-Fuentes, D.E., L.E. Fernandez-Garza, J.A. Samia-Meza, S.A. Barrera-Barrera, A.I. Caplan, and H.A. Barrera-Saldana, *Mesenchymal Stem Cells Current Clinical Applications: A Systematic Review.* Arch Med Res, 2020.
6. Majumdar, M.K., M. Keane-Moore, D. Buyaner, W.B. Hardy, M.A. Moorman, K.R. McIntosh, and J.D. Mosca, *Characterization and functionality of cell surface molecules on human mesenchymal stem cells.* J Biomed Sci, 2003. **10**(2): p. 228-41.
7. Goessler, U.R., K. Bieback, P. Bugert, T. Heller, H. Sadick, K. Hormann, and F. Riedel, *In vitro analysis of integrin expression during chondrogenic differentiation of mesenchymal stem cells and chondrocytes upon dedifferentiation in cell culture.* Int J Mol Med, 2006. **17**(2): p. 301-7.
8. Zwolanek, D., M. Flicker, E. Kirstatter, F. Zaucke, G.J. van Osch, and R.G. Erben, *beta1 Integrins Mediate Attachment of Mesenchymal Stem Cells to Cartilage Lesions.* Biores Open Access, 2015. **4**(1): p. 39-53.
9. Drury, J.L. and D.J. Mooney, *Hydrogels for tissue engineering: scaffold design variables and applications.* Biomaterials, 2003. **24**(24): p. 4337-4351.
10. Emsley, J., C.G. Knight, R.W. Farndale, M.J. Barnes, and R.C. Liddington, *Structural basis of collagen recognition by integrin alpha2beta1.* Cell, 2000. **101**(1): p. 47-56.
11. Davidenko, N., C.F. Schuster, D.V. Bax, R.W. Farndale, S. Hamaia, S.M. Best, and R.E. Cameron, *Evaluation of cell binding to collagen and gelatin: a study of the effect of 2D and 3D architecture and surface chemistry.* Journal of Materials Science-Materials in Medicine, 2016. **27**(10).
12. Thomas, D., G. Marsico, I.L. Mohd Isa, A. Thirumaran, X. Chen, B. Lukasz, G. Fontana, B. Rodriguez, M. Marchetti-Deschmann, T. O'Brien, and A. Pandit, *Temporal changes guided by mesenchymal stem cells on a 3D microgel platform enhance angiogenesis in vivo at a low-cell dose.* Proc Natl Acad Sci U S A, 2020. **117**(32): p. 19033-19044.
13. Drzeniek, N.M., A. Mazzocchi, S. Schlickeiser, S.D. Forsythe, G. Moll, S. Geissler, P. Reinke, M. Gossen, V.S. Gorantla, H.D. Volk, and S. Soker, *Bio-instructive hydrogel expands the paracrine potency of mesenchymal stem cells.* Biofabrication, 2021. **13**(4).
14. Ruoslahti, E. and M.D. Pierschbacher, *New perspectives in cell adhesion: RGD and integrins.* Science, 1987. **238**(4826): p. 491-7.

15. Humphries, J.D., A. Byron, and M.J. Humphries, *Integrin ligands at a glance.* J Cell Sci, 2006. **119**(Pt 19): p. 3901-3.
16. Peng, K.Y., Y.H. Liu, Y.W. Li, B.L. Yen, and M.L. Yen, *Extracellular matrix protein laminin enhances mesenchymal stem cell (MSC) paracrine function through alphavbeta3/CD61 integrin to reduce cardiomyocyte apoptosis.* J Cell Mol Med, 2017. **21**(8): p. 1572-1583.
17. Qazi, T.H., D.J. Mooney, G.N. Duda, and S. Geissler, *Biomaterials that promote cell-cell interactions enhance the paracrine function of MSCs.* Biomaterials, 2017. **140**: p. 103-114.
18. Arkenberg, M.R., H.D. Nguyen, and C.C. Lin, *Recent advances in bio-orthogonal and dynamic crosslinking of biomimetic hydrogels.* J Mater Chem B, 2020. **8**(35): p. 7835-7855.
19. Damasceno, P.K.F., T.A. de Santana, G.C. Santos, I.D. Orge, D.N. Silva, J.F. Albuquerque, G. Golinelli, G. Grisendi, M. Pinelli, R. Ribeiro dos Santos, M. Dominici, and M.B.P. Soares, *Genetic Engineering as a Strategy to Improve the Therapeutic Efficacy of Mesenchymal Stem/Stromal Cells in Regenerative Medicine.* Frontiers in Cell and Developmental Biology, 2020. **8**.
20. Moiani, A., Y. Paleari, D. Sartori, R. Mezzadra, A. Miccio, C. Cattoglio, F. Cocchiarella, M.R. Lidonnici, G. Ferrari, and F. Mavilio, *Lentiviral vector integration in the human genome induces alternative splicing and generates aberrant transcripts.* J Clin Invest, 2012. **122**(5): p. 1653-66.
21. Lee, H. and J.S. Kim, *Unexpected CRISPR on-target effects.* Nat Biotechnol, 2018. **36**(8): p. 703-704.
22. Baden, L.R., H.M. El Sahly, B. Essink, K. Kotloff, S. Frey, R. Novak, D. Diemert, S.A. Spector, N. Rouphael, C.B. Creech, J. McGettigan, S. Khetan, N. Segall, J. Solis, A. Brosz, C. Fierro, H. Schwartz, K. Neuzil, L. Corey, P. Gilbert, H. Janes, D. Follmann, M. Marovich, J. Mascola, L. Polakowski, J. Ledgerwood, B.S. Graham, H. Bennett, R. Pajon, C. Knightly, B. Leav, W. Deng, H. Zhou, S. Han, M. Ivarsson, J. Miller, T. Zaks, and C.S. Group, *Efficacy and Safety of the mRNA-1273 SARS-CoV-2 Vaccine.* N Engl J Med, 2021. **384**(5): p. 403-416.
23. Sahin, U., K. Kariko, and O. Tureci, *mRNA-based therapeutics--developing a new class of drugs.* Nat Rev Drug Discov, 2014. **13**(10): p. 759-80.
24. Karikó, K., M. Buckstein, H. Ni, and D. Weissman, *Suppression of RNA Recognition by Toll-like Receptors: The Impact of Nucleoside Modification and the Evolutionary Origin of RNA.* Immunity, 2005. **23**(2): p. 165-175.
25. Anderson, B.R., H. Muramatsu, B.K. Jha, R.H. Silverman, D. Weissman, and K. Karikó, *Nucleoside modifications in RNA limit activation of 2'-5'-oligoadenylate synthetase and increase resistance to cleavage by RNase L.* Nucleic acids research, 2011. **39**(21): p. 9329-9338.
26. Anderson, B.R., H. Muramatsu, S.R. Nallagatla, P.C. Bevilacqua, L.H. Sansing, D. Weissman, and K. Karikó, *Incorporation of pseudouridine into mRNA enhances translation by diminishing PKR activation.* Nucleic Acids Res, 2010. **38**(17): p. 5884-92.
27. Andries, O., S. Mc Cafferty, S.C. De Smedt, R. Weiss, N.N. Sanders, and T. Kitada, *N1-methylpseudouridine-incorporated mRNA outperforms pseudouridine-incorporated mRNA by providing enhanced protein expression and reduced immunogenicity in mammalian cell lines and mice.* Journal of Controlled Release, 2015. **217**: p. 337-344.
28. Li, B., X. Luo, and Y. Dong, *Effects of Chemically Modified Messenger RNA on Protein Expression.* Bioconjug Chem, 2016. **27**(3): p. 849-53.

29. Levy, O., W. Zhao, L.J. Mortensen, S. Leblanc, K. Tsang, M. Fu, J.A. Phillips, V. Sagar, P. Anandakumaran, J. Ngai, C.H. Cui, P. Eimon, M. Angel, C.P. Lin, M.F. Yanik, and J.M. Karp, *mRNA-engineered mesenchymal stem cells for targeted delivery of interleukin-10 to sites of inflammation.* Blood, 2013. **122**(14): p. e23-32.
30. Mazzocchi, A., M. Devarasetty, R. Huntwork, S. Soker, and A. Skardal, *Optimization of collagen type I-hyaluronan hybrid bioink for 3D bioprinted liver microenvironments.* Biofabrication, 2018. **11**(1): p. 015003.
31. Williams, D., H. Puhl, and S. Ikeda, *A Simple, Highly Efficient Method for Heterologous Expression in Mammalian Primary Neurons Using Cationic Lipid-mediated mRNA Transfection.* Frontiers in Neuroscience, 2010. **4**.
32. Zangi, L., K.O. Lui, A. von Gise, Q. Ma, W. Ebina, L.M. Ptaszek, D. Spater, H. Xu, M. Tabebordbar, R. Gorbatov, B. Sena, M. Nahrendorf, D.M. Briscoe, R.A. Li, A.J. Wagers, D.J. Rossi, W.T. Pu, and K.R. Chien, *Modified mRNA directs the fate of heart progenitor cells and induces vascular regeneration after myocardial infarction.* Nat Biotechnol, 2013. **31**(10): p. 898-907.
33. Carlsson, L., J.C. Clarke, C. Yen, F. Gregoire, T. Albery, M. Billger, A.C. Egnell, L.M. Gan, K. Jennbacken, E. Johansson, G. Linhardt, S. Martinsson, M.W. Sadiq, N. Witman, Q.D. Wang, C.H. Chen, Y.P. Wang, S. Lin, B. Ticho, P.C.H. Hsieh, K.R. Chien, and R. Fritsche-Danielson, *Biocompatible, Purified VEGF-A mRNA Improves Cardiac Function after Intracardiac Injection 1 Week Post-myocardial Infarction in Swine.* Mol Ther Methods Clin Dev, 2018. **9**: p. 330-346.
34. Drzeniek, N.M., N. Kahwaji, S. Schlickeiser, P. Reinke, S. Geißler, H.-D. Volk, and M. Gossen, *Immuno-engineered mRNA combined with cell adhesive niche for synergistic modulation of the MSC secretome.* Biomaterials, 2023. **294**: p. 121971.
35. Nance, K.D. and J.L. Meier, *Modifications in an Emergency: The Role of N1-Methylpseudouridine in COVID-19 Vaccines.* ACS Cent Sci, 2021. **7**(5): p. 748-756.
36. Lim, W.A., *The emerging era of cell engineering: Harnessing the modularity of cells to program complex biological function.* Science, 2022. **378**(6622): p. 848-852.
37. Kit-Anan, W., M.M. Mazo, B.X. Wang, V. Leonardo, I.J. Pence, S. Gopal, A. Gelmi, A. Nagelkerke, M. Becce, C. Chiappini, S.E. Harding, C.M. Terracciano, and M.M. Stevens, *Multiplexing physical stimulation on single human induced pluripotent stem cell-derived cardiomyocytes for phenotype modulation.* Biofabrication, 2021. **13**(2): p. 025004.
38. Sanchez Rezza, A., Y. Kulahci, V.S. Gorantla, F. Zor, and N.M. Drzeniek, *Implantable Biomaterials for Peripheral Nerve Regeneration–Technology Trends and Translational Tribulations.* Frontiers in Bioengineering and Biotechnology, 2022. **10**.
39. Kong, H.J., S. Hsiong, and D.J. Mooney, *Nanoscale Cell Adhesion Ligand Presentation Regulates Nonviral Gene Delivery and Expression.* Nano Letters, 2007. **7**(1): p. 161-166.
40. Dhaliwal, A., J. Lam, M. Maldonado, C. Lin, and T. Segura, *Extracellular matrix modulates non-viral gene transfer to mouse mesenchymal stem cells.* Soft Matter, 2012. **8**(5): p. 1451-1459.
41. Dimitroff, C.J., J.Y. Lee, S. Rafii, R.C. Fuhlbrigge, and R. Sackstein, *CD44 is a major E-selectin ligand on human hematopoietic progenitor cells.* J Cell Biol, 2001. **153**(6): p. 1277-86.
42. Schumann, J., K. Stanko, U. Schliesser, C. Appelt, and B. Sawitzki, *Differences in CD44 Surface Expression Levels and Function Discriminates IL-17 and IFN-gamma Producing Helper T Cells.* PLoS One, 2015. **10**(7): p. e0132479.

43. Sackstein, R., J.S. Merzaban, D.W. Cain, N.M. Dagia, J.A. Spencer, C.P. Lin, and R. Wohlgemuth, *Ex vivo glycan engineering of CD44 programs human multipotent mesenchymal stromal cell trafficking to bone.* Nat Med, 2008. **14**(2): p. 181-7.
44. Zhu, H., N. Mitsuhashi, A. Klein, L.W. Barsky, K. Weinberg, M.L. Barr, A. Demetriou, and G.D. Wu, *The role of the hyaluronan receptor CD44 in mesenchymal stem cell migration in the extracellular matrix.* Stem Cells, 2006. **24**(4): p. 928-35.
45. Tsai, C.W. and T.H. Young, *CD44 expression trends of mesenchymal stem-derived cell, cancer cell and fibroblast spheroids on chitosan-coated surfaces.* Pure and Applied Chemistry, 2016. **88**(9): p. 843-852.

Eidesstattliche Versicherung

„Ich, Norman Michael Drzeniek, versichere an Eides statt durch meine eigenhändige Unterschrift, dass ich die vorgelegte Dissertation mit dem Thema: "Mesenchymale Stromazellen der nächsten Generation für regenerative Zwecke - Manipulation des Zellphänotyps durch Biomaterialien und nichtviralen Gentransfer" (Englisch: "Next Generation Mesenchymal Stromal Cells for Regenerative Purposes - Manipulation of the Cellular Phenotype Using Biomaterials and Non-viral Gene Transfer") selbstständig und ohne nicht offengelegte Hilfe Dritter verfasst und keine anderen als die angegebenen Quellen und Hilfsmittel genutzt habe. Alle Stellen, die wörtlich oder dem Sinne nach auf Publikationen oder Vorträgen anderer Autoren/innen beruhen, sind als solche in korrekter Zitierung kenntlich gemacht. Die Abschnitte zu Methodik (insbesondere praktische Arbeiten, Laborbestimmungen, statistische Aufarbeitung) und Resultaten (insbesondere Abbildungen, Graphiken und Tabellen) werden von mir verantwortet.

Ich versichere ferner, dass ich die in Zusammenarbeit mit anderen Personen generierten Daten, Datenauswertungen und Schlussfolgerungen korrekt gekennzeichnet und meinen eigenen Beitrag sowie die Beiträge anderer Personen korrekt kenntlich gemacht habe (siehe Anteilserklärung). Texte oder Textteile, die gemeinsam mit anderen erstellt oder verwendet wurden, habe ich korrekt kenntlich gemacht.

Meine Anteile an etwaigen Publikationen zu dieser Dissertation entsprechen denen, die in der untenstehenden gemeinsamen Erklärung mit dem/der Erstbetreuer/in, angegeben sind. Für sämtliche im Rahmen der Dissertation entstandenen Publikationen wurden die Richtlinien des ICMJE (International Committee of Medical Journal Editors; www.icmje.og) zur Autorenschaft eingehalten. Ich erkläre ferner, dass ich mich zur Einhaltung der Satzung der Charité – Universitätsmedizin Berlin zur Sicherung Guter Wissenschaftlicher Praxis verpflichte.

Weiterhin versichere ich, dass ich diese Dissertation weder in gleicher noch in ähnlicher Form bereits an einer anderen Fakultät eingereicht habe.

Die Bedeutung dieser eidesstattlichen Versicherung und die strafrechtlichen Folgen einer unwahren eidesstattlichen Versicherung (§§156, 161 des Strafgesetzbuches) sind mir bekannt und bewusst.“

Datum Unterschrift

Anteilserklärung an den erfolgten Publikationen

Norman M. Drzeniek hatte folgenden Anteil an den folgenden Publikationen:

Publikation 1: Norman M. Drzeniek, Andrea Mazzocchi, Stephan Schlickeiser, Steven D. Forsythe, Guido Moll, Sven Geißler, Petra Reinke, Manfred Gossen, Vijay S. Gorantla, Hans-Dieter Volk, Shay Soker, *Bio-instructive hydrogel expands the paracrine potency of mesenchymal stem cells*, Biofabrication, 2021

Beitrag im Einzelnen:
Herr Drzeniek war an der Planung und Konzeptualisierung der Studie beteiligt und hat diese im Rahmen einer internationalen Zusammenarbeit und eines Laboraustausches am Wake Forest Institute for Regenerative Medicine (Winston-Salem, NC, USA) in Rücksprache mit den Professoren Volk, Gorantla und Soker organisiert und durchgeführt. Er etablierte die 3D Kultur der MSCs, plante die Versuche in Rücksprache mit seinen Betreuern und führte diese selbstständig durch. Bei der Elektronenmikroskopie erhielt er Unterstützung seitens der Core Facility Mitarbeiter der jeweiligen Einrichtung. Herr Drzeniek verfasste das Manuskript und betreute den Review Prozess im Journal in Rücksprache mit Prof. Soker. Analyse und Interpretation der Daten wurden in Rücksprache mit den Koautoren ebenfalls von Herrn Drzeniek durchgeführt, mit Ausnahme der Auswertung der Sekretomprofile in Abbildung 3 a-c, welche von Dr. Schlickeiser in Rücksprache mit Herrn Drzeniek ausgewertet und visualisiert wurden.

Publikation 2: Norman M. Drzeniek, Nourhan Kahwaji, Stephan Schlickeiser, Petra Reinke, Sven Geißler, Hans-Dieter Volk, Manfred Gossen, *Immuno-engineered mRNA combined with cell adhesive niche for synergistic modulation of the MSC secretome,* Biomaterials, 2021

Beitrag im Einzelnen:
Herr Drzeniek hat maßgeblich zum Konzept der Studie beigetragen, insbesondere die Kombination der Biomaterial- und Gentechnik-Ansätze. Er hat alle Versuche weitestgehend eigenständig geplant und die resultierenden Daten interpretiert und zu einem Manuskript gebündelt. Er verfasste das Manuskript und betreute den Review Prozess mit der Unterstützung von Dr. Gossen. Die Herstellung der in vitro transkribierten mRNA erlernte Herr Drzeniek im Labor von Dr. Gossen. Wesentliche weiterführende Teile der Methodologie etablierte Herr Drzeniek. Dazu gehören die mRNA-Transfektion der MSCs, die Beurteilung der zellulären Antwort auf die mRNA-Transfektion, sowie die Biomaterialarbeiten. Die Herstellung aller verwendeten mRNAs, sowie alle Biomaterialarbeiten wurden von Herrn Drzeniek durchgeführt. Aus Herrn Drzenieks Zellkulturversuchen gingen die Daten für Abbildungen 2g, 3d-h, 4e-f, sowie die Abbildungen 5 (bis auf ELISA Messungen) und 6 hervor. Die übrigen Versuche wurden von Frau Kahwaji in Rücksprache mit Herrn Drzeniek durchgeführt und formell ausgewertet, nachdem sie die notwendige Methodik von Herrn Drzeniek erlernt hatte. Diese Versuche wurden von Herrn Drzeniek geplant, methodisch betreut und interpretiert. Die Sekretomprofile in Abbildungen 3d-h und 4d wurden von Dr. Schlickeiser in Rücksprache mit Herrn Drzeniek ausgewertet und visualisiert.

_____

Unterschrift, Datum und Stempel des/der erstbetreuenden Hochschullehrers/in

_____

Unterschrift des Doktoranden/der Doktorandin

Publication 1: Journal Summary List

Journal Data Filtered By: **Selected JCR Year: 2019** Selected Editions: SCIE,SSCI
Selected Categories: **"ENGINEERING, BIOMEDICAL"** Selected Category Scheme: WoS
Gesamtanzahl: 87 Journale

Rank	Full Journal Title	Total Cites	Journal Impact Factor	Eigenfactor Score
1	Nature Biomedical Engineering	3,143	18.952	0.014180
2	Annual Review of Biomedical Engineering	4,698	15.541	0.004880
3	MEDICAL IMAGE ANALYSIS	9,028	11.148	0.017100
4	BIOMATERIALS	108,070	10.317	0.089110
5	Bioactive Materials	859	8.724	0.001650
6	Biofabrication	4,311	8.213	0.007470
7	Advanced Healthcare Materials	11,883	7.367	0.027520
8	Acta Biomaterialia	39,268	7.242	0.050720
9	npj Regenerative Medicine	417	7.021	0.001630
10	IEEE TRANSACTIONS ON MEDICAL IMAGING	21,657	6.685	0.030060
11	Bioengineering & Translational Medicine	595	6.091	0.001660
12	Photoacoustics	715	5.870	0.001760
13	Tissue Engineering Part B-Reviews	3,603	5.724	0.004190
14	IEEE TRANSACTIONS ON BIOMEDICAL ENGINEERING	23,928	4.424	0.021150
15	ARTIFICIAL INTELLIGENCE IN MEDICINE	2,953	4.383	0.003370
16	Journal of Neural Engineering	7,240	4.141	0.011940
17	Bio-Design and Manufacturing	99	4.095	0.000180
18	IEEE Transactions on Biomedical Circuits and Systems	3,534	4.042	0.006530
19	COMPUTERIZED MEDICAL IMAGING AND GRAPHICS	2,656	3.750	0.002940
20	EUROPEAN CELLS & MATERIALS	3,088	3.741	0.003140

IOP Publishing *Biofabrication* **13** (2021) 045002 https://doi.org/10.1088/1758-5090/ac0a32

Biofabrication

OPEN ACCESS

RECEIVED
22 March 2021

REVISED
13 May 2021

ACCEPTED FOR PUBLICATION
10 June 2021

PUBLISHED
8 July 2021

PAPER

Bio-instructive hydrogel expands the paracrine potency of mesenchymal stem cells

Norman M Drzeniek[1,2,*], Andrea Mazzocchi[6,7], Stephan Schlickeiser[1], Steven D Forsythe[7], Guido Moll[1,2], Sven Geißler[1,3], Petra Reinke[1,3], Manfred Gossen[4,5], Vijay S Gorantla[7], Hans-Dieter Volk[1,8] and Shay Soker[7,8,*]

[1] Berlin Institute of Health at Charité—Universitätsmedizin Berlin, BIH Center for Regenerative Therapies (BCRT), Charitéplatz 1, 10117 Berlin, Germany
[2] Berlin-Brandenburg School for Regenerative Therapies (BSRT), Charité—Universitätsmedizin Berlin, Augustenburger Platz 1, 13353 Berlin, Germany
[3] Berlin Center for Advanced Therapies (BeCAT), Charité—Universitätsmedizin Berlin, corporate member of Freie Universität Berlin and Humboldt-Universität zu Berlin, Augustenburger Platz 1, 13353 Berlin, Germany
[4] Berlin-Brandenburg Center for Regenerative Therapies (BCRT), Charité Campus Virchow-Klinikum, Augustenburger Platz 1, Berlin 13353, Germany
[5] Institute of Active Polymers, Helmholtz-Zentrum Hereon, Kantstr. 55, Teltow 14513, Germany
[6] Known Medicine Inc., 675 Arapeen Dr, Suite 103A-1, Salt Lake City, UT 84108, United States of America
[7] Wake Forest Institute for Regenerative Medicine, Wake Forest School of Medicine, Winston-Salem, NC 27101, United States of America
[8] Both authors contributed equally as senior authors.
[*] Authors to whom any correspondence should be addressed.

E-mail: norman.drzeniek@charite.de **and** ssoker@wakehealth.edu

Keywords: secretome, biomaterial, cell delivery, injectable hydrogel, 3D culture, collagen, hyaluronic acid, angiogenesis, mesenchymal stromal cells (MSCs), biomedical engineering, material structure, cell-material interactions, biochemical cues, biointerface, tissue engineering, regenerative medicine

Supplementary material for this article is available online

Abstract

The therapeutic efficacy of clinically applied mesenchymal stromal cells (MSCs) is limited due to their injection into harsh *in vivo* environments, resulting in the significant loss of their secretory function upon transplantation. A potential strategy for preserving their full therapeutic potential is encapsulation of MSCs in a specialized protective microenvironment, for example hydrogels. However, commonly used injectable hydrogels for cell delivery fail to provide the bio-instructive cues needed to sustain and stimulate cellular therapeutic functions. Here we introduce a customizable collagen I-hyaluronic acid (COL-HA)-based hydrogel platform for the encapsulation of MSCs. Cells encapsulated within COL-HA showed a significant expansion of their secretory profile compared to MSCs cultured in standard (2D) cell culture dishes or encapsulated in other hydrogels. Functionalization of the COL-HA backbone with thiol-modified glycoproteins such as laminin led to further changes in the paracrine profile of MSCs. In depth profiling of more than 250 proteins revealed an expanded secretion profile of proangiogenic, neuroprotective and immunomodulatory paracrine factors in COL-HA-encapsulated MSCs with a predicted augmented pro-angiogenic potential. This was confirmed by increased capillary network formation of endothelial cells stimulated by conditioned media from COL-HA-encapsulated MSCs. Our findings suggest that encapsulation of therapeutic cells in a protective COL-HA hydrogel layer provides the necessary bio-instructive cues to maintain and direct their therapeutic potential. Our customizable hydrogel combines bioactivity and clinically applicable properties such as injectability, on-demand polymerization and tissue-specific elasticity, all features that will support and improve the ability to successfully deliver functional MSCs into patients.

1. Introduction

Mesenchymal stromal (stem) cell (MSC) therapy is a promising regenerative treatment option for a variety of disease conditions, including but not limited to cardiovascular, neurological, musculoskeletal, immunological, and hematologic disorders [1–5]. Despite their multi-lineage differentiation potential,

recent evidence challenges the initial concept that transplanted MSCs can reliably engraft and replace damaged cells and tissues. Instead, MSCs are now thought to survive only temporarily after *in vivo* application and to primarily mediate their effects through the secretion of paracrine mediators, including pro-angiogenic, neuroprotective and immunomodulatory cytokines [6–8].

Intravenous injection, the most common route of cell administration, results in clearance of MSCs from the recipient body within hours. As a consequence of this fast clearance there is a low effective cell dose at the site of injury and a short time window for paracrine effects [7, 9–11]. As such, despite encouraging pre-clinical data and over 1,000 registered clinical trials using MSCs, clinical efficacy data has not lived up to initial expectations with only a few exceptions [10, 12]. Local injection of *in vitro* expanded MSCs either directly at the site of tissue damage, or intramuscularly, can improve cell engraftment and increase the local cell dose, resulting in stronger paracrine effects. However, the efficacy of this approach is dependent on whether MSCs remain functional in the harsh environment of the tissue into which they are administered. Fortunately, this intratissue administration route opens up the opportunity to deliver cells in a defined biomaterial carrier able to physically shield cells from challenging and highly variable microenvironments, sustain their paracrine activity and guide the MSCs' biological effects toward a specific healing scenario.

Several biomaterial strategies for cell delivery have been proposed, but most are limited by either a lack of bioactive cues that would support cell functionality or by poor usability that makes handling and local therapeutic application of the material difficult. Macroporous scaffolds are often fabricated from synthetic polymers or natural biopolymers, such as collagen, and excel in providing cell attachment sites, allowing for cell–matrix and cell–cell interactions and directing cell behavior [13–15]. Scaffold materials often undergo complex patterning methods, such as lyophilization and electrospinning. Whilst these methods provide great flexibility in generating scaffolds that can mimic microanatomical structures, they are often not possible to perform under physiological conditions and therefore can harm pre-seeded cells [16, 17]. Another major drawback to solid scaffolds is that, although they often recapitulate the native extracellular matrix (ECM) more closely than hydrogels and provide a myriad of biologically relevant cues, their application is limited to indications where surgical implantation is possible.

Aqueous hydrogels on the other hand are injectable and provide physical protection for encapsulated MSCs. They are broadly defined as polymer networks, commonly comprised of hyaluronic acid (HA), gelatin, polyethylene glycol (PEG), fibrin, alginate or polycaprolactone, which have the ability to swell in aqueous environments [18, 19]. Hydrogels can be prepared in a liquid phase and then crosslinked to a solid state with distinct mechanical properties. Hydrogel crosslinking can be achieved by different mechanisms, allowing for time- or temperature-dependent gelation and can even be triggered on demand by external stimuli such as light [20, 21]. These properties make hydrogels attractive for *in vivo* delivery of cells, where the cell suspension can be injected using a syringe or minimally invasive interventions [22]. Unfortunately, hydrogels often entrap cells in a highly hydrophilic environment that has few bioactive cues, thereby failing to support and instruct their therapeutic activity [14].

We hypothesized that increasing the presence of biologically relevant cues in an injectable hydrogel cell carrier could stimulate the secretion of therapeutically relevant mediators and that diversification of material-derived cues may further modulate the paracrine profile of encapsulated MSCs. To test this hypothesis, a biopolymer hydrogel (COL-HA) was formulated entirely from materials that are known to allow for cell–matrix interactions, such as collagen and HA, additionally functionalized with the glycoproteins laminin or fibronectin, and crosslinked through a mechanism that eliminated the need for additional bio-inert crosslinking components. The hydrogel stiffness and structure, cell viability, morphology and the paracrine profile were analyzed and compared to an industry standard gelatin-HA (Gel-HA) hydrogel. MSCs encapsulated within COL-HA formulations released different patterns of pro-regenerative factors than MSCs cultured in 2D or in other hydrogels. In depth secretome profiling predicted increased pro-angiogenic activity of COL-HA-encapsulated MSCs, which was confirmed using an assay to assess endothelial cell (EC) capillary network formation in the presence of COL-HA-encapsulated MSC conditioned media (CM).

Biomaterial-guided regulation of the MSC secretome adds important new insights to the current understanding of MSC therapy and the successful combination of usability and bio-instructive properties in COL-HA hydrogels can inform future studies into the next steps in improving methods for the successful delivery of MSC therapeutics into patients.

2. Materials and methods

2.1. Fabrication of hydrogels

Collagen-HA hydrogels (COL-HA) were prepared from telopeptide-intact methacrylated type 1 collagen (Advanced Biomatrix, Carlsbad, CA) and thiolated hyaluronic acid (Hystem; Advanced Biomatrix) and crosslinked through a light-initiated

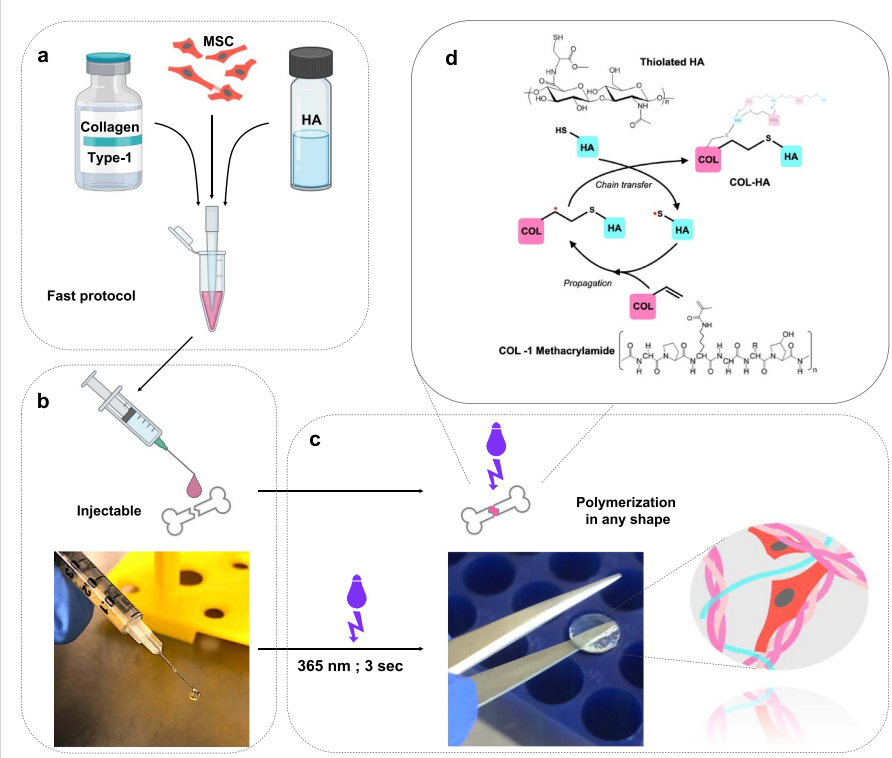

Figure 1. Fabrication of the COL-HA hydrogel (a) MSC are resuspended in collagen-HA hydrogel. (b) The cell-hydrogel mix can be applied using a pipette or syringe. (c) The hydrogel can be polymerized on demand with a short UVA light pulse and maintains its shape in the crosslinked state. (d) Crosslinking of the biopolymer network through radical mediated thiol-ene addition of thiolated HA to collagen methacrylamide.

thiol-ene radical addition (figure 1). Lyophilized collagen was dissolved in 20 mM acetic acid overnight at +4 °C to a concentration of 8 mg ml^{-1}. Thiolated HA was dissolved in PBS to a concentration of 10 mg ml^{-1}.

For COL-HA functionalization, 1 mg ml^{-1} solutions of thiolated glycoproteins (natural mouse laminin (ThermoFisher Scientic, Waltham, MA) or human plasma fibronectin (Sigma Aldrich, St. Louis, MO)) were prepared using a protein thiolation kit (Expedeon, Over Cambridgeshire, UK) according to the manufacturer's instructions.

Immediately before use, the collagen was brought to physiological pH and mixed with HA in a 3:1 ratio, then with laminin or fibronectin solution (or PBS) in a 2:1 ratio by volume for a final concentration of 4 mg collagen/ml, 1.67 mg HA/ml and optionally 0.33 mg ml^{-1} of glycoprotein. The liquid mix was used either for cell encapsulation or cast in a mold for photopolymerization. 0.02% (w/v) of 2-hydroxy-4′-(2-hydroxyethoxy)-2-methylpropiophenone (Sigma Aldrich, St. Louis, MO) was used to trigger the free-radical addition under exposure to UVA light of 1.4 W cm^{-2} for 3 s, resulting in instantaneous photo-initiated polymerization and hydrogel formation.

To prepare control Gel-HA gels, the Hystem™ kit components thiolated HA, thiolated porcine type A gelatin (Bloom 250) and Extralink, a linear 3.5 kDa PEGDA linker (Advanced Biomatrix) were dissolved in PBS to a concentration of 10 mg ml^{-1}, mixed in a 2:2:1 ratio by volume and photopolymerized under the same conditions as described for COL-HA, resulting in final concentrations of gelatin and HA of 4 mg ml^{-1} each. To modulate gel stiffness, the linear PEGDA linker was replaced by aqueous solutions of 4-(8-) arm PEG acrylate (2 kDa, 10 kDa, 20 kDa MW; Creative PEGWorks, Durham, NC) at 0.5 mM (1 mM; 5 mM; 10 mM) concentrations (table 1). The four-arm 20 kDa linker at a concentration of 5 mM matched closely the stiffness of COL-HA gels and was therefore chosen as a stiffness-matched control for COL-HA (Gel-HA stiff).

Table 1. Relationship between crosslinker type and concentration and resulting hydrogel stiffness in gelatin-HA control gels: mechanical characterization of different gelatin-HA-PEG gels shows a correlation between PEG linker concentration and hydrogel stiffness. A less prominent correlation can also be observed between stiffness and the arm length of the linker. The two conditions highlighted with an asterisk (*) were used as control hydrogels in this study.

Linker type	Linear PEGDA *	4 ARM-PEG	4 ARM-PEG	4 ARM-PEG	4 ARM-PEG	4 ARM-PEG	4 ARM-PEG*	8 ARM-PEG
Linker size (MW)	3.5 kDa	2 kDa	10 kDa	10 kDa	10 kDa	20 kDa	20 kDa	20 kDa
Linker arm length (MW/n arms)	1.75 kDa	1 kDa	2.5 kDa	2.5 kDa	2.5 kDa	5 kDa	5 kDa	2.5 kDa
Molar concentration (μmol ml^{-1})	2.86 mM	5 mM	1 mM	5 mM	10 mM	0.5 mM	5 mM	0.5 mM
Mass concentration (w/v)	**1%**	**1%**	**1%**	**5%**	**10%**	**1%**	**10%**	**1%**
Hydrogel stiffness (Pa); SD	**6069** 691	**6180** 788	**6845** 1723	**14 048** 1491	**22 760** 429	**8680** 2766	**28 744** 4724	**6822** 388

2.2. Physical characterization of hydrogels

Pore size was measured from scanning electron microscopy (SEM) images of cell-free hydrogels. Triplicates of each hydrogel condition were prepared side by side as described above, transferred into cylindrical molds (250 μl/gel) and photo-crosslinked. The gels were frozen at −80 °C overnight and lyophilized for 72 h. Dehydrated constructs were broken to expose the inner structure, sputter coated with gold/palladium particles and assessed with scanning electron microscopy at an accelerating voltage of 7.0 kV and a working distance of 5.6–8.1 mm (GeminiSEM 300, Zeiss, Oberkochen, Germany). Pore size was measured manually using ImageJ. Median values for each hydrogel condition were determined based on at least 50 measured pores and each individual value was shown in the scatter plot.

Elastic modulus ($E = \sigma/\varepsilon$) of the crosslinked hydrogel compositions was assessed using a uniaxial compression test using a Discovery HR-2 (TA Instruments, New Castle, DE) with an 8 mm parallel plate geometry in ambient conditions. Hydrogels were prepared as described above, the final mixture in its liquid phase was transferred into previously prepared polydimethylsiloxane (PDMS) molds and photo-crosslinked into a disc shape ($\oslash = 8$ mm; $V = 100$ μl/disc). Compression data was collected through outputs of axial force and height displacement. To determine the elastic modulus, stress and strain (y, x) were plotted and the linear portion of the plot was analyzed. Stress was calculated by dividing force by surface area of the hydrogels ($\sigma = F/A$) and strain was calculated by change in height divided by initial height of hydrogels ($\varepsilon = \Delta h/h$). Hydrogels were tested in quadruplicates ($n = 4$; for functionalized COL-HA the two variants COL-HA-Lam and COL-HA-Fn were tested in duplicate each) and average values were determined for each condition.

2.3. Cell culture and generation of CM

Human bone marrow (BM) mesenchymal stromal cells (MSCs) were received from the core facility 'Cell Harvesting' of the BIH Center for Regenerative Therapies (BCRT). The cells were derived from metaphyseal BM biopsies from two patients undergoing hip replacement at Charité—Universitätsmedizin Berlin, as previously stated [23–25]. Written informed consent was given, and ethics approval was obtained from the local ethics committee/institutional review board (IRB) of the Charité—Universitätsmedizin Berlin. All experiments in this study were performed in replicates from at least two different biological donors.

The cells were cultured in low glucose DMEM containing 10% v/v fetal calf serum (FCS), 1% v/v penicillin/streptomycin (both Biochrom AG), and 1% v/v Glutamax™ (Thermo Fisher Scientific Inc., Waltham, MA), passaged around 80% confluence and not used beyond passage 5.

For 3D culture MSCs were trypsinized, centrifuged and resuspended in the respective hydrogel formulations to a density of 5×10^6 cells ml^{-1} per 10 μl droplet and were distributed in a PDMS-precoated culture plate and photo-crosslinked as described above. Cells were allowed to interact with the biomaterial matrix for seven days. Medium was changed every other day. On day 6, constructs were washed with medium and 24 h CM were collected on day 7, centrifuged and stored at −80 °C until use for cytokine measurements. To generate stimulation medium for angiogenesis, constructs were washed with PBS instead and medium on MSC-constructs was replaced by FCS-free DMEM.

2.4. Quantification of MSC viability and morphology

LIVE/ DEAD viability assay (ThermoFisher Scientic, Waltham, MA) was performed on day 7 of 3D culture using calcein AM (1:2000) and ethidium homodimer-1 (1:500) in culture medium. MSC-hydrogel constructs were stained at 37 °C for 1 h before imaging on a Nikon eclipse Ti fluorescence microscope (Nikon Instruments Inc., Tokyo, Japan) or a Leica TCS LSI macro-confocal microscope (Leica, Wetzlar,

Germany). Viability for each experimental group was calculated by manually counting live and dead cells. For robust results, three biological replicates were assessed for each gelatin condition, four for the functionalized COL-HA conditions and five for unfunctionalized COL-HA. Four imaged areas were analyzed from each. To quantify the observed changes in cell shape, the Analyze Particles function in FIJI was used and spindle shape was expressed as the reciprocal of circularity [26], with a value of 1 representing a perfect circle. Biological triplicates $n = 3$ were analyzed, except for COL-HA: $n = 6$.

2.5. Cytokine profiling

Cytokine levels in CM from cell-hydrogel constructs were analyzed using an Olink Target 96 proximity extension assay (Olink Bioscience, Uppsala, Sweden). Biological quadruplicates were tested. Briefly, CM was mixed at a 1:3 ratio with a proprietary mix of cytokine-specific antibodies labeled with DNA oligonucleotides. When two specific probes bound an analyte they formed an amplicon that could be quantified by high-throughput RT-PCR. Details on this technology, including detection limits, validation data and reproducibility can be found on the company's website (www.olink.com/downloads). Relative concentration values for 266 different cytokines were given as normalized protein expression (NPX) units. A marker was considered as detected if more than three samples in any group had NPX values exceeding its limit of detection (LOD). The latter was defined as the larger of either the manufacturer provided LOD or the LOD estimated from own negative controls (blank medium measurements) plus three standard deviations. To validate the proximity extension assay and obtain absolute concentrations, the cell culture experiments were repeated using new batches of CM VEGF, basic fibroblast growth factor (bFGF) and OPG were quantified using ELISA (all R&D Systems, Minneapolis, MN) according to the manufacturer's instructions. Blank values from unconditioned DMEM were subtracted ($n \geqslant 8$ for VEGF and bFGF; $n = 4$ for OPG). Values were expressed as mean ± SEM.

2.6. Assessment of endothelial networks

An optimized protocol of a widely implemented endothelial tube formation assay was used to quantify pro-angiogenic effects [24, 25]. Briefly, HUVEC cells previously pre-screened for cytokine response (Promocell, Heidelberg, Germany) were starved for 10 h in serum-reduced basal endothelial medium and seeded at a density of 3×10^4 cells cm^{-2} in a 48 well cell culture plate coated with Geltrex (Thermo Fisher). Cells were stimulated with biological quadruplicates of hydrogel-MSC-derived 24 h CM in a 1:5 dilution in 2.5% supplemented basal endothelial medium (Promocell) and imaged after 16 h using a fluorescence microscope (Nikon). Unconditioned MSC medium was used for a negative control. For the positive control VEGF levels were previously measured by ELISA (R&D Systems) and the highest detected VEGF levels (stimulation group COL-HA-Lam) were matched using recombinant human VEGF-A165 (#293-VE R&D Systems, Minneapolis, MN).

Bright field images of formed networks were analyzed (at least $n = 13$ per condition) and network-associated parameters were quantified using FIJI and the Angiogenesis Analyzer macro [27]. For fluorescent images, cells were stained for 30 min using calcein AM (ThermoFisher).

2.7. Statistical data analysis

Values are depicted as mean (± standard error of the mean (SEM)) or median. Detailed information can be found in the figure legends. Experiments were repeated independently for $n = 4$ biological replicates, unless indicated otherwise. Levels of statistical significance were set at $^{*}p < 0.05$, $^{**}p < 0.01$, $^{***}p < 0.001$.

Statistical analysis was carried out in GraphPad Prism 8.0 (GraphPad Software Inc., USA) and R version 4.0.2. A two-tailed student's t-test (two groups) or one-way ANOVA with Holm–Sidak's post-hoc test (>two groups) was used as appropriate to test for significant differences between groups. Repeated measures ANOVA was carried out for quadruplicate measurements with Holm multiple comparisons adjustment using the *emmeans* package.

Heatmaps were generated with the *ComplexHeatmap* package. For clustering, a semantic distance matrix was computed using the *GOSemSim* package. Enriched gene ontology terms were derived for each cluster utilizing the *ClusterProfiler* package. Representative terms for angiogenesis, neuroprotection, immunomodulation, hemostasis and ECM remodeling were chosen and summarized for each detected cytokine under the five categories. The subterms can be found in supplementary figure 1.

3. Results

3.1. Hydrogel design and fabrication

The COL-HA hydrogels were designed as a cell delivery vehicle to modulate the paracrine effects of cells for human therapeutic application [18, 28, 29]. Collagen type 1 (COL) was chosen as the main hydrogel component because it is a highly bioactive substrate ideal for mimicking biological microenvironments, has been shown to promote MSC attachment and viability [13, 30, 31] and it is naturally enzymatically degradable [18, 28, 29, 32–34]. Native collagen crosslinks through fiber-self-assembly in a continuous, temperature-dependent process. However, these characteristics also limit the application of pure collagen as an injectable hydrogel due to lack of control over polymerization and mechanical properties.

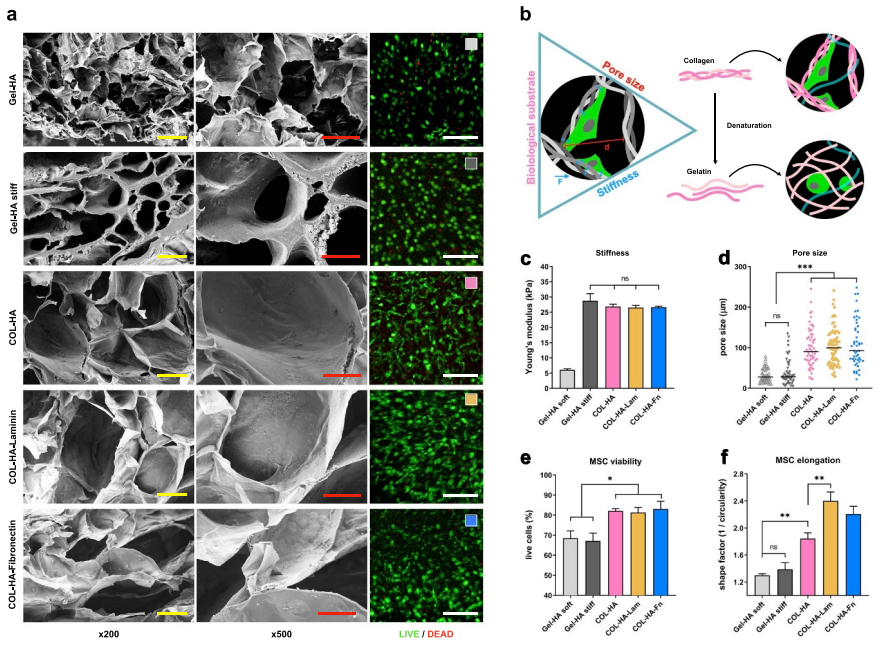

Figure 2. Microporous COL-HA hydrogels promote cell viability and stromal morphology of encapsulated MSCs. (a) From left to right: SEM images at two magnifications (×200; ×500) for all hydrogel conditions without cells show the inner structure of lyophilized hydrogels. Right column: representative confocal images of live/dead stained MSC at day 7 in the native hydrogel. Scale bars are 100 μm, 50 μm and 250 μm respectively. (b) A proposed model of biological cues, structure and stiffness exerting bio-instructive effects at the cell–material interface. Gelatin is derived from collagen and shares the same amino acid sequence but differs in its biological, mechanical and structural properties. (c) Hydrogel stiffness expressed as compressive modulus. (d) Individual pore diameters (short axis) of lyophilized gels were measured from SEM images. Median pore size is shown. (e) Viability of MSC cultured in hydrogels for 7 d. (f) Elongation of cells in the hydrogels on day 7 was quantified in Image J as circularity, then expressed as its reciprocal. ($^*p < 0.05$; $^{**}p < 0.01$; $^{***}p < 0.001$; ns: $p \geqslant 0.05$; all values except (d) are mean ± SEM).

Therefore, thiolated HA, a biodegradable glycosaminoglycan which is known to orchestrate tissue repair and angiogenesis [18, 28, 35], was used to crosslink collagen methacrylamide through a light-triggered thiol-ene reaction between the vinyl groups of the COL and sulfhydryls on HA (figure 1(d)). This eliminated the need for non-bioactive crosslinking molecules such as PEG (figure 1(a)). To diversify cell-instructive cues, the pure COL-HA formulation was functionalized with either laminin (COL-HA-Lam) or fibronectin (COL-HA-Fn; figure 1(d)). An advantage of the thiol-ene reaction, aside from its biocompatibility and bioorthogonality [21, 36, 37], is that the crosslinking can be spatially and temporally controlled with UVA light, allowing an on-demand phase transition from an injectable fluid state to a solid (form-stable) gel (figures 1(b) and (c)). This is important in the application context, where user-controlled crosslinking is beneficial for injection and precise immobilization of transplanted cells. The hydrogel design resulted in an injectable COL-HA formulation that consists exclusively of bioactive components, which can be prepared quickly using a clinician-friendly protocol and crosslinked on demand (figure 1).

3.2. Physical characterization of hydrogels

Cells in living tissues not only receive biochemical cues but are also subject to biomechanical load and themselves exert tensile and compressive forces on their surrounding matrix upon attachment (figure 2(b)). The resistance of a hydrogel to such deforming forces can be described by Young's elastic modulus (E) [38, 39]. E of the COL-HA hydrogels and the commercially available Gel-HA control hydrogels were determined by a uniaxial compression test in their cross-linked state. Physiologically relevant values between ∼26 kPa for COL-HA and ∼6 kPa for Gel-HA were obtained, which are similar to the stiffness of muscle and lung or liver, respectively (figure 2(c)) [38, 39]. There was no difference in stiffness between pure COL-HA hydrogels and those functionalized with laminin or fibronectin. Since the standard formulation of Gel-HA was found to have a significantly lower E than COL-HA, we engineered a stiffer variant of the control hydrogel (Gel-HA stiff),

which matched the E of COL-HA for better comparability (figure 2(c), table 1).

To characterize structural differences between hydrogel groups, the median pore diameter of lyophilized hydrogels was determined and quantified through SEM (figures 2(a) and (d)). COL-HA hydrogels were found to have larger pores than Gel-HA hydrogels. Pore size did not vary significantly between pure and functionalized COL-HA conditions. Despite the comparable median diameter, the pores of the stiff Gel-HA control were more heterogeneous and had thicker walls than the soft Gel-HA hydrogel (figure 2(a), 500× magnification).

The physical characterization of COL-HA hydrogels revealed that UV-triggered crosslinking resulted in reproducibly form-stable constructs that matched elasticity levels of native tissues, despite the crosslinker-free hydrogel design. Independently of differences in stiffness, COL-HA had larger pores in the lyophilized state than both Gel-HA controls.

3.3. COL-HA hydrogels promote cell viability and stromal morphology of encapsulated MSCs

To evaluate whether the different material properties affect viability and morphology of encapsulated cells, 5×10^6 MSCs/ml were resuspended in each gel formulation prior to photo-crosslinking. Cells remained viable inside the hydrogels for at least a week (figure 2(a) right column). Quantification of live to dead cell ratio at day 7 post-encapsulation revealed a significantly higher cell viability of COL-HA-encapsulated MSCs (COL-HA-MSC; viability > 80%) versus Gel-HA-encapsulated MSCs (Gel-HA-MSC; viability < 70%). Viability did not vary significantly between pure and functionalized COL-HA conditions (figure 2(e)). The lowest cell viability was observed in Gel-HA stiff hydrogels.

To assess morphological differences in MSC between all conditions, confocal imaging was used (figure 2(a) right column). Circularity of living cells was quantified using automatic image analysis and the elongation was expressed as the reciprocal of circularity, where a value of 1 corresponds to a perfect circle (figure 2(f)). Independent of the Gel-HA stiffness, Gel-HA-MSCs exhibited a predominantly round morphology, whereas COL-HA-MSC developed their typical elongated fibroblastic shape. This effect was significantly enhanced by functionalization of COL-HA; MSCs in COL-HA-Lam hydrogels showed the largest cell elongation compared to all other conditions.

The results suggest that COL-HA hydrogels supported high viability of encapsulated MSCs and allowed for cell attachment and spreading within the hydrogel, resulting in a different cell morphology compared to MSCs encapsulated in Gel-HA control hydrogels.

3.4. COL-HA increases the paracrine activity of encapsulated MSCs

It is widely recognized that the therapeutic properties of MSCs are related to paracrine or trophic effects determined by their specific secretion pattern [6, 40]. To investigate the influence of the different hydrogel microenvironments on the secretion profile, the cytokine compositions of the CM of COL-HA-MSC or Gel-HA-MSC 3D constructs were characterized and compared to 2D-cultured MSCs on tissue culture plates (TCPs) using a multiplex protein array. In line with our hypothesis, this analysis revealed a generally higher cytokine secretion of MSCs encapsulated in COL-HA constructs compared to Gel-HA or 2D TCP (figures 3(a) and (c)). Despite biological differences between MSC donors, 81 out of the 266 analytes were consistently detected (figure 3(a), supplementary table S1 available online at stacks.iop.org/BF/13/045002/mmedia) at different levels, thereby forming distinct cytokine profiles for the different experimental groups. To evaluate potential biological consequences resulting from these differences, gene ontology (GO) term enrichment analysis for biological processes was performed. Out of the 81 consistently detected cytokines, 56 analytes could be assigned to at least one of the following five categories: angiogenesis, neuro-regeneration, immunomodulation, hemostasis and ECM remodeling (figures 3(b) and S1). The concentrations of half of these analytes (28 out of 56) were significantly increased in the CM of all three COL-HA-MSC groups compared to all other experimental groups (figure 3(c)). These upregulated factors included classical pro-angiogenic growth factors, such as vascular endothelial growth factor A, placental growth factor and hepatocyte growth factor, but also other proteins, such as transforming growth factor beta 1 (TGF-β1) and interleukin-8 (IL-8), which are also known to exert pro-angiogenic effects [41–45]. Neuroprotective agents like osteopontin and glial cell-derived neurotrophic factor (GDNF) were also detected at increased concentrations in COL-HA-MSC CM compared to Gel-HA-MSC and 2D TCP-MSC [46, 47]. While only minor differences were observed between the CM from COL-HA-MSC and the COL-HA-Fn-MSC, the laminin modification further increased protein secretion. This increased secretion was especially pronounced for VEGF, bFGF and leukemia inhibitory factor (LIF) (figure 3(d)). The growth factor LIF has not only neurobiological and immunomodulatory functions but also mediates tolerogenic effects of MSCs [48, 49].

The cytokine pattern of soft Gel-HA-MSC contained lower levels of most cytokines compared to the pure COL-HA condition. For example, neuroprotective factors such as LIF or GDNF were detectable only at very low concentrations, whilst VEGF levels were lowest in the CM of Gel-HA-MSC compared to

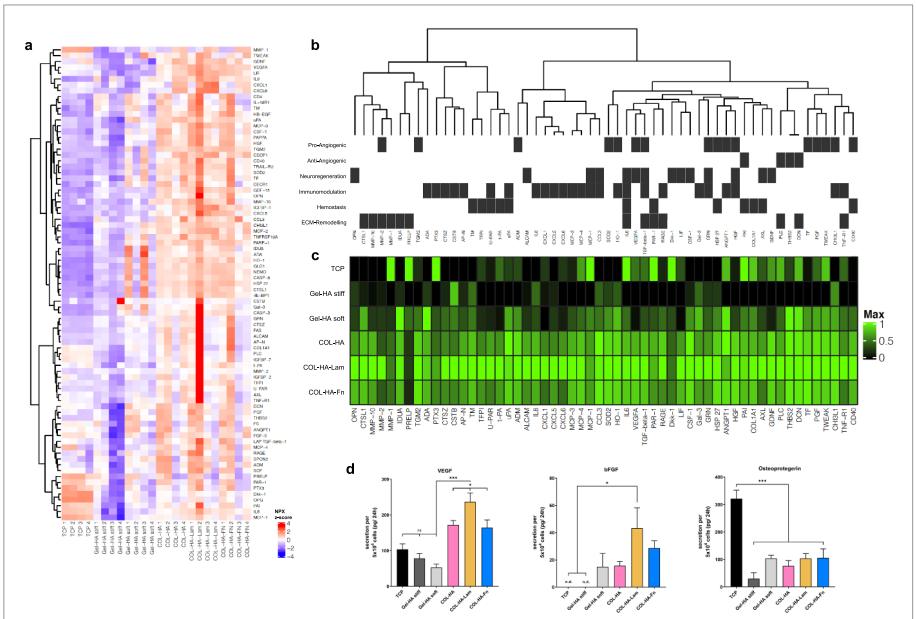

Figure 3. Cytokine profiling reveals expanded secretory profile of COL-HA-MSC. (a) Relative protein levels of all 81 detected analytes in CM from four biological replicates of six conditions. (b) Functional clustering of proteins relevant for angiogenesis, neuroregeneration, immunomodulation, hemostasis and ECM remodeling and (c) the detected levels of the respective proteins for each experimental group. (d) ELISA of VEGF, bFGF and osteoprotegerin. $^{*}p < 0.05$; $^{**}p < 0.01$; $^{***}p < 0.001$; ns: $p \geqslant 0.05$; all bar diagrams show mean ± SEM.

all other groups (figure 3(d)). Only five factors were either more highly secreted or their secretion levels were comparable to those in the COL-HA groups. These included the anti-angiogenic matrix proteins decorin (DCN) and thrombospondin-2, and the pro-angiogenic and vasculoprotective agent angiopoietin-1 [50–52]. Encapsulation of MSCs in the stiff Gel-HA hydrogel resulted in the lowest concentrations for most detectable analytes, compared to the other 3D hydrogel conditions.

The secretion profile of MSCs cultured on 2D TCP was entirely different compared to any 3D hydrogel condition. While most analytes were only detected at low concentrations, eight out of the 56 factors were detected at the highest concentrations in the 2D culture group. These included the inflammation marker interleukin-6 (IL-6) [53], pro-apoptotic factor dickkopf-1 (Dkk-1) and the pro-thrombotic factor plasminogen activator inhibitor-1 (PAI). Dkk-1 is associated with neuron death and Alzheimer's disease [54] and PAI regulates blood vessel formation, but is anti-angiogenic at high concentrations [55, 56]. The osteoblastic marker osteoprotegerin (OPG), which plays an important role in bone metabolism, was detected at significantly higher levels in CM from the TCP group compared to all hydrogels [57].

To validate the protein array data, VEGF and OPG, which showed very distinct regulation, were additionally measured by ELISA (figure 3(d)). The levels of bFGF were also quantified by ELISA, as it was not included in the array panel but has been described as a crucial MSC-derived trophic factor [40]. The ELISA values closely matched the results obtained from the protein array.

The comparison of paracrine profiles from MSCs exposed to different biomaterial microenvironments suggested complex biomaterial-guided regulation of the cellular secretome. In depth analysis revealed an especially strong secretion of pro-angiogenic factors from COL-HA-Lam encapsulated cells, predicting an increased pro-angiogenic potency of cells encapsulated in this cell carrier material.

3.5. ECs organize into capillary-like networks when stimulated with COL-HA-MSC CM

To confirm the increased pro-angiogenic potency from cells encapsulated in COL-HA hydrogels, a validated capillary-like structure formation assay was used [24, 25]. Primary human ECs were stimulated with CM derived from each of the hydrogel-MSC groups. Recombinant human VEGF (rhVEGF) was used as a positive control at a concentration equal to the determined VEGF level of COL-HA-Lam CM. Endothelial tube formation was quantified as the total master segment length (TMSL) detectable in an imaged field (figure 4(b)). Master segments are

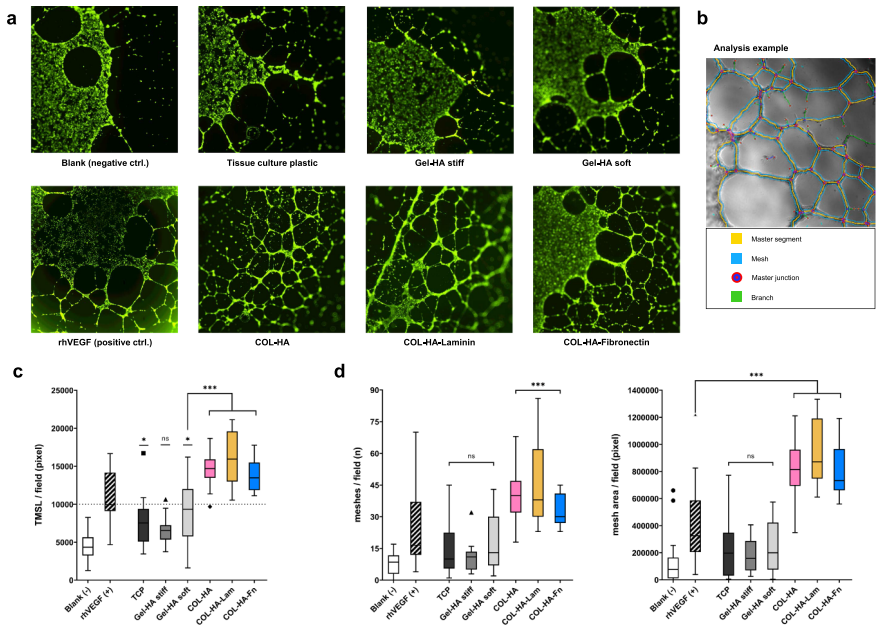

Figure 4. ECs organize into capillary-like networks when stimulated with pro-angiogenic CM. (a) Representative images of calcein AM stained endothelial tubes formed in response to the respective MSC/hydrogel CM indicated below. (b) Representative image of the analysis method to calculate TMSL and mesh area. To quantify the quality of formed networks, the total length of master segments (segments leading to a junction; TMSL) was quantified (c), along with the number of meshes and area covered by complete endothelial tube meshes (d) ($^{*}p < 0.05$; $^{**}p < 0.01$; $^{***}p < 0.001$; ns: $p \geqslant 0.05$; significance levels are relative to blank unless otherwise indicated; box plot whiskers show extreme values with Tukey's correction for outliers).

defined as capillary fragments leading to a junction and their total length is a good parameter for the extent of endothelial tube formation under the exclusion of loose branches. Except for Gel-HA stiff, the TMSL of all other conditions was found to be significantly increased compared to the blank control (figure 4(c)). The TMSL of the three COL-HA conditions was also significantly longer than in the Gel-HA soft group.

To subsequently assess whether the MSC-hydrogel constructs were able to induce the formation of interconnected capillary-like network structures, the number of intact meshes and the total area covered by complete meshes was determined (figure 4(d)). While CM from Gel-HA constructs and from 2D TCP induced some mesh formation, most of these network structures were incomplete and did not result in a significant increase in mesh number compared to the blank control. In contrast, all COL-HA conditions as well as the rhVEGF control significantly stimulated the formation of intact endothelial meshes compared to the unstimulated wells (blank). Network formation of EC stimulated with CM from functionalized and pure COL-HA was more robust and resulted in a significantly higher mesh area compared to rhVEGF (figure 4(d)). The COL-HA-Lam biomaterial induced longer master segments and slightly larger mesh areas compared to the pure COL-HA. Interestingly, a slightly higher median mesh count and tighter meshes were observed in response to CM from pure COL-HA-MSC compared to the functionalized COL-HA hydrogels.

The biological angiogenesis readout confirmed both the functional relevance of augmented pro-angiogenic factor secretion from COL-HA-encapsulated MSCs and additionally reflected the further enhanced pro-angiogenic potency predicted for COL-HA-Lam.

4. Discussion

The clinical success of MSC therapy is limited by the delivery method, therefore, the aim of this study was to fabricate, characterize and optimize an application-oriented carrier material with improved bio-instructive properties for the encapsulation and delivery of therapeutic MSCs.

Two bioactive polymers, collagen and HA, were used to photo-crosslink into a hydrogel with defined, tissue-compatible mechanical properties. Both polymers are used in reconstructive or surgical indications in patients and can therefore be considered safe and

clinically applicable [58–60]. In addition to the pure COL-HA formulation, two modified COL-HA variants were functionalized with either laminin (COL-HA-Lam) or fibronectin (COL-HA-Fn). Laminin is a major biological component of the basal lamina and is known to contain specific cell attachment motifs, while fibronectin is a dimer secreted from hepatocytes into the blood plasma, which plays a crucial role in blood clot formation, matrix remodeling and wound healing [61–63]. Prior studies have identified laminin as a beneficial substrate for MSC culture, capable of influencing the secretion of pro-regenerative mediators [62]. This was in line with our finding that the addition of laminin further promoted MSC elongation and secretion of angiogenic, neuroprotective and immunomodulatory mediators and induced a particularly potent pro-angiogenic MSC phenotype. However the predominant effects were seen in comparing collagen to gelatin-based materials, while the effect of glycoprotein modification was moderate in our study and could likely be blunted by glycoproteins in the serum that adsorb to the collagen matrix [63].

To put the properties of COL-HA into the context of commercially available biomaterials, an industry standard hydrogel kit, Hystem™ (Gel-HA), was used for comparison. Hystem™ has contributed to important advances in 3D cell culture and organoid development in recent years and exhibits a comparable photo-triggered phase change as COL-HA [19, 64, 65]. Gel-HA is composed of HA, PEG and gelatin, denatured collagen that shares the same amino acid sequence but has lost its tertiary triple-helical structure due to the denaturation process (figure 2(b)) [18, 28]. The loss of tertiary structure changes the availability of cell adhesion motifs on the protein surface, thereby resulting in different bio-instructive cues presented to cells by gelatin versus collagen [33, 34]. Another important difference between COL-HA and the Gel-HA control is that Gel-HA depends on a bio-inert PEG crosslinker that takes up to 20% of the hydrogel mixing volume. PEG does not allow for cells to attach, nor is it known to instruct cell behavior [66]. We eliminated the requirement for a PEG crosslinker in COL-HA since we hypothesized that a high PEG content might prevent cell–material interactions rather than provide them. Since the composition of the two Gel-HA control hydrogels differed only in the type and amount of PEG crosslinker (table 1), it is possible that the high concentration of four-arm PEG crosslinker reduced required cell–matrix interactions providing a potential explanation for the low cytokine levels in Gel-HA stiff CM.

Interestingly, structural differences were observed between collagen- and gelatin-based biomaterials (figure 2). Different studies have reported that MSCs lose their typical elongated fibroblastic shape and acquire round morphology after encapsulation in hydrogels with small pore sizes [14, 67–69]. Increased elongation of MSCs encapsulated in COL-HA, compared with poor elongation in both the soft and stiff Gel-HA conditions, suggest that the differences in cell morphology between COL-HA-MSC and Gel-HA-MSC constructs do not result from differences in bulk mechanical properties of the biomaterial, but rather depend on pore size and functionalization. The beneficial effect of large material pore size on MSC attachment and function has been demonstrated in prior studies [70]. In a setting where additional fabrication steps are added after hydrogel formation to create a porous hydrogel scaffold, differences in the material processing protocol can be used to create pores of different sizes and structures and study their effect on cells. For example, Matsiko *et al* achieved a difference in scaffold pore size by varying the lyophilization conditions between experimental groups of chemically identical scaffolds [70]. Consequently, the influence of pore size on cell function could be studied independently of the biochemical composition. In our study however, the cells were cultured in unprocessed hydrogels, while lyophilization was conducted on cell-free gels for analysis of the material structure, so that different processing protocols could not be used to fully uncouple structural parameters from biochemical cues. Because lyophilization was carried out side by side for all material groups, we assume that the observed differences in the lyophilized structure formed as a consequence of different biochemical hydrogel composition.

Encapsulation of MSCs in COL-HA demonstrated that the cells remained viable and assumed an elongated morphology within the hydrogel in comparison to commercially available hydrogels for cell culture. This observation suggested differences in interactions at the cell–material interface and we hypothesized that these differences would be reflected in the MSCs' secretory phenotype. While most studies that investigate cell–material interactions focus only on few cell-secreted mediators, we performed a detailed analysis of biomaterial-guided changes in the paracrine profile to validate our hypothesis. This analysis revealed complex regulation patterns and predicted a potent pro-angiogenic profile for MSCs encapsulated in COL-HA. Based on our previous studies, we hypothesized that the loss of cell attachment and spreading within the biomaterial negatively affects MSC's secretory phenotype [14]. In support of this hypothesis, the in depth secretome profiling revealed that hydrogel microenvironments differentially modulated the paracrine activity of encapsulated MSCs (figure 3). CM derived from MSCs encapsulated in COL-HA-biomaterials induced significantly stronger and more robust EC network formation compared to Gel-HA or 2D TCP (figure 4), with the strongest angiogenic effects mediated by COL-HA-Lam-MSCs. This finding validated the predicted paracrine pattern shift toward a pro-angiogenic secretome profile in a highly bioactive

biomaterial microenvironment. We propose that proteomics could be used to predict the resulting biological consequences of different material fabrication strategies at an early stage and to identify new applications for proven and established biomaterials. Our results also support the concept that the complex secretome of regenerative cells, such as MSCs, has stronger therapeutic potency than the administration of a single recombinant factor, such as rhVEGF.

The differences in paracrine activity between COL-HA and Gel-HA groups could be the consequence of different cell viabilities, however, 2D TCP cultures, which are known to maintain very high cell viability, showed a limited paracrine activity in our study. Another important influence on the paracrine activity could be the hydrogel stiffness. To test this possibility, the stiff Gel-HA control was included in this study. Although the modulus of this Gel-HA stiff biomaterial matched the COL-HA groups, their secretome profiles had very little similarity. Instead, the Gel-HA stiff biomaterial resulted in the lowest cytokine levels of all experimental groups, demonstrating that higher bulk stiffness alone does not augment the paracrine activity of MSCs. Tissue-specific bulk stiffness is a relevant design parameter for future *in vivo* studies, where the injected material would need to immobilize cells in a bone fracture gap, nerve gap or contracting muscle while complying to surrounding native tissue to avoid scarring and inflammation [71, 72]. However, bulk modulus might not accurately represent mechanical forces on the micro- or nanoscale sensed by cells, as recent literature highlights scale dependent differences in the stiffness of living tissues [39, 73, 74]. For example, while in our study the bulk stiffness values of different hydrogel substrates can be adjusted by changing crosslinking geometry and concentration, the microscale stiffness of a single collagen molecule lies in the GPa range and differs from the microscale stiffness of gelatin or other ECM components, regardless of bulk hydrogel properties [39, 75, 76]. By consequence, despite matched bulk stiffness, different substrates could trigger different mechanotransduction events in encapsulated cells.

As a standard reference we compared the secretome of COL-HA encapsulated cells to 2D MSC culture on polystyrene TCP. Interestingly, the osteoblastic marker OPG was one of the few factors that were secreted at highest levels from MSCs cultured on TCP. MSCs are known to be able to differentiate toward osteoblastic lineages and this result could be carefully interpreted in line with studies that demonstrate stiffness dependent regulation of cell fate [77], while on the other hand the many differences between the 2D and 3D microenvironments, such as culture dimensionality, stiffness, adhesion ligand type and density make causal attributions to a single factor difficult. The 2D culture condition resulted in a completely different secretome pattern than any of the 3D hydrogel conditions, implying that cell culture on polystyrene leads to non-physiological deviations in MSC biology.

Earlier studies have provided evidence that cell–cell and cell–matrix interactions within the 3D hydrogel are crucial for the regenerative function of MSCs [14, 78]. Here, we observed that functionally relevant shifts in the pattern of paracrine activity can be achieved by modifications of the biomaterial that support these cellular interactions, such as an attachment-enabling bioactive substrate, a microporous structure and the addition of specific ligands for integrin receptors. This observation is in line with the classic concept that cells derive cues about their phenotypic identity from their surrounding ECM and that decellularized ECM extracted from specific tissues can be used to guide cell differentiation in engineered tissues or organoids [41, 79, 80]. In this study, rather than focusing on cell differentiation, we extended the concept of matrix-guided cell behavior to shifts in the secretion pattern of therapeutically relevant proteins, which we analyzed using state of the art proteomics. Specifically, within a microenvironment composed of collagen, HA and laminin we observed the strongest MSC elongation. This correlated with the high angiogenic potency of COL-HA-Lam encapsulated MSCs, as predicted by a detailed analysis of their paracrine profile and functionally confirmed using in a model of endothelial tube formation.

5. Conclusion

This study demonstrates the fabrication and functionality of a biopolymer hydrogel to modulate the paracrine effects of therapeutic cells. We have combined biologically relevant material cues with important application-oriented features such as injectability and controlled crosslinking to produce a bio-instructive cell carrier for MSC encapsulation and protection. The fast fabrication protocol and on demand crosslinking mechanism are scalable and clinically translatable and were designed for human application, with all individual components of COL-HA or comparable biopolymers having been previously safely implanted into patients in a clinical setting [58–60]. Microporous COL-HA hydrogels promoted viability and elongation of encapsulated MSCs, which correlated with an expanded profile of secreted regenerative mediators. This effect was especially pronounced in COL-HA functionalized with laminin, with the paracrine profile inducing a strong EC capillary network formation. These results indicate that functionally relevant shifts in the pattern of paracrine activity can be achieved by specific modifications of the biomaterial substrate and

structure. Our tunable hydrogel platform creates the opportunity to generate user-defined libraries of bio-instructive hydrogels for targeted secretome modulation. In addition to the engineering of a suitable cell carrier matrix for future cell therapy studies, our study adds a new dimension to the current understanding of MSC secretome biology, suggests stronger therapeutic potency of a cell-derived secretome in comparison to the administration of a single recombinant factor and highlights important differences between 2D and 3D cell culture protocols. Our future studies will focus on *in vivo* characterization of COL-HA-encapsulated MSC in *in vivo* angiogenic and neuro-regenerative disease models as the next step towards bringing effective MSC therapies to patients.

Data availability statement

All data that support the findings of this study are included within the article (and any supplementary files).

Acknowledgments

This project has received funding from the European Union's Horizon 2020 research and innovation programme under Grant Agreement No. 733 006 (PACE) and No. 779 293. N M D.'s laboratory stay at Wake Forest Institute for Regenerative Medicine was made possible by funding of the travel grant by the Berlin-Brandenburg School for Regenerative Therapies GSC 203 and participation in the Visiting International Scholar Program (VISP) at the Wake Forest Institute for Regenerative Medicine. This work was also supported by Federal Ministry of Education and Research, Germany, in the Programme Health Research (BCRT Grant No. 13GW0098 and 13GW0099), through the German Research Foundation (DFG) "collaborative research center SFB1444-TP1/2" and the Helmholtz Association through program-oriented funding. The authors gratefully acknowledge the German Research Foundation (DFG) for funding S G (GE2512/2-2 & SFB 1444). S D F is supported by a grant from the National Institute of Health (T32CA247819). NMD acknowledges the advice of Dr. Fatih Zor, MD (Microsurgery Lab at WFIRM) in the planning of the experimental design and for his co-mentorship support during the follow on experiments. The authors thank the Core Facility for Electron Microscopy of the Charité for support in acquisition of the SEM data, Dr Aleksander Skardal (Ohio State University) for his support in initial discussions, Kenneth Gyabaah (Wake Forest Institute for Regenerative Medicine) for helpful advice regarding imaging techniques and Dr Nicola Brindle (BIH Center for Regenerative Therapies) for proof-reading the manuscript.

ORCID iDs

Norman M Drzeniek https://orcid.org/0000-0001-6562-2351
Andrea Mazzocchi https://orcid.org/0000-0002-5534-9678
Stephan Schlickeiser https://orcid.org/0000-0003-3142-2890
Steven D Forsythe https://orcid.org/0000-0003-4099-6642
Guido Moll https://orcid.org/0000-0001-6173-5957
Sven Geißler https://orcid.org/0000-0002-8750-6324
Petra Reinke https://orcid.org/0000-0003-0771-4375
Manfred Gossen https://orcid.org/0000-0002-1761-4063
Vijay S Gorantla https://orcid.org/0000-0003-0686-059X
Hans-Dieter Volk https://orcid.org/0000-0002-7743-6668
Shay Soker https://orcid.org/0000-0002-8458-9232

References

[1] Bagno L, Hatzistergos K E, Balkan W and Hare J M 2018 Mesenchymal stem cell-based therapy for cardiovascular disease: progress and challenges *Mol. Ther.* **26** 1610–23
[2] Mukai T, Tojo A and Nagamura-Inoue T 2018 Mesenchymal stromal cells as a potential therapeutic for neurological disorders *Regen. Ther.* **9** 32–7
[3] Steinert A F, Rackwitz L, Gilbert F, Nöth U and Tuan R S 2012 Concise review: the clinical application of mesenchymal stem cells for musculoskeletal regeneration: current status and perspectives *Stem. Cells Transl. Med.* **1** 237–47
[4] Burnham A J, Daley-Bauer L P and Horwitz E M 2020 Mesenchymal stromal cells in hematopoietic cell transplantation *Blood Adv.* **4** 5877–87
[5] Moll G, Drzeniek N, Kamhieh-Milz J, Geissler S, Volk H-D and Reinke P 2020 MSC therapies for COVID-19: importance of patient coagulopathy, thromboprophylaxis, cell product quality and mode of delivery for treatment safety and efficacy *Front. Immunol.* **11** 1091
[6] Caplan A I and Correa D 2011 The MSC: an injury drugstore *Cell Stem. Cell* **9** 11–5
[7] Lee S, Choi E, Cha M-J and Hwang K-C 2015 Cell adhesion and long-term survival of transplanted mesenchymal stem cells: a prerequisite for cell therapy *Oxid. Med. Cell. Longevity* **2015** 1–9
[8] Moll G, Drzeniek N, Kamhieh-Milz J, Geissler S and Reinke P 2020 Editorial comment: variables affecting the presence of mesenchymal stromal cells in the peripheral blood and their relationship with apheresis product *Br. J. Haematol.* **189** 593–6
[9] Moll G, Ankrum J A, Kamhieh-Milz J, Bieback K, Ringdén O, Volk H-D, Geissler S and Reinke P 2019 Intravascular mesenchymal stromal/stem cell therapy product diversification: time for new clinical guidelines *Trends Mol. Med.* **25** 149–63
[10] Caplan H *et al* 2019 Mesenchymal stromal cell therapeutic delivery: translational challenges to clinical application *Front. Immunol.* **10** 1645
[11] Wagner B and Henschler R 2013 Fate of intravenously injected mesenchymal stem cells and significance for clinical application *Adv. Biochem. Eng. Biotechnol.* **130** 19–37

[12] Rodriguez-Fuentes D E *et al* 2020 Mesenchymal stem cells current clinical applications: a systematic review *Arch. Med. Res.* **52** 93–101

[13] Dong C and Lv Y 2016 Application of collagen scaffold in tissue engineering: recent advances and new perspectives *Polymers* **8** 42

[14] Qazi T H, Mooney D J, Duda G N and Geissler S 2017 Biomaterials that promote cell-cell interactions enhance the paracrine function of MSCs *Biomaterials* **140** 103–14

[15] Murphy S V and Atala A 2014 3D bioprinting of tissues and organs *Nat. Biotechnol.* **32** 773–85

[16] Petcu E B *et al* 2018 3D printing strategies for peripheral nerve regeneration *Biofabrication* **10** 032001

[17] Zhang Z, Jørgensen M L, Wang Z, Amagat J, Wang Y, Li Q, Dong M and Chen M 2020 3D anisotropic photocatalytic architectures as bioactive nerve guidance conduits for peripheral neural regeneration *Biomaterials* **253** 120108

[18] Drury J L and Mooney D J 2003 Hydrogels for tissue engineering: scaffold design variables and applications *Biomaterials* **24** 4337–51

[19] Forsythe S *et al* 2020 Development of a colorectal cancer 3D micro-tumor construct platform from cell lines and patient tumor biospecimens for standard-of-care and experimental drug screening *Ann. Biomed. Eng.* **48** 940–52

[20] Arkenberg M R, Nguyen H D and Lin C-C 2020 Recent advances in bio-orthogonal and dynamic crosslinking of biomimetic hydrogels *J. Mater. Chem.* B **8** 7835–55

[21] DeForest C A, Polizzotti B D and Anseth K S 2009 Sequential click reactions for synthesizing and patterning three-dimensional cell microenvironments *Nat. Mater.* **8** 659–64

[22] Nih L R, Gojgini S, Carmichael S T and Segura T 2018 Dual-function injectable angiogenic biomaterial for the repair of brain tissue following stroke *Nat. Mater.* **17** 642–51

[23] Reinke S *et al* 2013 Terminally differentiated CD8(+) T cells negatively affect bone regeneration in humans *Sci. Transl. Med.* **5** 177ra36

[24] Glaeser J D, Geissler S, Ode A, Schipp C J, Matziolis G, Taylor W R, Knaus P, Perka C, Duda G N and Kasper G 2010 Modulation of matrix metalloprotease-2 levels by mechanical loading of three-dimensional mesenchymal stem cell constructs: impact on in vitro tube formation *Tissue Eng. Part* A **16** 3139–48

[25] Andrzejewska A *et al* 2019 Multi-parameter analysis of biobanked human bone marrow stromal cells shows little influence for donor age and mild comorbidities on phenotypic and functional properties *Front. Immunol.* **10** 2474

[26] Schindelin J *et al* 2012 Fiji: an open-source platform for biological-image analysis *Nat. Methods* **9** 676–82

[27] Carpentier G *et al* 2020 Angiogenesis analyzer for imageJ—a comparative morphometric analysis of "endothelial tube formation assay" and 'fibrin bead assay' *Sci. Rep.* **10** 11568

[28] Jorgensen A M, Yoo J J and Atala A 2020 Solid organ bioprinting: strategies to achieve organ function *Chem. Rev.* **120** 11093–127

[29] Murphy S V, De Coppi P and Atala A 2020 Opportunities and challenges of translational 3D bioprinting *Nat. Biomed. Eng.* **4** 370–80

[30] Kafi M A, Aktar M K, Phanny Y and Todo M 2019 Adhesion, proliferation and differentiation of human mesenchymal stem cell on chitosan/collagen composite scaffold *J. Mater. Sci. Mater. Med.* **30** 131

[31] Somaiah C, Kumar A, Mawrie D, Sharma A, Patil S D, Bhattacharyya J, Swaminathan R and Jaganathan B G 2015 collagen promotes higher adhesion, survival and proliferation of mesenchymal stem cells *PLoS One* **10** e0145068

[32] Forsythe S D, Sasikumar S, Moaven O, Sivakumar H, Shen P, Levine E A, Soker S, Skardal A and Votanopoulos K I 2020 Personalized identification of optimal HIPEC perfusion protocol in patient-derived tumor organoid platform *Ann. Surg. Oncol.* **27** 4950–60

[33] Davidenko N, Hamaia S, Bax D V, Malcor J-D, Schuster C F, Gullberg D, Farndale R W, Best S M and Cameron R E 2018 Selecting the correct cellular model for assessing of the biological response of collagen-based biomaterials *Acta Biomater.* **65** 88–101

[34] Davidenko N, Schuster C F, Bax D V, Farndale R W, Hamaia S, Best S M and Cameron R E 2016 Evaluation of cell binding to collagen and gelatin: a study of the effect of 2D and 3D architecture and surface chemistry *J. Mater. Sci. Mater.* M **27** 148

[35] Slevin M, Kumar S and Gaffney J 2002 Angiogenic oligosaccharides of hyaluronan induce multiple signaling pathways affecting vascular endothelial cell mitogenic and wound healing responses *J. Biol. Chem.* **277** 41046–59

[36] Hoyle C E, Lee T Y and Roper T 2004 Thiol-enes: chemistry of the past with promise for the future *J. Polym. Sci. Pol. Chem.* **42** 5301–38

[37] Ruskowitz E R and DeForest C A 2019 Proteome-wide analysis of cellular response to ultraviolet light for biomaterial synthesis and modification *ACS Biomater. Sci. Eng.* **5** 2111–6

[38] Skardal A, Mack D, Atala A and Soker S 2013 Substrate elasticity controls cell proliferation, surface marker expression and motile phenotype in amniotic fluid-derived stem cells *J. Mech. Behav. Biomed. Mater.* **17** 307–16

[39] Guimarães C F *et al* 2020 The stiffness of living tissues and its implications for tissue engineering *Nat. Rev. Mater.* **5** 351–70

[40] Maacha S, Sidahmed H, Jacob S, Gentilcore G, Calzone R, Grivel J-C and Cugno C 2020 Paracrine mechanisms of mesenchymal stromal cells in angiogenesis *Stem. Cells Int.* **2020** 4356359

[41] Ullah I, Abu-Dawud R, Busch J F, Rabien A, Erguen B, Fischer I, Reinke P and Kurtz A 2019 VEGF—Supplemented extracellular matrix is sufficient to induce endothelial differentiation of human iPSC *Biomaterials* **216** 119283

[42] Odorisio T, Cianfarani F, Failla C M and Zambruno G 2006 The placenta growth factor in skin angiogenesis *J. Dermatol. Sci.* **41** 11–9

[43] Chang H K *et al* 2016 Inducible HGF-secreting human umbilical cord blood-derived MSCs produced via TALEN-mediated genome editing promoted angiogenesis *Mol. Ther.* **24** 1644–54

[44] Yu Q and Stamenkovic I 2000 Cell surface-localized matrix metalloproteinase-9 proteolytically activates TGF-beta and promotes tumor invasion and angiogenesis *Genes Dev.* **14** 163–76

[45] Koch A E, Polverini P, Kunkel S, Harlow L, DiPietro L, Elner V, Elner S and Strieter R 1992 Interleukin-8 as a macrophage-derived mediator of angiogenesis *Science* **258** 1798–801

[46] Meller R, Stevens S L, Minami M, Cameron J A, King S, Rosenzweig H, Doyle K, Lessov N S, Simon R P and Stenzel-Poore M P 2005 Neuroprotection by osteopontin in stroke *J. Cereb. Blood Flow Metab.* **25** 217–25

[47] Oo T F, Kholodilov N and Burke R E 2003 Regulation of natural cell death in dopaminergic neurons of the substantia nigra by striatal glial cell line-derived neurotrophic factor *in vivo J. Neurosci.* **23** 5141–8

[48] Patterson P H 1994 Leukemia inhibitory factor, a cytokine at the interface between neurobiology and immunology *Proc. Natl Acad. Sci. USA* **91** 7833–5

[49] Lin J, Niimi Y, Clausi M G, Kanal H D and Levison S W 2020 Neuroregenerative and protective functions of leukemia inhibitory factor in perinatal hypoxic-ischemic brain injury *Exp. Neurol.* **330** 113324

[50] Grant D S *et al* 2002 Decorin suppresses tumor cell-mediated angiogenesis *Oncogene* **21** 4765–77

[51] Streit M, Riccardi L, Velasco P, Brown L F, Hawighorst T, Bornstein P and Detmar M 1999 Thrombospondin-2: a potent endogenous inhibitor of tumor growth and angiogenesis *Proc. Natl Acad. Sci. USA* **96** 14888–93

[52] Thurston G, Rudge J S, Ioffe E, Zhou H, Ross L, Croll S D, Glazer N, Holash J, McDonald D M and Yancopoulos G D

2000 Angiopoietin-1 protects the adult vasculature against plasma leakage *Nat. Med.* **6** 460–3
[53] Tanaka T, Narazaki M and Kishimoto T 2014 *IL-6 in inflammation, immunity, and disease Cold Spring Harb. Perspect. Biol.* **6** a016295
[54] Caricasole A *et al* 2004 Induction of Dickkopf-1, a negative modulator of the Wnt pathway, is associated with neuronal degeneration in Alzheimer's brain *J. Neurosci.* **24** 6021–7
[55] Wu J B *et al* 2015 Plasminogen activator inhibitor-1 inhibits angiogenic signaling by uncoupling vascular endothelial growth factor receptor-2-alpha(V)beta(3) integrin cross talk *Arterioscl. Throm. Vas.* **35** 111–20
[56] Devy L *et al* 2002 The pro- or antiangiogenic effect of plasminogen activator inhibitor 1 is dose dependent *FASEB J.* **16** 147–54
[57] Cawley K M *et al* 2020 local production of osteoprotegerin by osteoblasts suppresses bone resorption *Cell. Rep.* **32** 108052
[58] Volpi P, Zini R, Erschbaumer F, Beggio M, Busilacchi A and Carimati G 2020 Effectiveness of a novel hydrolyzed collagen formulation in treating patients with symptomatic knee osteoarthritis: a multicentric retrospective clinical study *Int. Orthop.* **45** 375–80
[59] Corcos J, Collet J P, Shapiro S, Herschorn S, Radomski S B, Schick E, Gajewski J B, Benedetti A, MacRamallah E and Hyams B 2005 Multicenter randomized clinical trial comparing surgery and collagen injections for treatment of female stress urinary incontinence *Urology* **65** 898–904
[60] Maheu E, Rannou F and Reginster J Y 2016 Efficacy and safety of hyaluronic acid in the management of osteoarthritis: evidence from real-life setting trials and surveys *Semin. Arthritis Rheum.* **45** S28–33
[61] Paulsson M 1992 The role of laminin in attachment, growth, and differentiation of cultured cells: a brief review *Cytotechnology* **9** 99–106
[62] Peng K Y *et al* 2017 Extracellular matrix protein laminin enhances mesenchymal stem cell (MSC) paracrine function through alphavbeta3/CD61 integrin to reduce cardiomyocyte apoptosis *J. Cell. Mol. Med.* **21** 1572–83
[63] Moretti F A, Chauhan A K, Iaconcig A, Porro F, Baralle F E and Muro A F 2007 A major fraction of fibronectin present in the extracellular matrix of tissues is plasma-derived *J. Biol. Chem.* **282** 28057–62
[64] Skardal A, Murphy S V, Crowell K, Mack D, Atala A and Soker S 2017 A tunable hydrogel system for long-term release of cell-secreted cytokines and bioprinted *in situ* wound cell delivery *J. Biomed. Mater. Res.* B **105** 1986–2000
[65] Mazzocchi A, Devarasetty M, Huntwork R, Soker S and Skardal A 2018 Optimization of collagen type I-hyaluronan hybrid bioink for 3D bioprinted liver microenvironments *Biofabrication* **11** 015003
[66] Zhu J 2010 Bioactive modification of poly(ethylene glycol) hydrogels for tissue engineering *Biomaterials* **31** 4639–56
[67] Levato R, Visser J, Planell J A, Engel E, Malda J and Mateos-Timoneda M A 2014 Biofabrication of tissue constructs by 3D bioprinting of cell-laden microcarriers *Biofabrication* **6** 035020
[68] Gao G, Schilling A F, Hubbell K, Yonezawa T, Truong D, Hong Y, Dai G and Cui X 2015 Improved properties of bone and cartilage tissue from 3D inkjet-bioprinted human mesenchymal stem cells by simultaneous deposition and photocrosslinking in PEG-GelMA *Biotechnol. Lett.* **37** 2349–55
[69] Du M, Chen B, Meng Q, Liu S, Zheng X, Zhang C, Wang H, Li H, Wang N and Dai J 2015 3D bioprinting of BMSC-laden methacrylamide gelatin scaffolds with CBD-BMP2-collagen microfibers *Biofabrication* **7** 044104
[70] Matsiko A, Gleeson J P and O'Brien F J 2015 Scaffold mean pore size influences mesenchymal stem cell chondrogenic differentiation and matrix deposition *Tissue Eng. Part* A **21** 486–97
[71] Moshayedi P, Ng G, Kwok J C F, Yeo G S H, Bryant C E, Fawcett J W, Franze K and Guck J 2014 The relationship between glial cell mechanosensitivity and foreign body reactions in the central nervous system *Biomaterials* **35** 3919–25
[72] Minev I R *et al* 2015 Biomaterials. Electronic dura mater for long-term multimodal neural interfaces *Science* **347** 159–63
[73] Herrera A, Hellwig J, Leemhuis H, Von Klitzing R, Heschel I, Duda G N and Petersen A 2019 From macroscopic mechanics to cell-effective stiffness within highly aligned macroporous collagen scaffolds *Mater. Sci. Eng.* C **103** 109760
[74] Harley B A, Freyman T M, Wong M Q and Gibson L J 2007 A new technique for calculating individual dermal fibroblast contractile forces generated within collagen-GAG scaffolds *Biophys. J.* **93** 2911–22
[75] Sasaki N and Odajima S 1996 Stress-strain curve and Young's modulus of a collagen molecule as determined by the x-ray diffraction technique *J. Biomech.* **29** 655–8
[76] Wenger M P E, Bozec L, Horton M A and Mesquida P 2007 Mechanical properties of collagen fibrils *Biophys. J.* **93** 1255–63
[77] Olivares-Navarrete R, Lee E M, Smith K, Hyzy S L, Doroudi M, Williams J K, Gall K, Boyan B D and Schwartz Z 2017 Substrate stiffness controls osteoblastic and chondrocytic differentiation of mesenchymal stem cells without exogenous stimuli *PLoS One* **12** e0170312
[78] Pumberger M *et al* 2016 Synthetic niche to modulate regenerative potential of MSCs and enhance skeletal muscle regeneration *Biomaterials* **99** 95–108
[79] Giobbe G G *et al* 2019 Extracellular matrix hydrogel derived from decellularized tissues enables endodermal organoid culture *Nat. Commun.* **10** 5658
[80] Jorgensen A M, Chou Z, Gillispie G, Lee S J, Yoo J J, Soker S and Atala A 2020 Decellularized skin extracellular matrix (dsECM) improves the physical and biological properties of fibrinogen hydrogel for skin bioprinting applications *Nanomaterials* **10** 1484

Publication 2: Journal Summary List

Journal Data Filtered By: **Selected JCR Year: 2021** Selected Editions: SCIE,SSCI Selected Categories: **"ENGINEERING, BIOMEDICAL"** Selected Category Scheme: WoS

Gesamtanzahl: 98 Journale

Rank	Full Journal Title	Total Cites	Journal Impact Factor	Eigenfaktor
1	Nature Biomedical Engineering	10,605	29.234	0.02704
2	Bioactive Materials	6,655	16.874	0.00480
3	Biomaterials Research	1,897	15.863	0.00224
4	BIOMATERIALS	131,366	15.304	0.05910
5	npj Regenerative Medicine	1,385	14.404	0.00251
6	MEDICAL IMAGE ANALYSIS	16,080	13.828	0.01971
7	Annual Review of Biomedical Engineering	5,968	11.324	0.00365
8	Advanced Healthcare Materials	24,096	11.092	0.02723
9	Biofabrication	7,979	11.061	0.00763
10	IEEE TRANSACTIONS ON MEDICAL IMAGING	32,367	11.037	0.03385
11	Materials Today Bio	796	10.761	0.00099
12	Bioengineering & Translational Medicine	1,581	10.684	0.00250
13	Acta Biomaterialia	58,946	10.633	0.04185
14	Photoacoustics	1,827	9.656	0.00293
15	COMPUTERIZED MEDICAL IMAGING AND GRAPHICS	3,973	7.422	0.00342
16	International Journal of Bioprinting	1,006	7.422	0.00109
17	Tissue Engineering Part B-Reviews	5,132	7.376	0.00285
18	Physical and Engineering Sciences in Medicine	862	7.099	0.00114
19	IEEE Reviews in Biomedical Engineering	2,213	7.073	0.00179
20	COMPUTER METHODS AND PROGRAMS IN BIOMEDICINE	16,120	7.027	0.01560

Biomaterials 294 (2023) 121971

Contents lists available at ScienceDirect

Biomaterials

journal homepage: www.elsevier.com/locate/biomaterials

Immuno-engineered mRNA combined with cell adhesive niche for synergistic modulation of the MSC secretome

Norman Michael Drzeniek [a,b,c], Nourhan Kahwaji [a,b], Stephan Schlickeiser [a,b], Petra Reinke [b,d], Sven Geißler [b,d,e], Hans-Dieter Volk [a,b,**], Manfred Gossen [f,g,*]

[a] Charité – Universitätsmedizin Berlin, Corporate Member of Freie Universität Berlin and Humboldt-Universität zu Berlin, Institute of Medical Immunology, Augustenburger Platz 1, 13353, Berlin, Germany
[b] Berlin Institute of Health at Charité – Universitätsmedizin Berlin, BIH Center for Regenerative Therapies (BCRT), Föhrer Straße 15, 13353, Berlin, Germany
[c] Berlin-Brandenburg School for Regenerative Therapies (BSRT; Graduate School 203 of the German Excellence Initiative), Augustenburger Platz 1, 13353, Berlin, Germany
[d] Charité – Universitätsmedizin Berlin, Corporate Member of Freie Universität Berlin and Humboldt-Universität zu Berlin, Berlin Center for Advanced Therapies (BeCAT), Augustenburger Platz 1, 13353, Berlin, Germany
[e] Berlin Institute of Health at Charité – Universitätsmedizin Berlin, Julius Wolff Institute (JWI), Augustenburger Platz 1, 13353, Berlin, Germany
[f] Institute of Active Polymers, Helmholtz-Zentrum Hereon, Kantstraße 55, 14513, Teltow, Germany
[g] Berlin-Brandenburg Center for Regenerative Therapies (BCRT), Augustenburger Platz 1, 13353, Berlin, Germany

ARTICLE INFO

Keywords:
mRNA
Innate immune response
Collagen
Secretome
Angiogenesis
Mesenchymal stromal/stem cell

ABSTRACT

In vitro transcribed (IVT-)mRNA has entered center stage for vaccine development due to its immune co-stimulating properties. Given the widely demonstrated safety of IVT-mRNA-based vaccines, we aimed to adopt IVT-mRNA encoding VEGF for secretory phenotype modulation of therapeutic cells. However, we observed that the immunogenicity of IVT-mRNA impairs the endogenous secretion of pro-angiogenic mediators from transfected mesenchymal stromal cells, instead inducing anti-angiogenic chemokines. This inflammatory secretome modulation limits the application potential of unmodified IVT-mRNA for cell therapy manufacturing, pro-angiogenic therapy and regenerative medicine.

To uncouple immunogenicity from the protein expression functionality, we immuno-engineered IVT-mRNA with different chemically modified ribonucleotides. 5-Methoxy-uridine-modification of IVT-mRNA rescued the endogenous secretome pattern of transfected cells and prolonged secretion of IVT-mRNA-encoded VEGF.

We found that high secretion of IVT-mRNA-encoded protein further depends on optimized cell adhesion. Cell encapsulation in a collagen-hyaluronic acid hydrogel increased secretion of IVT-mRNA-encoded VEGF and augmented the endogenous secretion of supporting pro-angiogenic mediators, such as HGF.

Integrating minimally immunogenic mRNA technology with predesigned matrix-derived cues allows for the synergistic combination of multiple dimensions of cell manipulation and opens routes for biomaterial-based delivery of mRNA-engineered cell products. Such multimodal systems could present a more biologically relevant way to therapeutically address complex multifactorial processes such as tissue ischemia, angiogenesis, and regeneration.

1. Introduction

Biological processes requiring a high degree of tissue plasticity, such as embryogenesis and organ formation but also revascularization and regeneration, are orchestrated by a complex interplay of multiple cytokines and growth factors [1]. However, most therapeutic strategies addressing these processes rely on the administration of a single factor. For example, vascular endothelial growth factor A (VEGF-A) is a driving growth factor behind angiogenesis, but not as effective when used as a single agent. Administration of VEGF-A to ischemic tissues can be key to

* Corresponding author. Institute of Active Polymers, Helmholtz-Zentrum Hereon, Kantstraße 55, 14513, Teltow, Germany.
** Corresponding author. Charité – Universitätsmedizin Berlin, Corporate Member of Freie Universität Berlin and Humboldt-Universität zu Berlin, Institute of Medical Immunology, Augustenburger Platz 1, 13353, Berlin, Germany.
E-mail addresses: hans-dieter.volk@charite.de (H.-D. Volk), manfred.gossen@hereon.de (M. Gossen).

https://doi.org/10.1016/j.biomaterials.2022.121971
Received 14 July 2022; Received in revised form 5 December 2022; Accepted 16 December 2022
Available online 26 December 2022

cardiovascular regeneration, however, VEGF-A gene therapy for revascularization in critical limb ischemia, with the aim to deliver high levels of VEGF, has not conclusively shown benefits in clinical trials, with side effects becoming evident at high doses [2,3]. Used as a stand-alone factor, VEGF-A increases vessel permeability leading to edema [4,5] and may lack angiogenic potency despite high doses. Physiologically, VEGF-mediated angiogenesis requires support by other pro-angiogenic mediators such as hepatocyte growth factor (HGF), which possesses similar angiogenic signalling properties as VEGF but stabilizes the endothelial cell barrier [6,7].

Therefore, the development of multimodal and/or multifactorial therapeutic regimens that allow multidimensional control over synergistic mediator patterns is a promising concept to address complex biological processes, such as angiogenesis or tissue regeneration [1].

Mesenchymal stromal/stem cells (MSCs) are secretory active cells that hold promise as a sustained *in situ* source of pro-angiogenic growth factors, including VEGF-A as well as other synergistic factors such as HGF [8–10]. However, a recent Phase III multi center trial of placenta derived MSC-like cells for critical limb ischemia ultimately failed to reach statistically significant efficacy [11]. This suggests that while cell transplantation is, in principle, a valid multifactorial strategy to support revascularization, augmenting MSCs' therapeutic potency through targeted shifts in their secretome profile may be necessary to achieve satisfactory therapeutic efficacy.

Additionally, MSC functionality also depends on cell adhesion and *in situ* persistence [12], therefore requiring a viable delivery strategy. As such, encapsulation in a pre-designed biomaterial prior to transplantation has established itself as a preferred strategy for local delivery of adherent cells. Aside from physically protecting cells *in situ* and improving engraftment [13] a synthetic interactive biomaterial microenvironment provides an opportunity to modulate therapeutically relevant cell functions such as the secretion of growth factors through presentation of bioactive cues and adhesion motifs [14]. We and others have previously shown that a type-I collagen 3D niche shifts the secretome pattern of MSCs toward a stronger pro-angiogenic phenotype through integrin signalling [15,16]. Such matrix-mediated effects can affect multiple signalling molecules relevant for a given biological process in a broad fashion. However, they are inherently unselective and difficult to limit to specific factors. Thus, a mechanistic understanding of the processes at the matrix-cell biointerface is an important field of research.

In addition to the broad modulation that can be achieved by matrix-derived cues, the secretion of selected key factors, such as VEGF for angiogenesis, can be achieved with high precision and selectivity by genetic modification of cells and forced overexpression of the desired factor. The use of traditional methods for stable genetic modification of cells, such as viral vectors, transposon, or CRISPR/Cas-mediated chromosomal integration, carries the safety risk of oncogene activation and tumour formation [17,18]. Therefore, the clinical translation of such therapeutics has been challenging. Additionally, integrative DNA strategies often suffer from their susceptibility to epigenetic mechanisms of gene silencing. In contrast, transient gene expression via in vitro transcribed (IVT) mRNA, the driving technology behind SARS-CoV2 vaccines, has established itself as the first recombinant nucleic acid therapeutic to be routinely applied in a broad population [19]. In contrast to traditional DNA-based cell editing, IVT-mRNA does not enter the cell nucleus upon transfection, instead directly utilizing the cytoplasmic translation machinery. This results in fast and highly efficient protein expression in the cytoplasm and eliminates any risk for genotoxicity or mutagenesis [20].

Given its excellent efficacy and safety profile, IVT-mRNA also has the potential to transform the treatment of ischemic and cardiovascular disease. IVT-VEGF-mRNA is the first clinically applied mRNA drug coding for a secreted protein. It has been shown to increase skin blood flow in patients with type 2 diabetes mellitus [21] and is currently being investigated for angiogenesis-mediated regeneration of myocardial ischemia (ClinicalTrials.gov : NCT03370887) [22,23].

The turnover of synthetic mRNAs in the cytoplasm in absence of ongoing re-synthesis or re-delivery limits the time window for therapeutically relevant protein synthesis to a few days at best. On the upside, this eliminates the long-term risks associated with permanent growth factor overexpression. On the downside, however, for applications requiring longer-term protein synthesis this transient mode of action is often considered a major limitation of mRNA technology [20]. Prolonging the expression duration of IVT-mRNA has become one of the major challenges in its adoption for widespread pharmaceutical use.

The intrinsic immune adjuvant functionality of IVT-mRNA places the technology at centre stage for vaccine development against malignant and infectious diseases, whilst potentially limiting its application in cell editing and regenerative therapy, where excessive inflammation is not desired. Immunogenicity and intracellular instability of IVT-mRNA results from its recognition by intracellular pattern recognition receptors (PRR; Fig. 1b) [24]. Optimization of the RNA design toward low uridine (U) content can minimize recognition by PRR, but U cannot be eliminated completely from the RNA sequence [25]. Replacement of U by chemically modified nucleotides such as pseudo-uridine (ψ) [24], and more recently N1-methylpseudouridine (m1ψ) [26] and 5-methoxyuridine (5moU) [27] has been proposed to reduce immunogenicity and increase protein expression (Fig. 1c). Most comparative studies have been conducted in cell lines, but the efficacy and potential side effects of nucleotide-modified IVT-mRNA on primary (therapeutically relevant) human cells remains poorly characterized.

We propose IVT-mRNA as a powerful tool to improve the potency of therapeutic cells or other advanced therapy medicinal products (ATMPs; Fig. 1a). Yet to harness the full potential of IVT-mRNA in cardiovascular regeneration, its immunogenicity needs to be uncoupled from its protein expression functionality, which is facilitated by the availability of said chemical nucleotide modifications. Otherwise, unchecked immune stimulation might impair the function of the transfected cells, alter paracrine signalling toward other cells and cause excessive inflammation, which in turn could disrupt the angiogenic cascade or exacerbate pathological processes, for example in cardiovascular disease (Fig. 1b and c) [28–30].

Here, we investigate whether immuno-engineering of IVT-mRNA can allow overexpression of a pro-angiogenic paracrine mediator without disturbing the natural pro-angiogenic secretome of MSCs. We systematically investigate the effects of long established and more recently introduced IVT-mRNA nucleotide modifications on protein expression kinetics, innate immune response, metabolic activity, and paracrine signalling of transfected cells, with special attention to angiogenic mediators.

Additionally, we propose that combining mRNA-mediated editing of cells with their encapsulation in a predesigned microenvironment could allow to orchestrate cellular paracrine effects in multiple dimensions, including (I) broad matrix-mediated pro-angiogenic secretome modulation, (II) targeted overexpression of a key growth factor (here VEGF-165), as well as (III) inflammatory signalling in response to unmodified and immuno-engineered mRNAs. To the best of our knowledge, multimodal biofabrication strategies that combine genetic modification of cells and encapsulation in a predesigned microenvironment remain so far unexplored. Cell transfection and encapsulation require different processing steps, timing and technique and may cause accumulated cell stress. Here we demonstrate a low stress, easily translatable process for cell transfection and encapsulation in an injectable hydrogel, combining mRNA- and matrix-mediated effects on angiogenic signalling. We investigate the role that IVT-mRNA immune engineering and cell attachment within the biomaterial play for cell survival, IVT-mRNA expression and endogenous production of angiogenic cytokines, such as HGF.

In summary, by uncoupling the protein expression functionality of IVT-mRNA from its immunogenicity and pairing it with optimized cell adhesion in biomaterial niche, we propose a multimodal cell

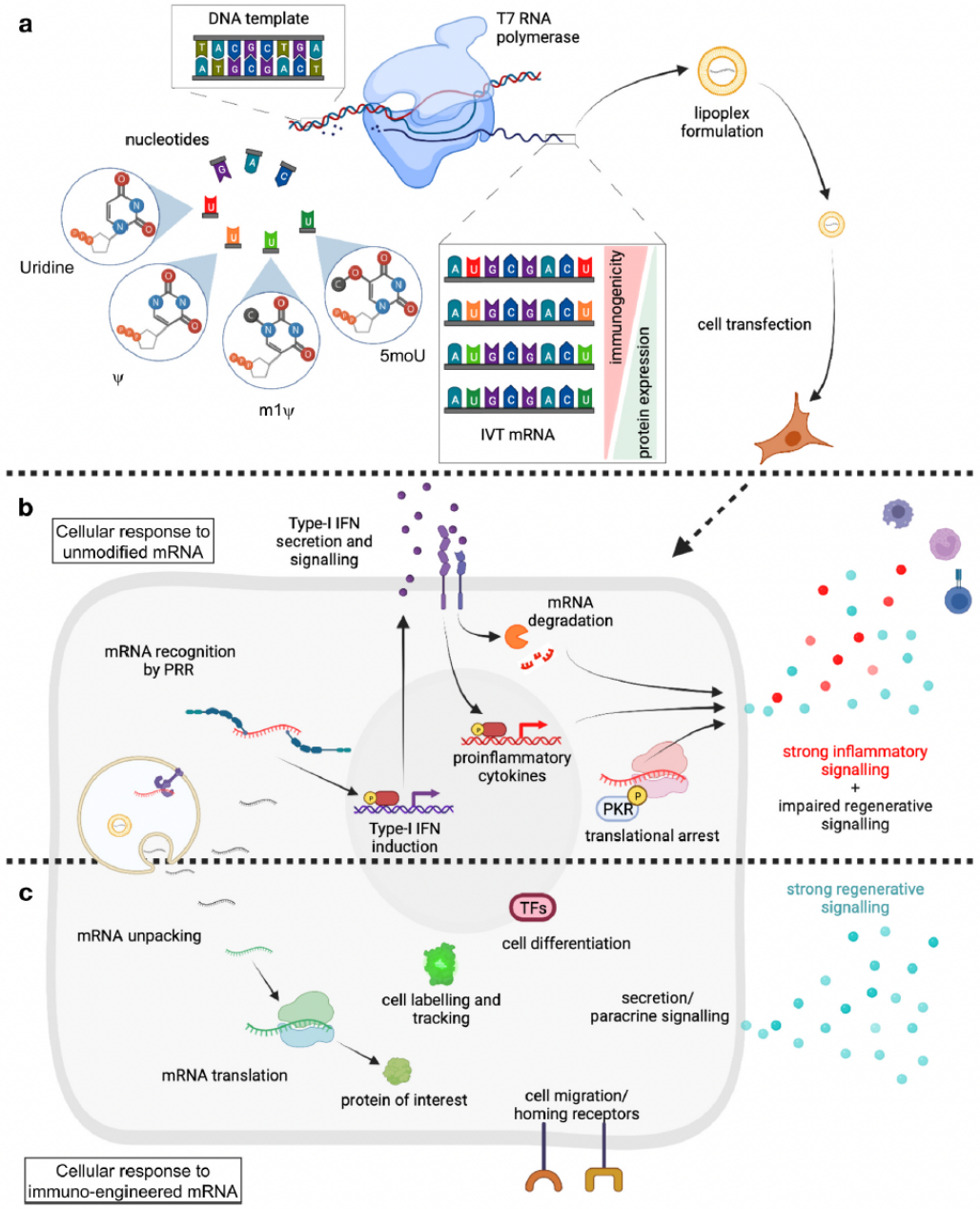

Fig. 1. Chemical nucleotide modification of IVT-mRNA determines cellular response, expanding potential mRNA applications.

a) Synthetic mRNA was transcribed in vitro (IVT) using a DNA template, a polymerase and nucleotides with or without different chemical modifications. Chemical modification of uridine (pseudouridine (ψ), N1-methylpseudouridine (m1ψ) or 5-methoxyuridine (5moU)) influences both the immunogenicity and expression duration of IVT-mRNA. The IVT-mRNA is complexed with a delivery vehicle, such as a cationic lipid nanoparticle, to facilitate cell transfection.

b) Unmodified mRNA is recognized by pattern recognition receptors (PRR), which triggers the expression and secretion of type-I interferons. Autocrine or paracrine interferon signalling results in the expression of interferon-stimulated genes, mRNA degradation, translational arrest by protein kinase R and the secretion of chemokines (red) which attract immune cells.

c) Immuno-engineered IVT-mRNA is minimally immunogenic and minimizes PRR recognition. It is translated efficiently at the ribosome without any risk of genomic integration or oncogene activation. No or minimal interferon response is triggered, less degradation results in longer expression windows and the natural paracrine signalling of the transfected cell remains unaffected. This opens up new applications for immuno-engineered mRNA, especially in the regenerative and cardiovascular fields where an excessive immune response is undesirable. Potential applications range from modification of therapeutic cell products with secretable proteins or homing receptors, fluorescent cell tracking to cell differentiation through expression of transcription factors.

engineering system to orthogonally control and orchestrate patterns of angiogenesis-promoting cytokines and growth factors. Such multi-level control over patterns of soluble factors is an important step toward therapeutically addressing complex biological processes at a molecular level.

2. Materials and methods

2.1. In vitro culture of human bone marrow mesenchymal stromal/stem cells

Human bone marrow mesenchymal stromal/stem cells (MSCs) were provided by the 'Cell Harvesting' core facility at the BIH Center for Regenerative Therapies (BCRT). MSCs were derived from bone marrow biopsies of patients undergoing hip replacement at Charité—Universitätsmedizin Berlin, as previously stated [16]. Written informed consent was given, and ethics approval was obtained from the local ethics committee/institutional review board (IRB) of the Charité—Universitätsmedizin Berlin (number of approval: EA2/089/20). All experiments in this study were performed in biological replicates using primary cells from at least two different donors. The cells were cultured in low glucose DMEM supplemented with 10% v/v fetal calf serum (FCS), 1% v/v penicillin/streptomycin (both Biochrom AG), and 1% v/v Glutamax™ (Thermo Fisher Scientific Inc., Waltham, MA) at 37 °C in a humidified 5% CO2 atmosphere, with medium changed every other day and passaged around 80% confluence.

2.2. In vitro transcription of modified and unmodified mRNA

In vitro transcription of synthetic mRNA encoding GFP or VEGF-165 was performed using T7 RNA polymerase and modified (ψ, m1ψ or 5moU – for VEGF additionally 5 mC) or unmodified (U) uridine-nucleoside triphosphates. The plasmid vector template pRNA2-(A)128 [31], containing a T7 promoter, a 5′-UTR, the coding region for GFP or VEGF (Supplementary Data 1), a human β-globin 3′-UTR and a 128-base polyadenine tail, was linearized enzymatically and the fragment of interest was purified by agarose gel electrophoresis. Synthesis of mRNA was performed using the TranscriptAid T7 Kit (Thermo Fisher Scientific). For co-transcriptional capping of the 5′ end, anti-reverse cap analog (ARCA) was added at a concentration of 30 mM and chemically modified nucleotides (ψ, m1ψ,5moU, 5 mC) (all Jena Bioscience, Germany) were added at 100 mM as complete substitution of unmodified nucleotides (U, C). mRNA was purified by lithium chloride precipitation, resuspended in RNAse-free water containing 0.1 mM EDTA. Concentration was determined using NanoDrop 1000 Spectrophotometer (Peqlab, Germany) and stored at −80 °C until further use.

2.3. mRNA transfection

Transfection was performed by complexing mRNA with Lipofectamine MessengerMAX reagent (Thermo Fisher Scientific) at a 1:2 ratio (w:v). The reagent was mixed with Opti-MEM reduced serum medium (Thermo Fisher Scientific) at a 1:50 vol ratio and incubated for 10 min at room temperature. The equal volume of Opti-MEM was mixed with the mRNA. Both solutions were gently mixed and incubated at room temperature for 5 min, allowing the formation of mRNA-lipoplexes. All experiments were conducted using 125 ng mRNA per cm^2 surface area (approx. $2{,}5 \times 10^4$ cells), except for dose response experiments in Fig. 2, as indicated in the figure legend. Negative controls containing only the carrier lipid Lipofectamine MessengerMAX and Opti-MEM without any mRNA (indicated as lipofectamine) and an untreated MSC control (untransfected) were included in all experiments. To evaluate the relationship between lipoplex incubation time and transfection efficacy, the mRNA-lipoplexes were removed at the indicated timepoints with two additional washing steps using warm medium, ensuring complete removal of the mRNA. Expression was quantified 24 h after the lipoplexes were added.

2.4. GFP-mRNA expression and flow cytometry

For assessment of GFP-mRNA expression, MSCs were imaged with an inverted fluorescent microscope (ELIPSE Ti–U equipped with pE-300lite LED light source; Nikon, Düsseldorf, Germany) every 24 h for 7 days post transfection and for analysis NIS-Elements imaging software version 4.51 (Nikon) was used. To ensure robustness of observed effects, the observation was repeated for two independently synthesized mRNA batches, with two cell donors respectively (Supplementary Fig. 1). Additionally, quantitative analysis of GFP-mRNA expression was conducted at different timepoints post transfection by flow cytometry. Cells were detached, stained with DAPI for LIVE/DEAD distinction and analyzed with MACSQuant VYB (Miltenyi Biotec). The flow cytometric data was analyzed with FlowJo V10 according to the gating strategy as illustrated in (Supplementary Fig. 2). Briefly, for differentiation of cells from cell debris, forward (FSC) vs. side scatter (SSC) was applied and doublets were excluded using FSC-area against FSC-height (FSC-A against FSC-H). Live cells were defined using a DAPI negative control and GFP + cells were determined within live cells in relation to untransfected cells. All measurements were conducted with at least 4 biological replicates (2 cell donors * 2 independent transfection experiments).

2.5. Protein detection

VEGF secretion and HGF secretion were quantified from cell culture supernatants by ELISA (R&D Systems, Minneapolis, MN) according to the manufacturer's instructions. Conditioned media (CM) were collected at different timepoints post transfection and stored at −80 °C until analysis. Unconditioned DMEM +10% FCS was also stored and used as a blank. Secretion of IL-6, IFN-β was quantified 24 h post transfection using ELISA (R&D Systems, Minneapolis, MN) according to the manufacturer's instructions. For secretome analysis the concentrations of 266 proteins in the MSC supernatant were evaluated using an Olink Target 96 proximity extension assay (Olink Bioscience, Uppsala, Sweden), as previously described [16]. Briefly, CM was mixed at a 1:3 ratio with a proprietary mix of cytokine-specific antibodies barcoded with DNA oligonucleotides. When two distinct specific probes bind an analyte, they anneal via complementary DNA sequences forming the basis for an amplicon that is quantified by high-throughput RT-PCR. Details on this technology, including detection limits, validation data and reproducibility can be found on the company's website (www.olink.com/downloads). Relative concentration values were given as normalized protein expression (NPX) units. A marker was considered as detected if more than three samples in any group had NPX values exceeding its limit of detection (LOD). The latter was defined as the larger of either the LOD defined by the manufacturer or the LOD estimated from our own negative controls (blank medium measurements) plus three standard deviations. Heatmaps were generated with the ComplexHeatmap package. Principal component analysis (PCA) was carried out to identify which analytes most contributed to the total variation in the data and influenced differences between secretome profiles of MSC conditions. Biplots were generated using the prcomp function and *factoextra* package version 1.0.7. The assay was carried out in triplicates. Two were from the same cell donor but different experiments and the third replicate was derived from cells of a different patient donor. The experiment assessing proteomic time courses of MSC under different treatment conditions was performed using two biological replicates. For this experiment, biological variation has been regressed out prior to conducting PCA using the ComBat function of the *sva* package. All analyses were performed using R version 4.1.1, available free online at https://www.r-project.org.

2.6. Caspase activity

Caspase 3 and 7 activity of transfected MSCs was measured 24 h post transfection using the Caspase-Glo 3/7 or Caspase-Glo 3/7 3D kits

(Promega, Madison, WI) for plated cells or 3D cultured cells respectively, according to the manufacturer's instructions. Briefly, cells were incubated in a 1:2 reagent: medium for 1 h at room temperature and luminescence was measured with a GloMax luminometer (Promega).

2.7. Metabolic activity

Mitochondrial metabolic activity of transfected MSCs was measured at day 0, 1 and 5 post transfection using PrestoBlue® cell viability reagent (Thermo Fisher Scientific) according to the manufacturer's instructions. Briefly, cells were incubated in a 1:10 ratio of reagent: medium for 1 h at 37 °C and fluorescence was measured at 570 nm with a fluorescent plate reader (Tecan, Männedorf, Switzerland).

2.8. Assessment of angiogenic activity in endothelial cells

Endothelial network formation was analyzed in response to CM derived from transfected and untransfected MSCs by use of an improved endothelial tube formation assay, as reported previously [16]. Briefly, HUVEC cells (Promocell, Heidelberg, Germany) were seeded in a cell culture plate coated with Geltrex (Thermo Fisher) and stimulated with biological quadruplicates of MSC-derived 24 h or 72 h CM in a 1:20 dilution in 2.5% supplemented basal endothelial medium (Promocell). Images were taken after 16 h using a fluorescence microscope (Nikon). For negative controls, CM of untransfected MSCs and unconditioned MSC medium (−) was used. As a positive control (+), recombinant human VEGF-165 (#293-VE R&D Systems, Minneapolis, MN) was added matching the previously highest detected VEGF concentration. Additionally, the positive control and CM from 5moU+5 mC-VEGF--transfected MSCs were blocked with an anti-VEGF-antibody (R&D Systems) to confirm the relationship between VEGF and the observed effects. Bright field images of resulting networks were analyzed (at least n = 12 per condition) and quantification of network-associated parameters was performed by FIJI and the Angiogenesis Analyzer macro. Cells were stained for 30 min using calcein AM ((1:2000; ThermoFischer) allowing visualization of networks by fluorescence microscopy.

2.9. Hydrogel formulation and cell encapsulation

MSCs were encapsulated using a collagen I (Col) and hyaluronic acid (HA) hydrogel as described previously [16]. Briefly, methacrylated collagen (8 mg/mL) was mixed with thiolated hyaluronic acid (10 mg/mL; both from Advanced Biomatrix, Carlsbad, CA) and DMEM in a 3:1:2 ratio (v/v) and used for resuspension of MSCs 1 h post transfection. The resulting cell-hydrogel mixture was cross-linked using UV-light (dose: 1 J/cm^2) and cultured in a 48 well cell culture plate as 10 μL droplets with a density of 3.5–5 × 10^6 cells/mL. Media were changed daily and collected for ELISA. For investigation of cell attachment, a control gel composed of polyethylene glycol (PEG) and HA, but no collagen was used: PEG-diacrylate (Extralink; Advanced Biomatrix) was mixed with thiolated hyaluronic acid (both 10 mg/mL) in a 1:4 ratio (v/v). The procedure was identical to Col-HA encapsulation. Viability of encapsulated cells was analyzed by staining with calcein AM (1:2000) and ethidium homodimer-1 (1:1000) (ThermoFisher Scientific, Waltham, MA) in culture medium at 37 °C for 1 h before imaging on a Leica TCS LSI macro-confocal microscope (Leica, Wetzlar Germany). Cell elongation was calculated from automatic measurement of circularity (reciprocal) in FIJI using the "analyze particles" function.

2.10. UV irradiation

MSCs from two different donors were seeded and cultured on a 48 well plate (1 cm^2/well) until 80% confluent. The energy dose of a UV-A spot-lamp with an 8 mm light guide (Dymax, Torrington, CT) was calibrated to values of 0.5 J, 1 J, 2 J and 10 J/cm^2 at 1 cm distance using a UV intensity meter (Dymax). Cells were irradiated at 1 cm distance with the respected light dose and supplemented with fresh medium. Caspase activity was measured 24 h later. For cell encapsulation experiments a dose of 1 J/cm^2 was used.

2.11. Localized angiogenesis assay

Localized endothelial network formation was evaluated in response to hydrogels containing VEGF-transfected MSCs, while hydrogels containing untransfected MSCs served as a negative control. 5 μL microgels containing 2,5 × 10^4 cells were implanted asymmetrically on the edge of a Geltrex coated well and network formation in areas local and distant from the microgel was analyzed as described above. The assay was performed in biological quadruplicates and for each, three random areas were imaged.

2.12. Statistical data analysis

Values are depicted as mean (± standard derivative (SD) or standard error of the mean (SEM)). Experiments were repeated independently for at least n = 8 (4x biological, 2x technical replicates), unless indicated otherwise. Levels of statistical significance were set at *p < 0.05, **p < 0.01, ***p < 0.001. Statistical analysis was carried out in R version 4.0.2 and GraphPad Prism 9.0 (GraphPad Software Inc., USA). Two-way (repeated measures) ANOVA with Holm–Sidak's or Tukey's post-hoc test or mixed-effects analysis (if values were missing) was used to test for significant differences between groups (details in figure legends). Repeated measures ANOVA was carried out for quadruplicate measurements with Holm multiple comparisons adjustment using the emmeans package.

3. Results

3.1. Chemical modifications of uridine differentially modulate mRNA peak expression and duration at minimal toxicity

The relatively short expression window can be both an advantage and a major limitation of mRNA technology. The ability to control IVT-mRNA expression kinetics would allow for tailoring the technology to the desired application. To evaluate if we could control protein synthesis capacity using specific mRNA modifications, IVT-mRNA coding for GFP was transcribed in vitro containing either UTP or the complete substitution of this nucleotide by classic or advanced uridine modifications. IVT-mRNA was complexed with lipofectamine and added to cell media for transfection. Transfection efficiency was above 70% in all groups, except for unmodified mRNA (U-mRNA) which resulted in a slightly lower transfection efficacy than modified mRNAs (Fig. 2b). Time-course fluorescence microscopy of cells transfected with lipoplexes revealed highest peak fluorescence in m1ψ- and 5moU-modified mRNA at 24 h post transfection (Fig. 2c). A marked decline was seen between day 2 and 3 for all conditions except 5moU. Surprisingly, GFP fluorescence of 5moU-transfected MSCs was high for more than a week. Results were validated using two independently synthesized mRNA batches and cells from different donors (Supplementary Fig. 1). Cytometric quantification of GFP fluorescence at day 1, 4 and 7 confirmed the different expression kinetics between the distinct nucleotide modifications (Fig. 2d; Supplementary Fig. 2). ψ did not affect fluorescence intensity or kinetics compared to U. m1ψ showed the highest initial fluorescence intensity, followed by a rapid decline between day 1 and 4, so that despite high initial expression levels the observed kinetic was similar to the unmodified IVT-mRNA (U-mRNA) control. The 5moU modification yielded high and stable fluorescence between day 1 and 4 and still exceeded fluorescence levels of all other modifications at day 7.

To evaluate the toxicity of the IVT-mRNAs, caspase activity, cell viability and metabolic activity were measured. At the moderate mRNA dose used in this study (125 ng/cm^2), significant upregulation of caspase was only detected in cells exposed to U-mRNA. At a 4-fold higher dose

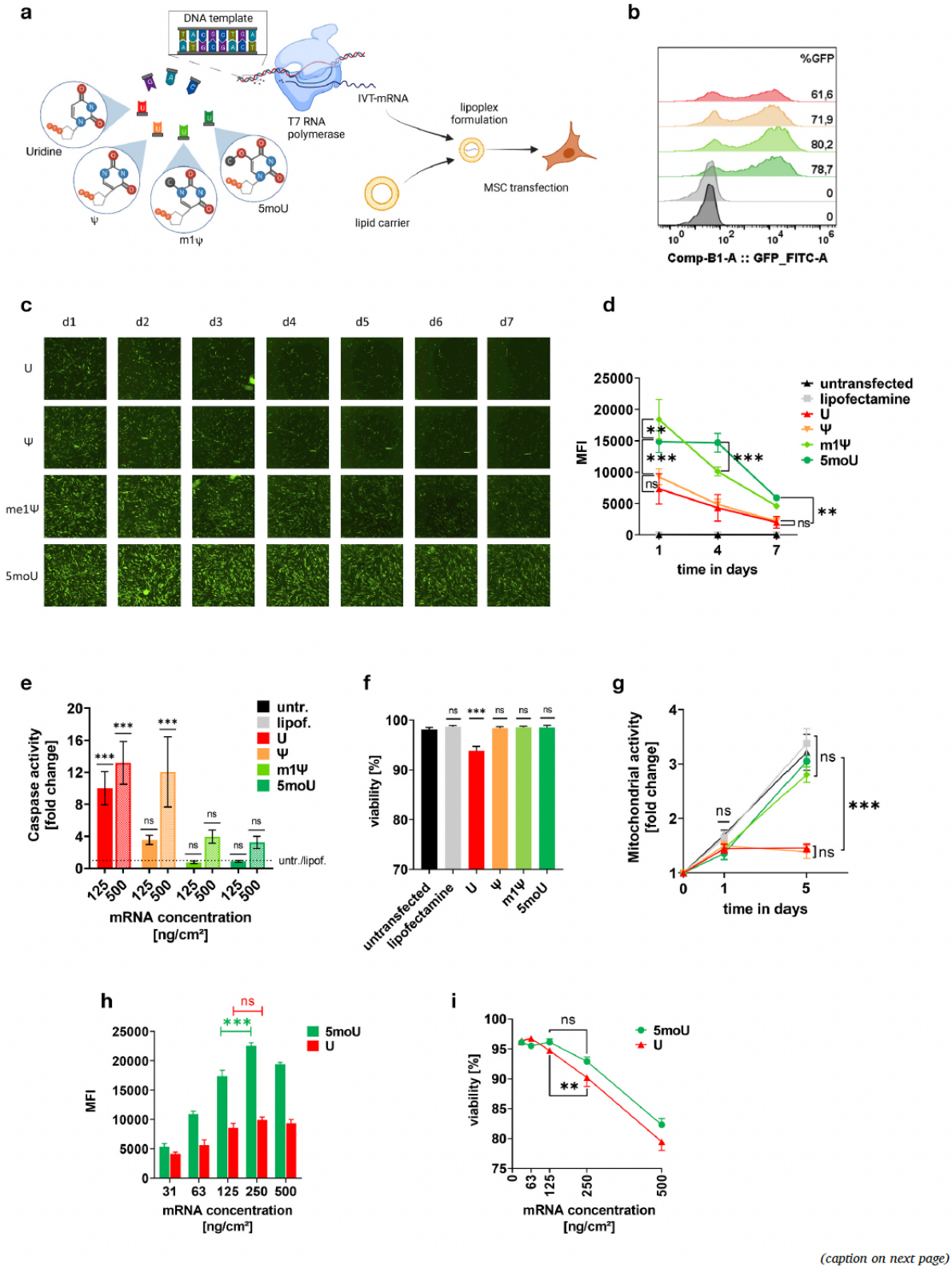

(caption on next page)

Fig. 2. Chemical nucleotide modification results in high and long lasting IVT-mRNA expression at minimal toxicity.

a) Schematic: In vitro transcription of mRNA using chemically modified uridine nucleotides yields IVT-mRNAs that result in different protein expression levels and prolonged expression periods.
b) MSC transfection efficacy is similar for all IVT-mRNA modifications. The percentage of cells gated for GFP+ is indicated. All events from n = 4 were pooled together to draw representative histograms. Quantitative values (%GFP) are means derived from GFP positive gates in dot plots.
c) Fluorescent imaging of MSCs transfected with GFP-mRNA synthesized with non-modified uridine (U); pseudouridine (ψ), N1-methylpseudouridine (m1ψ) or 5-methoxyuridine (5moU). Cells were imaged every day for 7 days (scale bar = 100 μm).
d) Flow cytometric quantification of GFP mean fluorescence (MFI) of transfected MSCs at days 1, 4 and 7 reveals a distinct influence of uridine modifications on the expression kinetic of IVT-mRNA encoding GFP.
e) Caspase activity is increased in cells transfected with a moderate dose of unmodified mRNA or a high dose of ψ-modified mRNA.
f) IVT-mRNA transfection results in excellent cell viability for all modifications (24 h post transfection). Only the unmodified IVT-mRNA leads to a small loss in cell viability.
g) Mitochondrial metabolic activity of mRNA-transfected cells measured at day 0, 1, and 5 post-transfection.
h) - i) Selection of the optimal non-toxic IVT-mRNA dose (125 ng/cm^2) based on dose-response regarding expression and toxicity: peak expression is reached at a dose of 250 ng mRNA/cm^2 (h). 5moU-mRNA is non-toxic up to a dose of 250 ng mRNA/cm2, while unmodified IVT-mRNA shows significant reduction of cell viability above 125 ng mRNA/cm^2 (i).

Data shown as mean ± SEM. Two-way ANOVA with Tukey's multiple comparisons test was used for statistical analysis. Significance levels are shown in relation to the untransfected group, unless indicated otherwise. *p < 0,05; **p < 0,01; ***p < 0,001; ns = not significant. All data n = 4, except for e and g: n = 6.

(500 ng/cm^2), increased caspase activity was observed in all IVT-mRNA groups but was only significant for U-mRNA and ψ-mRNA (Fig. 2e). In accordance with this result, only U-mRNA reduced cell viability, as measured by flow cytometry. For all modified mRNA groups, cell viability exceeded 95% (Fig. 2f). To evaluate the impact of IVT-mRNA on cell metabolic activity and detect any lasting impairment thereof, the mitochondrial activity of cells was evaluated before transfection with GFP-mRNA and 1 and 5 days after transfection (Fig. 2g). Before and one day after transfection, no differences in metabolic activity between groups were found. By day 5 the metabolic activity of m1ψ and 5moU groups increased 3-fold, similarly to the untransfected and lipofectamine-exposed groups. U-mRNA and ψ-mRNA significantly reduced cell metabolic activity on day 5, suggesting long-term impairment of cells transfected with these mRNAs, beyond the stress potentially triggered by lipoplex exposure.

To determine the dose-dependent effect of IVT-mRNA on protein expression level and toxicity, 5moU-modified mRNA and U-mRNA were compared at concentrations of 31 –500 ng/cm^2. Above 250 ng/cm^2 expression yields for both mRNAs reached their plateau (Fig. 2h). No significant viability loss was observed up to 125 ng/cm^2, but at higher concentrations U-mRNA significantly affected cell viability (Fig. 2i). The subsequent evaluation of side effects of mRNA uptake on paracrine activity (Fig. 3) was performed at subtoxic concentrations (125 ng IVT-mRNA/cm^2).

3.2. The innate immune response against unmodified IVT-mRNA is marked by profound changes in paracrine signalling and can be averted by nucleotide modification

Upon transfection, exogenous mRNA is recognized by intracellular pattern recognition receptors (PRR). The activation of PRR leads to the transcription, expression, and secretion of type-1 interferons (IFN), which triggers secondary effects by autocrine and paracrine signalling [32]. High concentrations of IFN-β were detected in supernatants from U-mRNA transfected cells (Fig. 3b). While all nucleotide modifications significantly reduced IFN-β secretion, only 5moU did so below detection levels. Secretion of IL-6, a pro-inflammatory cytokine secreted by MSCs showed a similar trend, with only U- and ψ-mRNA significantly increasing IL-6 secretion compared to untransfected cells (Fig. 3c).

To investigate effects of IVT mRNA immunogenicity on a broader profile of secreted factors, a screen for inflammatory and angiogenic mediators was performed in the supernatant of untransfected MSCs versus cells transfected with U-mRNA and 5moU-mRNA coding for GFP. More than 250 different proteins were analyzed and among them 106 analytes showed a concentration above the detection limit (Fig. 3d).

The secretome profiles of the 5moU-mRNA-transfected MSCs were comparable to the profile of the untransfected controls and the transfection vehicle control (lipofectamine). Regardless of biological variance between the tested cell donors, U-mRNA transfected MSCs presented a completely different secretome compared to all other groups. Principal component analysis (PCA) revealed that donor variance contributed to 3.1% of variation within the secretome data, whereas 94.1% of differences could be attributed to the effect of U-mRNA. Among the 25 proteins that contributed most to the characteristic secretome profile of U-mRNA transfected MSCs, chemokines of the CC and CXC families, which support immune cell attraction and activation, were the most prominent (Fig. 3e). The pro-inflammatory chemokine CXCL10, which also has a pronounced anti-angiogenic function [29], showed the largest increase. Accordingly, secretome data from U-mRNA-transfected MSCs showed not only increased levels of inflammatory proteins compared to 5moU-mRNA-transfected cells but also significantly lower levels of proangiogenic mediators such as VEGF-A, hepatocyte growth factor (HGF), and angiopoietin 1 (ANGPT1) (Fig. 3f–h).

Together, these data indicate that transfection of U-mRNA triggers a pro-inflammatory and anti-angiogenic shift in the secretion profile of MSCs, which may negatively affect their regenerative properties. This impairment was not observed for 5moU-mRNA, suggesting that targeted overexpression of IVT-mRNA-encoded proteins can be uncoupled from the immunogenicity of IVT-mRNA by using chemically modified uridine analogs. These results were validated following transfection with VEGF-mRNA (Fig. 4d), demonstrating that they are not sequence-specific or related to the overexpressed protein, but rather a cellular response toward exogenous mRNA as a biochemical entity.

3.3. Immune engineering of VEGF-mRNA has long lasting effects on VEGF expression and natural paracrine patterns

Secretion of pro-regenerative and pro-angiogenic paracrine mediators is considered to be the main mechanism of action of MSC therapy [33]. To investigate the effect of immunogenic and immuno-engineered IVT-mRNA on the pro-angiogenic effects of MSCs and to determine the extent to which these effects may be enhanced by overexpression of human VEGF-165, cells were transfected with differently modified VEGF mRNAs (Fig. 4a).

Secreted VEGF was measured in supernatants of transfected cells (Fig. 4b). U and ψ resulted in low VEGF secretion, which dropped below baseline secretion (untransfected) after 24 h and 48 h respectively. M1ψ led to the highest initial secretion among all single-substitution uridine modifications, but secretion dropped by an order of magnitude within 48 h 5moU-mRNA yielded slightly lower initial expression compared to m1ψ but maintained high VEGF secretion for over 120 h. In addition to the uridine modifications, 5-methyl-cytidine (5mC) as a substitute for

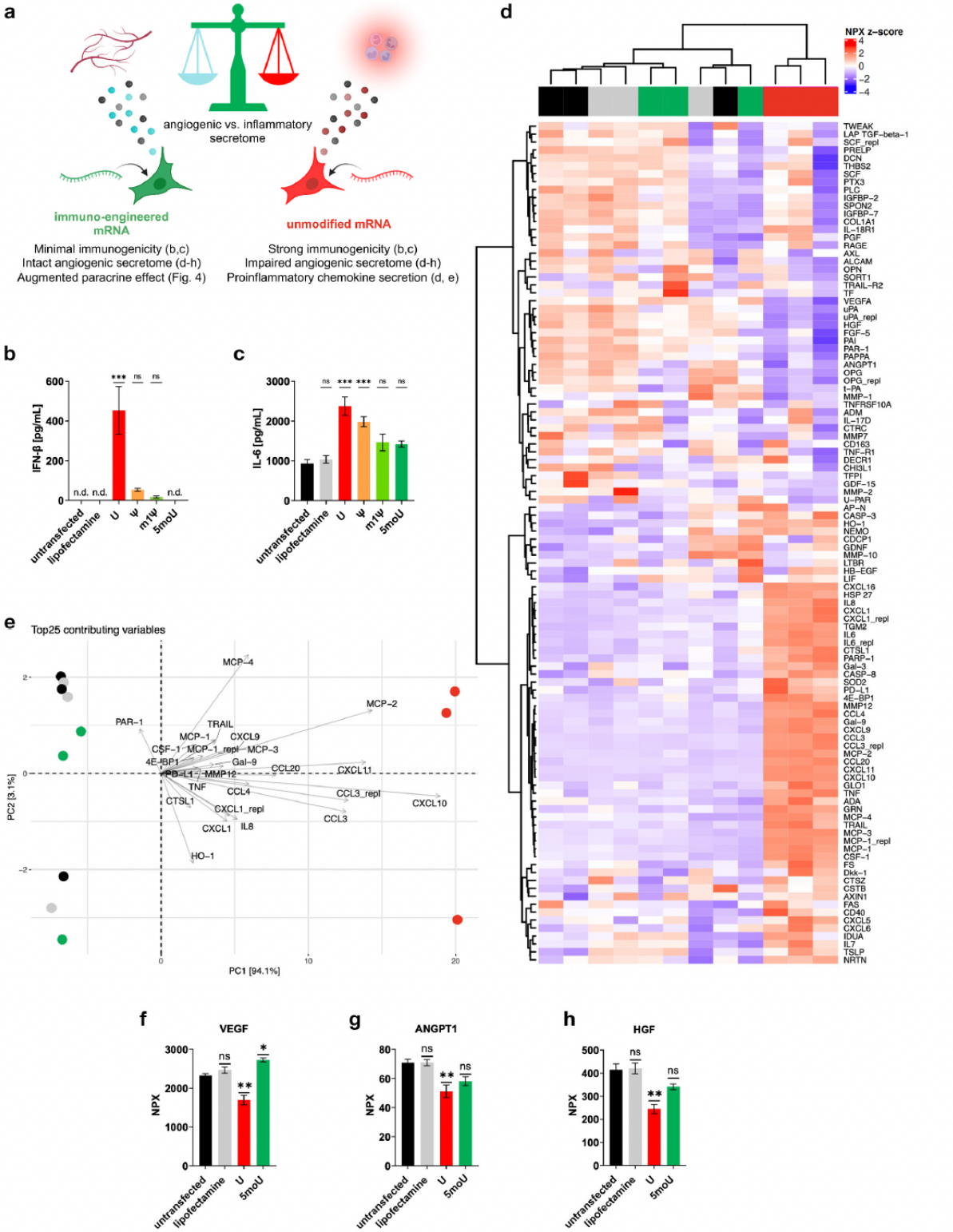

(caption on next page)

Fig. 3. Effects of immuno-engineered versus unmodified IVT-mRNA on paracrine activity of transfected MSCs.

a) Schematic: While unmodified mRNA induces a pro-inflammatory MSC secretome dominated by chemokines, mRNA immuno-engineering (IE) uncouples the immune response against IVT-mRNA from its protein expression template functionality and restores balance to the endogenous paracrine pattern of transfected cells.
b) Intracellular recognition of unmodified mRNA induces type-I interferon secretion and is significantly reduced by uridine modification.
c) IL-6 production is increased by unmodified and ψ-mRNA but not by m1ψ- and 5moU-modified mRNA.
d) Secretome profiling of mRNA-transfected and untransfected MSCs. Complex shifts in the paracrine pattern are induced by unmodified mRNA (red), regardless of cell batch or donor. The secretome of 5moU-transfected MSC (green) and lipofectamine treated cells (grey) is similar to untreated cells (black).
e) Principal Component Analysis (PCA) shows that secretion of chemokines mainly contributes to differences between unmodifed and immuno-engineered (5moU) GFP-mRNA, with CXCL10 being the strongest contributing analyte. The PCA biplot shows scores (coloured dots) of the first two principal components overlaid with loading vectors (arrows) of the top 25 variables contributing to the total variation in the data.
f)- h) The natural secretion of pro-angiogenic mediators VEGF-A, Angiopoietin-1 and HGF is impaired by unmodified mRNA but can be salvaged by 5moU nucleotide modification.

Data shown as mean ± SEM. One-way ANOVA with Holm-Sidak's multiple comparisons test was used for statistical analysis. Significance levels are shown in relation to the untransfected group, unless indicated otherwise. *p < 0,05; **p < 0,01; ***p < 0,001; ns = not significant; n.d. = not detectable. b, c: n = 6; *d*-h: n = 3.

cytidine was tested. The combination with 5 mC consistently augmented protein secretion levels for each uridine-substituted IVT-mRNA, but did not affect the secretion kinetics. For the remainder of the study, 5moU+5 mC-modified mRNA was chosen as the optimal immuno-engineered mRNA (IE-mRNA) and compared against unmodified, uridine-containing mRNA (U-mRNA).

A longer time course experiment, with measurements of VEGF and IFN-β on days 1, 4, 7 and 10 post-transfection (Fig. 4c) revealed that IE-mRNA-transfected cells secreted augmented VEGF levels, compared to untransfected cells even up to day 7. They maintained similar secretion levels to untreated cells for the remaining 3 days of the observation period, indicating that their natural baseline production of VEGF was not impaired after mRNA overexpression had ended. IFN-β was not detected in the media of untreated cells or IE-mRNA transfected cells at any time.

In contrast, cells transfected with U-mRNA showed high secretion of IFN-β, which remained detectable for 7 days post-transfection. These cells secreted high levels of VEGF only on day 1 post-transfection and showed lasting impairment of VEGF secretion for the remaining observation period, even several days after the expression of U-mRNA had ended.

To investigate delayed and long-lasting changes in the secretory phenotype related to IVT-mRNA (coding for VEGF) transfection, a time course proteomic analysis of cell conditioned media collected on days 1, 4, 7 and 10 post-transfection was performed (Fig. 4d, Supplementary Fig. 3). Secretomes of untransfected and IE-mRNA-transfected cells clustered together on all days and showed relatively little change over time. Between day 1 and later timepoints these cells increased their production of proteins related to connective tissue matrix deposition and remodelling, such as type I collagen (COL1A1), prolargin (PRELP) and osteoprotegerin (OPG), as would be expected of healthy MSCs in culture.

For U-mRNA transfected cells an upregulation of inflammatory factors and reduced secretion of pro-angiogenic factors was evident, which validates the data obtained with GFP-mRNA (Fig. 3d and e). Interestingly, U-mRNA transfected cells showed a clear temporal change in their secretome. While part of the upregulated inflammatory factors remained high throughout the observed 10 days (e.g. CXCL10, CXCL11), while a different cluster of pro-inflammatory cytokines was upregulated only briefly after transfection (e.g. Caspase 3, CXCL-1, IL-8; Supplementary Fig. 3). In U-mRNA transfected MSCs, the upregulation of extracellular matrix proteins was delayed and occurred only between days 7 and 10, implicating that these cells slowly return to their original phenotype after more than one week post-transfection.

3.4. Immuno-engineered, but not unmodified VEGF-mRNA augments the pro-angiogenic effect of MSCs

To evaluate the biological effect of VEGF-transfected MSCs, endothelial cells were stimulated with MSC-conditioned media (CM). Their capacity to self-organize into an endothelial tube network was observed and network formation was quantified using Fiji (Fig. 4e and f). Fresh assay medium was used as a negative control (−) and supplemented with hrVEGF-165 for the positive control (+). CM from untransfected MSCs (untr), GFP-transfected MSCs (IE-GFP) and U-VEGF-transfected MSCs (U-VEGF) did not stimulate endothelial tube formation, compared to the negative control. Only CM from MSCs transfected with immuno-engineered VEGF mRNA (IE-VEGF; 5moU+5 mC) significantly augmented endothelial network formation. No difference was observed between the effect of CM conditioned between 0 and 24 h post transfection (d1) or 48–72 h post transfection (d3), indicating a lasting effect of transfection of modified mRNA on the angiogenic potency of MSCs.

To verify whether the observed endothelial network formation is directly linked to the overexpressed VEGF, CM from IE-mRNA transfected MSCs and the recombinant positive control were both blocked with anti-VEGF-antibody. Upon blocking of VEGF endothelial tube formation dropped to background levels.

3.5. Combined IVT-mRNA transfection and hydrogel encapsulation allows for multimodal control of cells' functional phenotype

Through their multifactorial mode of action, cell therapies offer potential advantages over the administration of single molecules to address complex biological networks [1]. Combining gene modification and biomaterial encapsulation could allow for orthogonal modulation of multiple therapeutically relevant cell functions.

A hydrogel consisting of type-I telocollagen photo-crosslinked with thiolated HA (Col-HA), that has previously been shown to improve the pro-angiogenic signalling of MSCs [16], was prepared to encapsulate VEGF-mRNA-transfected cells, thereby combining the pro-angiogenic effects of transfection with the material niche (Fig. 5a).

For gel photo-crosslinking UV-A light (365 nm) at an energy dose of 1 J/cm^2 was used. To make sure that the UV irradiation is not harmful to the cells, caspase activity in irradiated cells was measured as a function of energy dose (Fig. 5b). Only a very high UV dose of 10 J/cm^2 led to caspase activation, whereas lower doses of 2 J/cm^2 and less did not.

As shown in Fig. 4b, the secretion of mRNA-encoded VEGF peaks at 24 h post transfection. To ensure that as much of this secretion window occurs after cell encapsulation and is not lost in pre-processing of cells, the incubation time between mRNA transfection and cell detachment and encapsulation was minimized. To this end the transfection efficacy in dependence of mRNA-lipoplex incubation time was investigated. Transfection largely occurred within the first few hours after adding lipoplexes to the cells: When lipoplexes were incubated on cells for only 1 h and were then removed, >33% of all cells were transfected. Following 6 h of lipoplex exposure ~60% were transfected with only a slow increase over the following 18 h by an additional ~15% transfected cells (Supplementary Fig. 4). We therefore chose to incubate lipoplexes on the cells for 1 h prior to washing and detaching the cells for

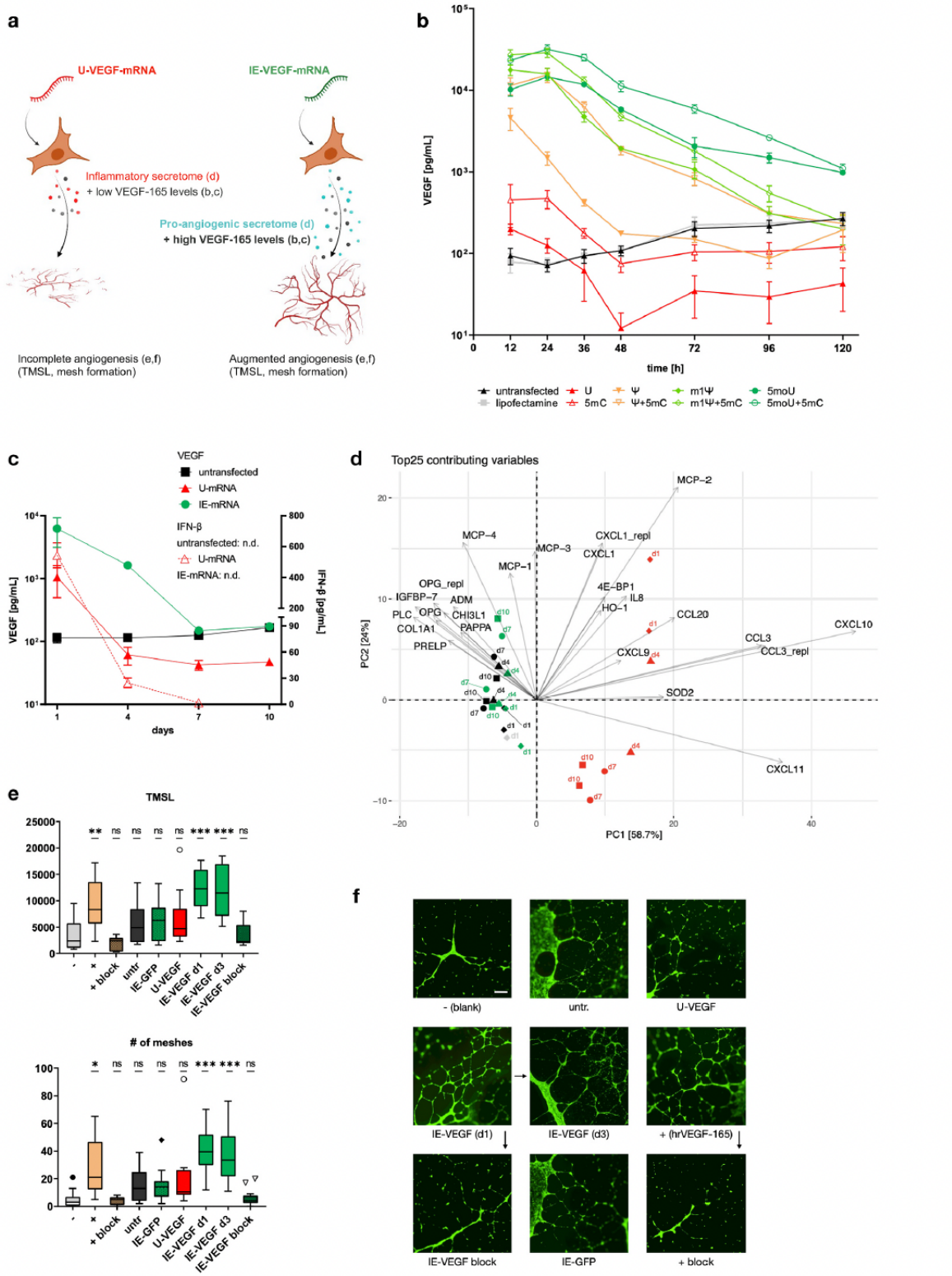

(caption on next page)

Fig. 4. Immuno-engineered VEGF mRNA augments the pro-angiogenic effect of MSCs.

a) Schematic: Transfection of MSCs with U-VEGF-mRNA impairs the angiogenic properties of MSCs, results in low VEGF-165 overexpression and does not improve the cells' angiogenic effects. Immuno-engineering of VEGF-mRNA yields higher levels of VEGF-165 in addition to a preserved endogenous secretome. This enhanced secretome has an augmented pro-angiogenic effect on endothelial cells.
b) VEGF secretion from transfected MSCs is influenced by chemical modification of uridine and cytidine. Uridine modification with 5moU additionally extends the VEGF secretion window.
c) VEGF secretion from IE-mRNA transfected cells (green) lasts for 7 days and continues at baseline levels, similar to untransfected cells (black). VEGF secretion from U-mRNA transfected cells (red) is high only on day 1 and remains reduced compared to untransfected cells. IFN-β secretion is high following U-mRNA transfection and remains detectable for 7 days (dashed red line). Untransfected MSCs or IE-mRNA-transfected MSCs do not secrete IFN-β (n.d.; not detectable).
d) Proteomic time course of MSC conditioned media (days 1, 4, 7, 10). The Principal Component Analysis (PCA) biplot shows scores (coloured shapes) of the first two principal components for samples collected on days 1 (diamonds), 4, (triangles), 7 (circles) and 10 (squares), overlaid with loading vectors (arrows) of the top 25 variables contributing to the total variation in the data. The PCA shows that cells treated with IE-VEGF-mRNA (green), untreated cells (black) and lipofectamine-treated cells (grey; only day 1) cluster together on all days and show little change over 10 days of culture. The secretion pattern of cells transfected with unmodifed VEGF-mRNA (red) undergoes changes in time but high secretion of pro-inflammatory chemokines (e.g., CXCL10) distinguishes it from all other groups throughout the entire observation period.
e) Quantified endothelial network formation. CM from MSCs transfected with IE-mRNA encoding VEGF-165 significantly augments endothelial network formation compared to blank media, whereas CM from untransfected MSC or MSCs transfected with unmodified mRNA do not. Blocking of VEGF shows that the angiogenic effect is VEGF-dependent. TMSL = total master segment length of endothelial tubes/field.
f) Representative images of the endothelial cell networks that formed in response to MSC CM (scale bar = 300 μm)

Significance levels are shown in relation to blank, unless indicated otherwise. Box plot whiskers show extreme values with Tukey's correction for outliers. Two-way ANOVA with Tukey's multiple comparisons test was used for statistical analysis. *$p < 0,05$; **$p < 0,01$; ***$p < 0,001$; ns = not significant. b: n = 6; c: n = 4; d: n = 2; e: n = 12.

encapsulation.

Cells transfected with either immuno-engineered mRNA (IE-mRNA) or unmodified mRNA (U-mRNA) encoding VEGF-165 or untreated cells were encapsulated in the Col-HA hydrogel and observed at days 1, 4, 7 and 10 post-encapsulation (Fig. 5c). Upon encapsulation, caspase activity was strongly increased in U-mRNA transfected cells (16-fold) and only slightly increased in IE-mRNA transfected cells (4-fold) (Fig. 5d). Untreated cells and cells transfected with IE-mRNA showed high viability ~85% inside the hydrogel throughout the observation period, while the cell viability for U-mRNA was strikingly low at day 1 (~45%) and remained low at later timepoints (Fig. 5c, e). In all three conditions, viable cells elongated over time within the Col-HA hydrogel, indicating cell adhesion to the collagen substrate. By day 4 this resulted in a stromal morphology and approximation of pseudopodia of the initially separated cells (Fig. 5c,f).

Both groups of VEGF-transfected cells showed expression of the IVT-mRNA (Fig. 5g). However, in the U-mRNA group VEGF secretion declined beneath the baseline secretion level of the untransfected group by day three and did not recover. In contrast, VEGF secretion in the IE-mRNA group was approximately one log level higher than for U-mRNA and remained above baseline levels (untransfected) for more than 7 days.

In addition to overexpressed VEGF, HGF was measured as a relevant example of a naturally produced complementary proangiogenic factor (Fig. 5h). In the U-mRNA group, HGF levels were very low and detected only in few samples. In contrast, in both untransfected and IE-mRNA transfected cells HGF-secretion increased 3-fold within the first 3 days post-encapsulation. IE-mRNA transfected cells and untransfected cells secreted similar HGF levels throughout the observation period, indicating that cell-material-interactions were not altered by the transfection and consequently mRNA technology can be implemented orthogonally to bioinstructive materials to edit the phenotype of cells.

To test whether the hydrogel-encapsulated MSCs could also induce a localized angiogenic effect, Col-HA gel microspheres containing either VEGF-mRNA transfected MSCs or untransfected MSCs were implanted asymmetrically into a layer of matrigel bulk gel and endothelial cells were seeded on top (Fig. 6a). Endothelial tube formation was observed only in the vicinity of the microgels but not on the opposite side of the bulk gel (Fig. 6b and c), indicating a strong but locally confined angiogenic effect. Though untransfected Col-HA-encapsulated MSCs promoted significant endothelial cell self-organization, VEGF-transfected cells induced a stronger angiogenic effect.

3.6. Secretion of IVT-mRNA encoded proteins is sensitive to cell attachment

To investigate whether the high expression of IE VEGF-mRNA in Col-HA encapsulated cells and the observed increase in HGF secretion were sensitive to the cell attachment within the collagen gel, cells were encapsulated for comparison in a PEG-HA control gel, which does not allow for cell attachment. Cells transfected with IE VEGF-mRNA or untransfected cells were encapsulated and observed between days 1 and 4 post-encapsulation, as an increase in HGF-secretion had been observed between these time points.

Cell viability was initially slightly lower in the non-adhesive PEG gel (- adh) than in Col-HA (+adh; Fig. 5i). This difference became significant at day 4 with approximately 20% lower cell viability in the non-adhesive gel. VEGF secretion was approximately 3 to 4-fold reduced in the PEG gel, compared to Col-HA (Fig. 5j). This was true both for untransfected MSCs naturally secreting VEGF-A (untransfected + adhesion vs. untransfected - adhesion), as well as MSCs transfected with VEGF-165-mRNA (VEGF-mRNA + adhesion vs. VEGF-mRNA - adhesion), indicating a general dependence of secretory activity on cell adhesion. For GFP, which is expressed in the cytoplasm but not secreted, no evident difference was observed between cells in an adhesive versus non-adhesive gel (Supplementary Fig. 5), suggesting that protein secretion rather than mRNA translation is attachment sensitive.

Consistent with the previous experiments, MSC cultured in Col-HA (transfected and untransfected) showed an increase in HGF secretion, while in the PEG-HA control group HGF levels also increased slightly over time but could not be reliably detected in all samples even at day 4 (Fig. 5k).

4. Discussion

In an early pioneer study, Levy et al. successfully improved the anti-inflammatory properties of MSCs and their homing to an inflamed ear in a rodent model by overexpressing IL-10, PSGL-1 and SLeX using IVT-mRNA modified with ψ [34]. While the report showed an important proof of concept of efficacy, it did not investigate the side effects of unmodified or modified IVT-mRNA on cell fitness and phenotype. As technological progress in vitro transcription, chemical nucleotide modification and nucleic acid delivery have transformed IVT-mRNA into a new clinically applied drug class, these questions of cellular response and potential side effects have gained translational relevance. Furthermore, SARS-CoV2 vaccines recently developed by Moderna and

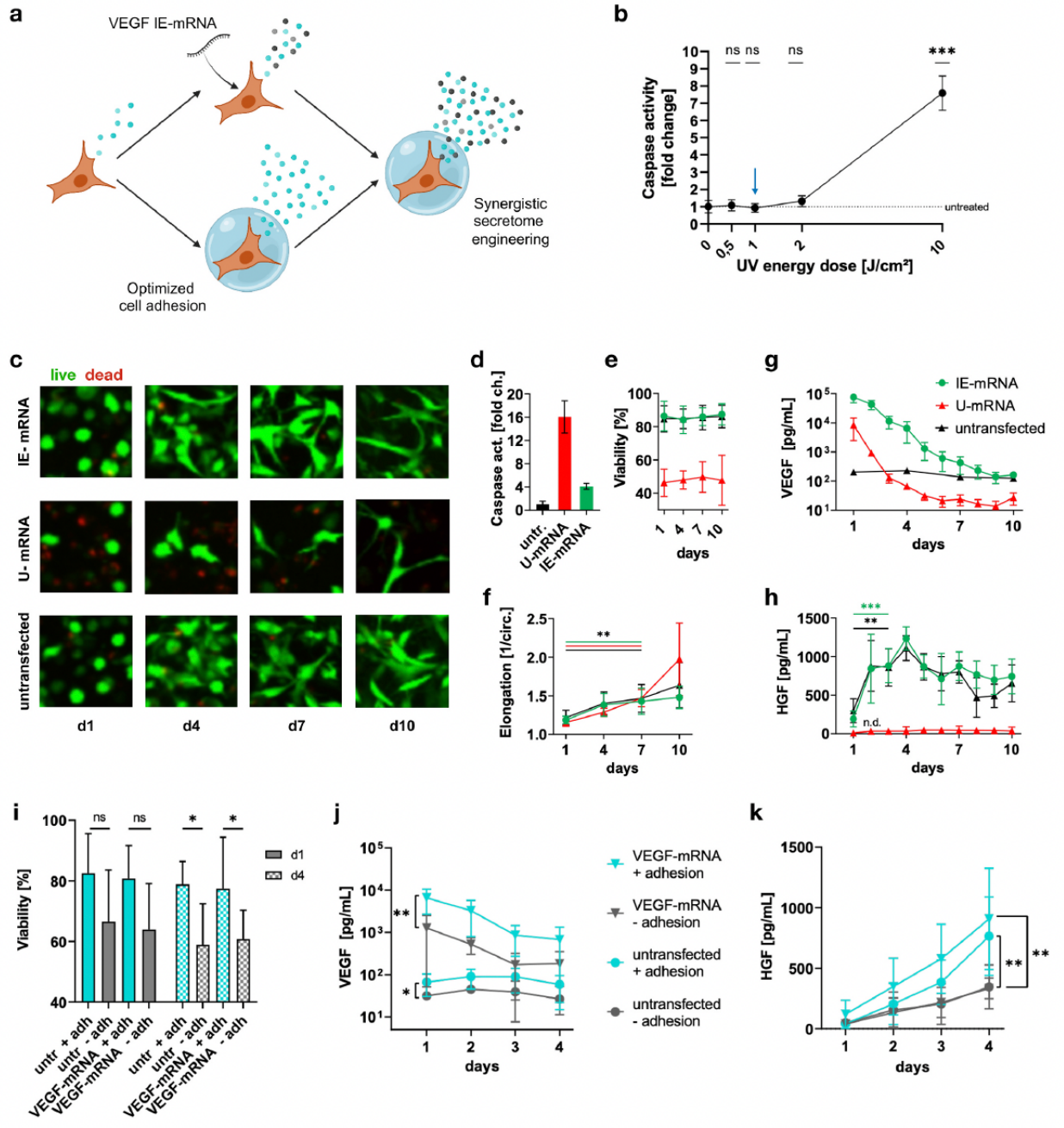

(caption on next page)

Fig. 5. Orthogonal and synergistic effects of IVT-mRNA transfection and optimized cell attachment on MSC phenotype and angiogenic signalling.

a) Schematic: Transfection of MSCs with IE-mRNA allows for overexpression of a selected factor such as VEGF-165. Encapsulation of MSCs in a hydrogel that provides cell attachment sites augments the endogenous secretion of angiogenic growth factors such as HGF. When both cell manipulation techniques are combined, cell attachment increases the secretion of IVT-mRNA-expressed proteins.
b) UV irradiation at a dose of 1 J/cm^2, as used for photo-crosslinking of cell-loaded hydrogels (blue arow), does not increase caspase activity in irradiated cells. Only a 10-fold higher dose results in significantly upregulated caspase activity.
c) Untransfected MSCs or MSCs transfected with U-mRNA versus IE-mRNA encoding VEGF-165 were encapsulated in a Col-HA gel and cultured for 10 days. Live cells = green (calcein AM); dead cells = red (ethidium homodimer). Representative images taken on days 1, 4, 7 and 10 show high cell viability for untransfected and IE-mRNA transfected cells and continuous elongation of live cells in all three groups.
d) Caspase 3/7 activity 24 h post-encapsulation. Consecutive mRNA-transfection, detachment and hydrogel UV-encapsulation of cells results in slight increase in caspase activity in the IE-mRNA group but high caspase activation in U-mRNA-treated cells.
e) Viability in the Col-HA gel remains high for untransfected and IE-mRNA transfected MSCs, while transfection with U-mRNA results in low viability upon encapsulation.
f) Live cells attach and elongate in the Col-HA gel regardless of transfection conditions.
g) VEGF secretion from cells encapsulated in Col-HA. Untransfected cells (black) show stable baseline VEGF secretion over 10 days. VEGF secretion of U-mRNA transfected cells (red) drops below baseline levels after two days, while IE-mRNA transfected cells (green) secrete high levels for > one week.
h) HGF secretion in untransfected (black) and IE-mRNA transfected cells (green) increases within the first four days post-encapsulation and is very low in U-mRNA transfected cells (red; n. d. = not detectable).
i) Cell viability within the Col-HA gel, which provides cell adhesion sites (+adh), remains high over 4 days. In the control hydrogel, which does not allow adhesion (-adh), cell viability is reduced slightly on day 1 and significantly on day 4.
j) Endogenous VEGF-A secretion from untransfected MSCs (circles) is higher in the Col-HA gel (teal line; untransfected + adhesion) compared to PEG-HA (grey line; untransfected - adhesion). Furthermore, secretion of overexpressed VEGF-165 from VEGF-mRNA transfected cells (triangles) is also higher in the presence of cell adhesion motifs.
k) The increase of endogenous HGF secretion from encapsulated cells is less pronounced in a hydrogel which does not provide cell adhesion motifs (grey line), compared to Col-HA hydrogel (teal line), regardless of whether the cells were transfected with IE-VEGF-mRNA (triangles) or untransfected (circles).

Data shown as mean ± SD. Two-way ANOVA (or mixed effect analysis for f) with Holm-Sidak's multiple comparisons test was used for statistical analysis. *p < 0,05; **p < 0,01; ***p < 0,001; ns = not significant. b: n = 5 or 6; d: n = 10; e: n = 16; f, h, i: n = 8; g: n = 4; j, k, = 12.

Biontech/Pfizer contain IVT-mRNA modified with the more recently proposed uridine analog m1ψ [35], in contrast to the early IVT-mRNA technology used by Levy et al., in 2013 [24,34]. Therefore, we have followed up on the concept of using IVT-mRNA to improve properties of therapeutic cells, while using state-of-the-art mRNA technology, systematically comparing the effects of classic and recently proposed nucleotide modifications, and giving special attention to cellular responses and potential biomaterial-based delivery strategies of mRNA-transfected cells.

We observed two distinct cellular responses toward IVT-mRNA transfection, the first, protein expression and the second, immune response, which, importantly, can be decoupled from each other and modulated by nucleotide modifications. The expression of the protein of interest depends on the sequence of the open reading frame of the mRNA and is usually the primary aim of IVT-mRNA transfection. The intracellular immune response is directed against the IVT-mRNA due to recognition as an exogenous biochemical entity. From the study of viruses it is known that exogenous nucleic acid introduced into a human cell, as occurs upon viral infection, upregulates interferon-stimulated genes and triggers inflammatory signalling [32,36]. In a vaccination context this can be desirable, as the IVT-mRNA acts as its own immune activating adjuvant. However, we show that for other applications the mRNA's immunogenicity could be problematic, leading to excessive inflammatory signalling and altering the properties of therapeutic cells. We show that chemical nucleotide modification, especially of uridine, affects IVT-mRNA mediated protein expression and immunogenicity, allowing the two processes to be uncoupled. Protein expression can be increased and prolonged whilst the inflammatory response and associated phenotypic changes are reduced.

A limitation of IVT-mRNA, which is frequently mentioned in the literature and has so far prevented its widespread application, is its intracellular instability and short-lived effect. In accordance with this, we have observed a dramatic decline in the effect of IVT-mRNA containing uridine or ψ after only two days (Figs. 2c and 4b). However, both newer uridine modifications (m1ψ and 5moU) resulted in increased peak protein expression. We found that 5moU also led to a prolonged expression period compared to m1ψ. The initial expression peak of 5moU was slightly lower than that of m1ψ-mRNA, thus there appears to be a distinct difference in the expression kinetics between both modifications (Figs. 2c and 4b, c). This finding is in line with observations made by Li et al. who first identified 5moU as a promising ribonucleotide modification [27] and implies that IVT-mRNA expression level and duration can be decoupled to a certain degree.

The influence of IVT-mRNA nucleotide modification on the expression kinetics could have several underlying mechanisms, as chemically modified nucleotides influence both the translatability and stability of the mRNA. Translatability could be influenced either directly by affecting the translation speed at the ribosome or the tRNA selection [37], or indirectly through the degree of immune response-related activation of protein kinase R [38]. The intracellular stability of IVT-mRNA is also mediated directly through increased resistance to cleavage by RNAses and indirectly by immune response-related activation of these RNAses [39].

We were interested in understanding and controlling the effects of IVT-mRNA immunogenicity on transfected cells. We found that upon transfection with unmodified mRNA secretion of angiogenic mediators is diminished (Fig. 3g–i) and instead pro-inflammatory chemokines (most prominently the anti-angiogenic CXCL10) are released (Fig. 3d and e). This anti-angiogenic and pro-inflammatory shift involves large portions of the secretome and lasts for more than 10 days, making unmodified IVT-mRNA unsuitable for applications in revascularization and cardiovascular regeneration.

Aside from immunogenicity, we also hypothesized that overexpression of exogenous IVT-mRNA at supraphysiological levels might exceed the cells' capacity for mRNA translation, thereby downregulating naturally expressed proteins. However, transfection with immuno-engineered mRNA (uridine substituted by 5moU ± 5 mC), which did not trigger any detectable immune response, resulted in a secretome which was indistinguishable from untreated cells (Fig. 3d and e). This suggests that MSCs possess sufficient secretory capacity for IVT-mRNA overexpression, and that the observed secretome changes induced by unmodified IVT-mRNA transfection are mainly, if not exclusively, related to its immunogenicity.

Thus, immuno-engineered IVT-mRNA allows for the overexpression of very high levels of a selected protein in stromal cells, orthogonally to the cells' natural secretion pattern. Immune engineering of IVT-mRNA

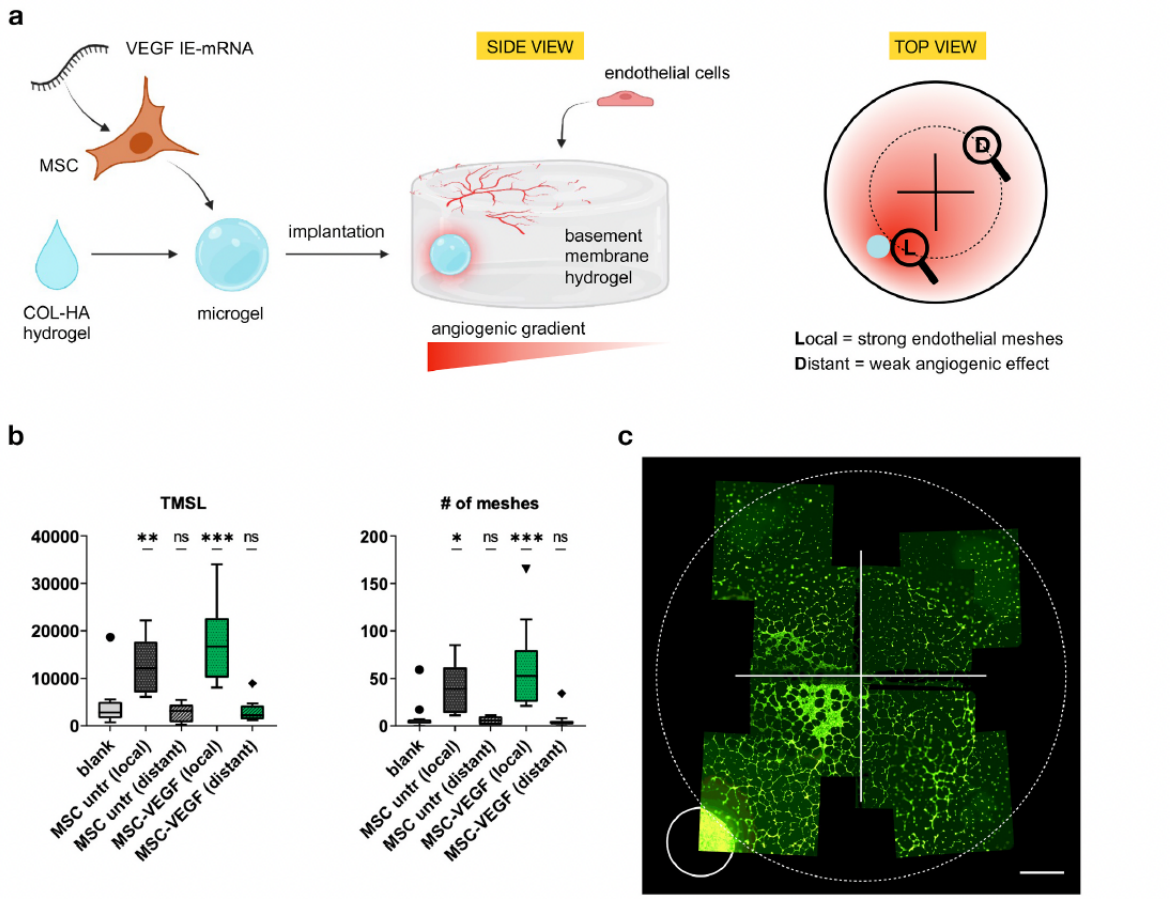

Fig. 6. VEGF-MSC microgel implants locally promote endothelial network formation.

a) Assay schematic: MSCs were encapsulated into Col-HA gels 1 h post-transfection with VEGF-IE-mRNA. 5 μL microgels were then implanted asymmetrically into a basement membrane bulk gel to establish a gradient of released growth factors. Endothelial cells were seeded on the basement membrane gel and endothelial network formation in areas local and distant from the microgel was compared.

b) Quantification of endothelial network parameters (total master segment length and number of formed meshes per field) reveals extensive mesh formation in the vicinity of the implant, while on the opposite side of the assay gel no formation of longer endothelial tube fragments can be observed. This was observed for both untransfected and VEGF-IE-mRNA transfected MSCs encapsulated in the Col-HA hydrogel, although the angiogenic effect of MSC-VEGF was stronger.

c) Fluorescent imaging of endothelial tube formation on a basement membrane gel with an asymmetrically placed MSC-VEGF implant (lower left corner; cf. a)). Calcein AM was used for staining. The angiogenic effect is localized mainly in the quadrant closest to the MSC implant (scale bar = 1 mm).

Significance levels are shown in relation to blank. Box plot whiskers show extreme values with Tukey's correction for outliers. Two-way ANOVA with Tukey's multiple comparisons test was used for statistical analysis. *$p < 0{,}05$; **$p < 0{,}01$; ***$p < 0{,}001$; ns = not significant. b: n = 12.

was found to be a prerequisite for effective pro-angiogenic effects (Fig. 4) and increases resilience of IVT-mRNA engineered cells for further use, such as encapsulation in a predesigned biomaterial carrier without excessive cell stress and viability loss (Fig. 5).

The compatibility of mRNA engineered cells with biomaterial encapsulation is crucial, as the function of MSCs is dependent on cell adhesion, requiring a delivery strategy that ensures such optimized cell attachment [12]. Biomaterial encapsulation also provides the opportunity to modulate genetically engineered cells through cell-material interactions. We have previously developed a bioinstructive collagen-hyaluronic acid hydrogel (Col-HA) for cell delivery, which can be injected and photo-crosslinked on demand [16]. We [16] and others [15,40] have shown that collagen-based biomaterials improve the pro-angiogenic paracrine pattern of MSCs through cell-matrix attachment and integrin signalling. Accordingly, in this study untransfected MSCs encapsulated in the Col-HA hydrogel showed high cell viability over 10 days, attachment and elongation, as well as increased secretion of angiogenic factors (exemplified by HGF; Fig. 5).

To harness this augmented natural pro-angiogenic secretome as a synergistic support for the mRNA-overexpressed VEGF, we combined IVT-mRNA transfection with a material-based niche effect (Fig. 5a). The effective combination of both techniques was found to depend on two factors:

First, the minimization of IVT-mRNA immunogenicity is a prerequisite for subjecting transfected cells to further stress. U-mRNA transfected cells which already show signs of stress under normal culture conditions did not tolerate subsequent cell encapsulation, resulting in poor viability and strongly diminished growth factor secretion. IE-mRNA-transfected cells were more resilient upon encapsulation (only slight increase in caspase activity, high long-term viability) and

performed similarly to untransfected cells in every respect, with the additional feature of high VEGF overexpression (Fig. 5d, e, g, h).

Second, strong secretion of growth factors, including the IVT-mRNA-encoded VEGF-165 required a cell-adhesive environment: Secretion of naturally produced HGF (Fig. 5k) and naturally produced VEGF-A (Fig. 5j) was higher in the collagen hydrogel, which provided cell attachment motifs, than in the PEG hydrogel with no such motifs. The same was true for IVT-mRNA encoded VEGF-165 (Fig. 5j). MSC viability was reduced in the control PEG hydrogel (no cell adhesion motifs) which is consistent with the principle of anoikis [41]. However, a ~3-fold reduced secretion of IVT-mRNA expressed VEGF-165 in the non-adhesive control gel is not fully explained by the ~20% difference in cell viability (Fig. 5i, h).

There was an interesting difference between the secretion kinetic of VEGF and HGF. VEGF secretion (both endogenous and overexpressed) was augmented in cell-adhesive Col-HA gels starting from day 1 and remained stable throughout the observation period, while HGF secretion robustly increased between day 1 and 4, implying that the qualitative composition of the cellular growth factor pattern changed over time. This could be explained by different opportunities for cellular interaction being present at days 1 vs 4: On day 1 MSCs were able to attach to collagen, which is a ligand for α1β1-and α2β1-integrins [42] expressed on MSCs [43], but remained round and isolated from each other. By day 4, MSCs were elongated and in closer proximity to each other, which could facilitate cell-cell interactions in addition to cell-material interaction. This would be in line with our previous studies, which showed a distinct role for N-cadherin mediated cell-cell interactions in the paracrine function of MSCs [44,45].

Using a widely accepted in vitro model of endothelial cell self-organization to confirm the biological relevance of observed MSC secretome changes, we demonstrate that pro-angiogenic factors overexpressed using immune engineered IVT-mRNA in MSCs are biologically active and furthermore, that encapsulation in a Col-HA hydrogel further boosts their proangiogenic functions (Figs. 4 and 6). The in vivo fate and performance of MSCs delivered in biomaterial carriers (also including collagen) has been extensively studied by us [46] and others [15,40,47]. Without a biomaterial carrier, engraftment and persistence of MSCs is low and they are cleared within few hours-days [12,48]. Biomaterial encapsulation has been used to prolong the effects of MSCs, but the cell persistence observed in these studies rarely exceeds a week, thus eliminating concerns about undesired long-term engraftment of these cells [15,47]. Given the transient, non-integrating nature of mRNA transfection and the minimal phenotypical differences between untreated cells and those transfected with IE-mRNA, we have no reason to believe that the technique we propose would significantly alter the in vivo fate of our proposed system, compared to that which has been reported for untransfected MSCs. The demonstration of in vivo efficacy of our multimodal system is an important next step but requires a clear therapeutic aim in a relevant disease model. Choosing the appropriate indication and developing a relevant disease models and intervention technique pose entirely new questions of a translational nature, which will inspire future studies.

5. Conclusions

In this study we have combined in vitro transcribed (IVT-) mRNA transfection with biomaterial encapsulation to manipulate the pattern of cell-secreted growth factors in three complementary dimensions: we have successfully uncoupled (i) the overexpressed gene-of-interest (here VEGF165) from (ii) the IVT-mRNA-triggered inflammatory secretome shift and found a synergy between IVT-mRNA expression and (iii) the adhesion-dependent secretome modulation mediated by the encapsulating hydrogel.

We have demonstrated the crucial importance of IVT-mRNA immuno-engineering in a non-vaccine context and adopted minimally immunogenic mRNA technology for applications in cell editing and regeneration: an unchecked immune response against IVT-mRNA in primary human cells results in a compromised cell phenotype with an unbalanced pro-inflammatory secretome and reduced pro-angiogenic functionality. This immune response is effectively minimized by the synthetic ribonucleotide 5moU, thereby restoring the balance in the cells' secretory phenotype. Additionally, immuno-engineering of IVT-mRNA augments and prolongs the secretion of the mRNA-encoded protein and allows for encapsulation of transfected MSCs in an injectable hydrogel without sacrificing cell viability or secretory activity.

Successful integration of mRNA-transfection with hydrogel encapsulation opens routes for potential clinical delivery of mRNA-engineered cell products. Importantly, we have found that optimized cell attachment is also a prerequisite for strong secretion of IVT-mRNA encoded protein, which is a newly described synergism between mRNA transfection of cells and their microenvironment. Material-mediated effects allow for an additional level of control over the cells' secretome in synergy with IVT-mRNA overexpression, as demonstrated by an increased secretion of endogenous HGF and mRNA-overexpressed VEGF in collagen hydrogels. We believe that multimodal control over synergistic cell functions is an important enabling step toward therapeutics which adequately target complex multifactorial processes such as angiogenesis or tissue regeneration.

Credit author statement

Norman Michael Drzeniek: Project administration, Conceptualization, Methodology, Investigation, Formal analysis, Visualization, Writing – original draft. Nourhan Kahwaji: Investigation, Formal analysis, Visualization. Stephan Schlickeiser: Formal analysis, Software. Petra Reinke: Conceptualization, Writing – review & editing. Sven Geißler: Conceptualization, Writing – review & editing, Resources. Hans-Dieter Volk: Supervision, Conceptualization, Writing – review & editing, Funding acquisition. Manfred Gossen: Supervision, Conceptualization, Methodology, Resources, Writing – original draft.

Declaration of competing interest

The authors declare that they have no known competing financial interests or personal relationships that could have appeared to influence the work reported in this paper.

Data availability

Data will be made available on request.

Acknowledgements

This project has received funding from the European Union's Horizon 2020 research and innovation programme under Grant Agreement No. 733 006 (PACE) and No. 779 293 and from the Einstein Center for Regenerative Therapies (ECRT) Kickbox. N.D., S.G. and H-D.V. acknowledge funding from the German Research Foundation (DFG) through funding the Collaborative Research Center 1444 (CRC 1444). N. D. would like to thank the Berlin-Brandenburg School for Regenerative Therapies GSC 203 for its support. S.G. was supported by German Federal Ministry of Education and Research (BMBF, 031L0234B). Funding was provided by the Helmholtz Association and by the Federal Ministry of Education and Research, Germany, in the Program Health Research (BCRT grant no. 13GW0098 and 13GW0099).

The authors would also like to thank the BCRT Cell Harvesting Core Unit (BCRT-CH) of the Berlin Institute of Health, Charité - Universitätsmedizin Berlin for their excellent technical assistance and support and Dr. Nicola Brindle for critical discussion and proof-reading the manuscript. Figures were created using BioRender.com and GraphPad Prism.

Appendix A. Supplementary data

Supplementary data to this article can be found online at https://doi.org/10.1016/j.biomaterials.2022.121971.

Graphical abstract: Multi-level secretome engineering with immuno-engineered mRNA and biomaterial niche augments the pro-angiogenic paracrine potency of therapeutic cells.

Conventional mesenchymal stromal/stem cell (MSC) therapeutics achieve incomplete effects in pro-angiogenic therapy.

The pro-angiogenic paracrine effects of MSCs are improved by combining biomaterial-based secretome modulation with immuno-engineered in vitro transcribed (IVT-) mRNA:

By immuno-engineering the IVT-mRNA, targeted overexpression of VEGF is uncoupled from the inflammatory secretome shift caused by unmodified mRNA, and instead can be combined with adhesion-mediated upregulation of supporting pro-angiogenic mediators (e.g. HGF). Optimized cell adhesion synergistically increases the secretion of IVT-mRNA encoded VEGF. Orchestration of pro-angiogenic growth factor patterns within the MSC secretome augments the pro-angiogenic potency of the MSC product.

References

[1] W.A. Lim, The emerging era of cell engineering: harnessing the modularity of cells to program complex biological function, Science 378 (6622) (2022) 848–852.
[2] Y.H. Kusumanto, V. van Weel, N.H. Mulder, et al., Treatment with intramuscular vascular endothelial growth factor gene compared with placebo for patients with diabetes mellitus and critical limb ischemia: a double-blind randomized trial, Hum. Gene Ther. 17 (6) (2006) 683–691.
[3] F. Sanada, Y. Taniyama, Y. Kanbara, et al., Gene therapy in peripheral artery disease, Expet Opin. Biol. Ther. 15 (3) (2015) 381–390.
[4] I. Vajanto, T.T. Rissanen, J. Rutanen, et al., Evaluation of angiogenesis and side effects in ischemic rabbit hindlimbs after intramuscular injection of adenoviral vectors encoding VEGF and LacZ, J. Gene Med. 4 (4) (2002) 371–380.
[5] I. Baumgartner, G. Rauh, A. Pieczek, et al., Lower-extremity edema associated with gene transfer of naked DNA encoding vascular endothelial growth factor, Ann. Intern. Med. 132 (11) (2000) 880–884.
[6] E. Sulpice, S. Ding, B. Muscatelli-Groux, et al., Cross-talk between the VEGF-A and HGF signalling pathways in endothelial cells, Biol. Cell. 101 (9) (2009) 525–539.
[7] F. Liu, K.L. Schaphorst, A.D. Verin, et al., Hepatocyte growth factor enhances endothelial cell barrier function and cortical cytoskeletal rearrangement: potential role of glycogen synthase kinase-3beta, Faseb. J. 16 (9) (2002) 950–962.
[8] T. Kobayashi, K. Hamano, T.S. Li, et al., Enhancement of angiogenesis by the implantation of self bone marrow cells in a rat ischemic heart model, J. Surg. Res. 89 (2) (2000) 189–195.
[9] A. Blum, W. Balkan, J.M. Hare, Advances in cell-based therapy for peripheral vascular disease, Atherosclerosis 223 (2) (2012) 269–277.
[10] A. Liew, T. O'Brien, Therapeutic potential for mesenchymal stem cell transplantation in critical limb ischemia, Stem Cell Res. Ther. 3 (4) (2012) 28.
[11] [press release], Pluristem Announces DMC Recommendation Following Interim Analysis of its Phase III CLI Study, 2020.
[12] S. Lee, E. Choi, M.J. Cha, K.C. Hwang, Cell adhesion and long-term survival of transplanted mesenchymal stem cells: a prerequisite for cell therapy, Oxid. Med. Cell. Longev. 2015 (2015) 632902.
[13] A.S. Mao, J.W. Shin, S. Utech, et al., Deterministic encapsulation of single cells in thin tunable microgels for niche modelling and therapeutic delivery, Nat. Mater. 16 (2) (2017) 236–243.
[14] M.E. Wechsler, V.V. Rao, A.N. Borelli, K.S. Anseth, Engineering the MSC secretome: a hydrogel focused approach, Adv Healthc Mater 10 (7) (2021), e2001948.
[15] D. Thomas, G. Fontana, X. Chen, et al., A shape-controlled tuneable microgel platform to modulate angiogenic paracrine responses in stem cells, Biomaterials 35 (31) (2014) 8757–8766.
[16] N.M. Drzeniek, A. Mazzocchi, S. Schlickeiser, et al., Bio-instructive hydrogel expands the paracrine potency of mesenchymal stem cells, Biofabrication 13 (4) (2021), 045002.
[17] H. Lee, J.S. Kim, Unexpected CRISPR on-target effects, Nat. Biotechnol. 36 (8) (2018) 703–704.
[18] A. Moiani, Y. Paleari, D. Sartori, et al., Lentiviral vector integration in the human genome induces alternative splicing and generates aberrant transcripts, J. Clin. Invest. 122 (5) (2012) 1653–1666.
[19] L.R. Baden, H.M. El Sahly, B. Essink, et al., Efficacy and safety of the mRNA-1273 SARS-CoV-2 vaccine, N. Engl. J. Med. 384 (5) (2021) 403–416.
[20] U. Sahin, K. Kariko, O. Tureci, mRNA-based therapeutics–developing a new class of drugs, Nat. Rev. Drug Discov. 13 (10) (2014) 759–780.
[21] L.-M. Gan, M. Lagerström-Fermér, L.G. Carlsson, et al., Intradermal delivery of modified mRNA encoding VEGF-A in patients with type 2 diabetes, Nat. Commun. 10 (1) (2019) 871.
[22] A. Collén, N. Bergenhem, L. Carlsson, et al., VEGFA mRNA for regenerative treatment of heart failure, Nat. Rev. Drug Discov. 21 (1) (2022) 79–80.
[23] A. Mullard, mRNA-based drug approaches Phase I milestone, Nat. Rev. Drug Discov. 15 (9) (2016), 595-595.
[24] K. Karikó, M. Buckstein, H. Ni, D. Weissman, Suppression of RNA recognition by toll-like receptors: the impact of nucleoside modification and the evolutionary origin of RNA, Immunity 23 (2) (2005) 165–175.
[25] A. Thess, S. Grund, B.L. Mui, et al., Sequence-engineered mRNA without chemical nucleoside modifications enables an effective protein therapy in large animals, Mol. Ther. 23 (9) (2015) 1456–1464.
[26] O. Andries, S. Mc Cafferty, S.C. De Smedt, R. Weiss, N.N. Sanders, T. Kitada, N1-methylpseudouridine-incorporated mRNA outperforms pseudouridine-incorporated mRNA by providing enhanced protein expression and reduced immunogenicity in mammalian cell lines and mice, J. Contr. Release 217 (2015) 337–344.
[27] B. Li, X. Luo, Y. Dong, Effects of chemically modified messenger RNA on protein expression, Bioconjugate Chem. 27 (3) (2016) 849–853.
[28] S.S. Signorelli, V. Fiore, G. Malaponte, Inflammation and peripheral arterial disease: the value of circulating biomarkers (Review), Int. J. Mol. Med. 33 (4) (2014) 777–783.
[29] L. Lasagni, M. Francalanci, F. Annunziato, et al., An alternatively spliced variant of CXCR3 mediates the inhibition of endothelial cell growth induced by IP-10, Mig, and I-TAC, and acts as functional receptor for platelet factor 4, J. Exp. Med. 197 (11) (2003) 1537–1549.
[30] R.C. Hoogeveen, A. Morrison, E. Boerwinkle, et al., Plasma MCP-1 level and risk for peripheral arterial disease and incident coronary heart disease: atherosclerosis Risk in Communities study, Atherosclerosis 183 (2) (2005) 301–307.
[31] D. Williams, H. Puhl, S. Ikeda, A simple, highly efficient method for heterologous expression in mammalian primary neurons using cationic lipid-mediated mRNA transfection, Front. Neurosci. 4 (2010) 181.
[32] M.M.H. Li, M.R. MacDonald, C.M. Rice, To translate, or not to translate: viral and host mRNA regulation by interferon-stimulated genes, Trends Cell Biol. 25 (6) (2015) 320–329.
[33] A.I. Caplan, D. Correa, The MSC: an injury drugstore, Cell Stem Cell 9 (1) (2011) 11–15.
[34] O. Levy, W. Zhao, L.J. Mortensen, et al., mRNA-engineered mesenchymal stem cells for targeted delivery of interleukin-10 to sites of inflammation, Blood 122 (14) (2013) e23–e32.
[35] P. Morais, H. Adachi, Y.-T. Yu, The critical contribution of pseudouridine to mRNA COVID-19 vaccines, Front. Cell Dev. Biol. 9 (2021) 789427.
[36] D. Walsh, I. Mohr, Viral subversion of the host protein synthesis machinery, Nat. Rev. Microbiol. 9 (12) (2011) 860–875.
[37] D.E. Eyler, M.K. Franco, Z. Batool, et al., Pseudouridinylation of mRNA coding sequences alters translation, Proc. Natl. Acad. Sci. USA 116 (46) (2019) 23068–23074.
[38] B.R. Anderson, H. Muramatsu, S.R. Nallagatla, et al., Incorporation of pseudouridine into mRNA enhances translation by diminishing PKR activation, Nucleic Acids Res. 38 (17) (2010) 5884–5892.
[39] B.R. Anderson, H. Muramatsu, B.K. Jha, R.H. Silverman, D. Weissman, K. Karikó, Nucleoside modifications in RNA limit activation of 2'-5'-oligoadenylate synthetase and increase resistance to cleavage by RNase L, Nucleic Acids Res. 39 (21) (2011) 9329–9338.
[40] D. Thomas, G. Marsico, I.L.M. Isa, et al., Temporal changes guided by mesenchymal stem cells on a 3D microgel platform enhance angiogenesis in vivo at a low-cell dose, P Natl Acad Sci USA 117 (32) (2020) 19033–19044.
[41] S.M. Frisch, H. Francis, Disruption of epithelial cell-matrix interactions induces apoptosis, J. Cell Biol. 124 (4) (1994) 619–626.
[42] N. Davidenko, C.F. Schuster, D.V. Bax, et al., Evaluation of cell binding to collagen and gelatin: a study of the effect of 2D and 3D architecture and surface chemistry, J. Mater. Sci. Mater. Med. 27 (10) (2016) 148.
[43] M.K. Majumdar, M. Keane-Moore, D. Buyaner, et al., Characterization and functionality of cell surface molecules on human mesenchymal stem cells, J. Biomed. Sci. 10 (2) (2003) 228–241.
[44] T.H. Qazi, D.J. Mooney, G.N. Duda, S. Geissler, Biomaterials that promote cell-cell interactions enhance the paracrine function of MSCs, Biomaterials 140 (2017) 103–114.
[45] T.H. Qazi, D.J. Mooney, G.N. Duda, S. Geissler, Niche-mimicking interactions in peptide-functionalized 3D hydrogels amplify mesenchymal stromal cell paracrine effects, Biomaterials 230 (2020), 119639.
[46] M. Pumberger, T.H. Qazi, M.C. Ehrentraut, et al., Synthetic niche to modulate regenerative potential of MSCs and enhance skeletal muscle regeneration, Biomaterials 99 (2016) 95–108.
[47] A.S. Mao, B. Ozkale, N.J. Shah, et al., Programmable microencapsulation for enhanced mesenchymal stem cell persistence and immunomodulation, Proc. Natl. Acad. Sci. U. S. A. 116 (31) (2019) 15392–15397.
[48] B. Wagner, R. Henschler, Fate of intravenously injected mesenchymal stem cells and significance for clinical application, Adv. Biochem. Eng. Biotechnol. 130 (2013) 19–37.

Mein Lebenslauf wird aus datenschutzrechtlichen Gründen in der elektronischen Version meiner Arbeit nicht veröffentlicht.

Mein Lebenslauf wird aus datenschutzrechtlichen Gründen in der elektronischen Version meiner Arbeit nicht veröffentlicht.

Publication list

	Publication	IF at subm.**	IF 2021
1	Drzeniek, N.M., N. Kahwaji, S. Schlickeiser, P. Reinke, S. Geißler, H.-D. Volk*, and M. Gossen*, *Immuno-engineered mRNA combined with cell adhesive niche for synergistic modulation of the MSC secretome.* **Biomaterials, 2023**. 294: p. 121971.	15.304 (2021)	15.304
2	Sanchez Rezza, A., Y. Kulahci, V.S. Gorantla, F. Zor*, and N.M. Drzeniek*, *Implantable Biomaterials for Peripheral Nerve Regeneration–Technology Trends and Translational Tribulations.* **Frontiers in Bioengineering and Biotechnology, 2022**. 10.	5.89 (2020)	6.064
3	Drzeniek, N.M., A. Mazzocchi, S. Schlickeiser, S.D. Forsythe, G. Moll, S. Geissler, P. Reinke, M. Gossen, V.S. Gorantla, H.D. Volk*, and S. Soker*, *Bio-instructive hydrogel expands the paracrine potency of mesenchymal stem cells.* **Biofabrication, 2021**. 13(4).	8.213 (2019)	11.092
4	Moll, G*., N. Drzeniek*, J. Kamhieh-Milz, S. Geissler, H.D. Volk, and P. Reinke, *MSC Therapies for COVID-19: Importance of Patient Coagulopathy, Thromboprophylaxis, Cell Product Quality and Mode of Delivery for Treatment Safety and Efficacy.* **Front Immunol, 2020**. 11: p. 1091.	4.716 (2018)	8.786
5	Moll, G., N. Drzeniek, J. Kamhieh-Milz, S. Geissler, and P. Reinke, *Editorial comment: variables affecting the presence of mesenchymal stromal cells in the peripheral blood and their relationship with apheresis product.* **British Journal of Haematology, 2020**. 189(4): p. 593-596.	5.206 (2018)	8.615

* shared first or last author position

** impact factor at the time of submission (year indicated in parentheses)

Acknowledgements

First, I want to thank my advisors Hans-Dieter Volk, Manfred Gossen and Petra Reinke, who are not only true experts in their fields but were also incredibly supportive mentors at every step of my journey. Through your example you have shown me, each in your own way, what it means to be a great scientist and inspired me to pursue this difficult, yet exciting and incredibly rewarding path. Thank you for always being a pillar of support, while giving me enough freedom to make mistakes, learn from them and find my own path. While taking the first steps of my professional life under your guidance I have learned a lot, not only professionally, but also as a person and for this, above all, I feel incredibly grateful.

I want to thank all my colleagues from Volk and Gossen labs, without whom completing this work would have been -probably- impossible and -certainly- not as much fun! I want to thank Nourhan Kahwaji, who completed her undergraduate thesis in my PhD project, and who was an immense help. Thank you for always being as engaged and dependable as you are and for making us laugh with those sophisticated Christmas tree decorations. I also want to thank Guido Moll, who has been a wonderful colleague, mentor, and friend! Thanks for the fun lunch breaks, the late-night steakhouse dinners and for teaching me so much about everything, from MSC biology to the inner workings of academia. Thank you Sven Geißler, Stephan Schlickeiser, Katrin Witte, Cornelia Heindrich, Jörg Contzen and Hanieh Moradian for teaching me how to keep my cells alive, understand my data and not to burn down the lab.

I also want to thank the great colleagues I have met at WFIRM. Thank you, Shay Soker and Vijay Gorantla, for making me feel welcome in your labs and for giving me the opportunity to learn and broaden my horizon as a visiting scientist. Thank you, Steve Forsythe, for sharing your expertise and your whisky with me. Thank you, Diana Lim, Mahesh Devarasetty, Andrea Mazzocchi, Ethan Shelkey and Giorgio Orofino.

I dedicate this work to my family who has supported me throughout my entire life with unwavering love and trust. Thanks Mom and Dad for always looking out for my best interest, for providing me with wonderful opportunities and giving me the freedom to find my own path. Thank you, Grandpa and Grandma, for exposing me to so many interesting thoughts, scientific theories and concepts at a young age, inspiring me to become a scientist and sparking in me an endless curiosity about the inner workings of this beautiful

world. I also want to thank my friends and especially Lisa who have supported me over the years and showed me remarkable understanding for my irregular work schedule.

Finally, I wish to thank the German Federal Ministry of Education and Research, Amgen Inc. and Verband Deutsche Nierenzentren (DN) e.V. for supporting me throughout my studies.